Yannick Wijmans

4354516

Horizontal negatively buoyant jets in deep sea mining

The influence of initial concentration of discharged slurries on the spatial spread of turbidity currents

14-11-2021

TU Delft

[This page is intentionally left blank]

Horizontal negatively buoyant jets in deep sea mining

The influence of initial concentration of discharged slurries on the spatial spread of turbidity currents

By

Y. R. Wijmans

4354516

in partial fulfilment of the requirements for the degree of

Master of Science
in Offshore and Dredging Engineering

at the Delft University of Technology

Supervisor:	Dr. Ir. R.L.J. Helmons	TU Delft
Thesis committee:	Dr. Ir. R.L.J. Helmons,	TU Delft
	Dr. Ir. A.M. Talmon,	TU Delft
	Dr. A Kirichek,	TU Delft

TU Delft

[This page is intentionally left blank]

Acknowledgements

This thesis marks the end point of a 7-year study period at the TU Delft, after having successfully finished a bachelor in Maritime Technology and a master in Offshore and Dredging Engineering, something I could not have done without the help of a few others.

I would like to sincerely thank my parents for always supporting me in my choices and always being there to support me both financially and mentally when needed. I would also like to thank my girlfriend, sister and friends who helped me through tough times, and with whom I created unforgettable memories during my time in Delft and Rotterdam.

The completion of this MSc thesis specifically would not have been possible without the help of my supervisors and laboratory staff. Therefore I would like to thank Dr. Ir. Rudy Helmons for all the time he devoted to being my main supervisor during this research. The results accomplished would not have been possible without the weekly meetings, discussions, suggestions and feedback provided by him. I would also like to thank Dr. Ir. Arno Talmon for supervising this research and providing feedback and suggestions. Lastly, I want to thank Ed Stok and Andre van den Bosch for providing technical support in the 3mE dredging lab.

[This page is intentionally left blank]

Summary

Recently, deep-sea mining has acquired renewed interest from commercial companies due to a rise in the demand of minerals and metals. Deep-sea mining is focussed on different minerals and rare earth elements that are increasingly used in the manufacturing of goods and products related to renewable energy. The focus lies on polymetallic nodules, seafloor massive sulphides and cobalt-rich crusts. In order to collect these minerals, a mining operation at several kilometres depth has to be undertaken. Apart from the technical challenges that mining at several kilometres depth poses, also the environmental consequences receive a lot of attention. Deep-sea mining receives a lot of criticism from environmental agencies. Deep-sea mining operations are believed to cause damage to the environment by the sediment plume, as well as by producing light and noise which are absent under normal conditions at the deep ocean floor. Among other things, more knowledge is required about the sediment plume. This plume is generated by the movement of the miner, but more importantly by the discharging of the picked up and unwanted sediment. This happens at the back of the miner using a set of diffusers. A knowledge gap exists in the understanding that changing the initial concentration of the discharged slurry has on the spread of the sediment plume and subsequent turbidity current. In order to acquire a better understanding of the effect that the initial concentration of the slurry has on the spatial spread of the sediment plume and turbidity current caused by the deep sea mining vehicle, experiments have been performed in which the initial concentration has been altered so that the characteristics of the ensuing current can be compared. The main objective of this research has been defined as the following:

*'Determine how changing the **initial volumetric concentration** of the discharge mixture influences the flow parameters after impingement and sediment flux inside the turbidity current for a **constant sediment flux and discharge velocity** through measurement of velocity and concentration profiles. Subsequently use the findings to **identify how the spread of sediment can be limited** for the benefit of the ecosystems around the mining area.'*

Important aspects of the diffuser are called the source parameters. The diffuser in these experiments is a source of both momentum and buoyancy. The momentum flux is a function of the volume flow and discharge velocity, while the buoyancy flux is determined by the volume flow and apparent gravity. For a horizontal jet, the momentum flux is what causes the horizontal motion of the jet and plume, and the buoyancy flux caused deflection towards the bottom and is therefore responsible for the downwards motion of the plume. These parameters together can be used for determining several characteristic lengths of the jet. Increasing the concentration of the slurry increases the density and thereby apparent gravity. As a result, the ratio between momentum and buoyancy differs for different concentrations, which forms an important characteristic for comparing experiments.
One of the most important assumptions for investigating the influence of initial concentration of the slurries has to do with the different phases of the discharged flow. During the initial phase, in which the negatively buoyant jet deflects towards the bottom and transforms into a plume, the density difference between the slurry and ambient mixture is thought to be dominant for the settling process, as the mixture behaves as one coherent fluid. After impingement on the bottom, the mixture spreads as a short-lived wall jet after which the mixture continues its way downstream as a turbidity current. During this phase it is the weight of the solids inside the slurry that causes it to settle. Because there are a lot of solids present in these slurries this process of settling is controlled by both hindered settling and flocculation. Flocculation is the aggregation of cohesive particles, forming a larger, heavier particle. Clay, which is cohesive, is expected to be present at most mining sites, resulting in flocculation to be an important factor in the process.

The research has been performed by conducting a total of three different experiments. These experiments consist of pumping a pre-mixed slurry of water and spherical glass particles into a large modular tank, where is it discharged through a diffuser. For each experiment a mixture is prepared with a different concentration (140, 80 and 20 g/L), which is discharged into the modular tank with three different flow rates in order to keep the sediment flux constant between each experiment. A total of three diffusers are used, one for each

concentration. The diffusers differ in cross section in order to achieve a constant discharge velocity for all experiments. Inside this modular tank measurements were performed to gather data. Experiments have been performed using both spherical glass particles and clay. The sediment flux is kept constant between different experiments as it is assumed that the sediment flux of real deep sea mining operations will be mainly determined by the width, cutting depth and velocity of the mainly vehicle. The discharge velocity is based on a scaled down 0.5 m/s, which is assumed to be the discharge velocity for full scale deep sea mining operations. The discharge velocity will most likely be equal to the forward velocity of the miner vehicle to minimize the kinetic energy added to the discharged slurry.
For performing measurements during the experiments an ADV was used. This device is capable of measuring the velocity in three directions over a profile of 30 mm with 1 mm intervals. The ADV also measures the signal-to-noise ratio, which after performing a calibration can be used for calculating the concentration inside the turbidity current. Together this data can be used for determining the spatial spread of the turbidity current. It is important to note that this calibration depends on the sediment type and size. The range of concentrations to which this method is applicable is mostly dependent on the size and type of the sediment and the acoustic frequency of the ADV. It is known that for some frequencies the absorption losses become high for certain ranges of particles diameters which causes the backscatter signal strength to diminish. This leads to concentration measurements only being possible for a limited range of values.

Experiment results consist of velocity profiles, concentration profiles and video images. Statistical analysis of the data and observations of the visualized data and video imagery of the experiments allowed for an analysis of the concentration influence on the spatial spread of the turbidity current.
Based on the findings of this research, it is believed that a higher concentration than the 1% volumetric concentration that is currently being assumed by deep sea mining companies could prove to be beneficial in preventing the spatial spread of the sediment plume and subsequent turbidity current resulting from the sediment discharge of the deep sea mining vehicle. It is believed that in general, increasing the initial concentration of the discharged slurry, and thereby decreasing the momentum/buoyancy ratio of the buoyant jet, directly leads to both the velocity and concentration of the turbidity current to decrease over a shorter distance after impingement, while the impingement distance itself is also decreased for a higher initial concentration. As such, the total reach of the turbidity current resulting from the slurry discharge from a deep sea mining vehicle can be decreased by using a higher initial concentration of said slurry. It should however be noted that a large increase in concentration has the adverse effect of an aggressive impingement, leading to larger velocities in the ensuing wall jet than would otherwise be the case, and further research is required to determine the exact effect that the concentration has on this, as a too large velocity could cause the resuspension of bed material. It is believed that mainly the higher density difference with the ambient water plays a vital role in decreasing the spatial spread of the sediment plumes produced by deep sea mining operations. The higher density achieved by a high concentration results in the plume to deflect towards to bottom over a shorter distance and a decrease in turbidity current height. This decrease in height is beneficial for the later stage of the turbidity current in which the dying out is dominated by the settling velocity of individual particles.

Table of contents

List of figures and tables

Figures:

Tables:

Abbreviations

3D	Three-dimensional
ADV	Acoustic Doppler velocimeter
AR	Aspect ratio
BAT	Best available technology
BEP	Best environmental practice
CCZ	Clarion-Clipperton Zone
CLB	Continuous-line-bucket-dredging
DSM	Deep-sea mining
EEZ	Exclusive economic zone
ISA	International seabed authority
MR	Mining rate
NA	Nodule abundance
NTU	Nephelometric Turbidity Units
PDF	Probability density function
PSD	Particle size distribution
REE	Rare earth elements
SMS	Seafloor massive sulphides
SNR	Signal-to-noise ratio
SSC	Suspended solids concentration
UN	United nations
VTS	Vertical transport system

List of symbols

Symbols	Description	Unit
A_0	Cross sectional area of discharge source	m^2
C_0	Initial concentration	-
C_m	Mass concentration	-
C_{pr}	Pressure recovery coefficient	-
C_v	Volumetric concentration	-
C_{vd}	Delivered volumetric concentration	-
C_{vi}	In-situ volumetric concentration	-
d	Diameter of solids	µm
d	Flow thickness	m
D	Diameter of pipeline	m
D_H	Hydraulic diameter	m
F_s	Sediment deposition rate	$gm^{-1}s^{-1}$
Fr	Froude number	-
g	Gravity constant	m/s^2
g’	Apparent gravity	m/s^2
h	Cutting layer depth of the miner/Duct height	m
J_0	Buoyancy flux at (discharge) source	m^4/s^3
k	Wave number	m^{-1}
L	Characteristic dimension	m
L_m	Momentum-settling length scale	m
L_M	Momentum-buoyancy (jet/plume transition) length scale	m
L_Q	Discharge length scale	m
M_0	Momentum flux at (discharge) source	m^4/s^2
P	Nodule production of a mining vehicle	kg/s
P	Wetted perimeter	m
Q_{sed}	Volume flow of sediment	m^3/s
Q_0	Volume flow at (discharge) source	m^3/s
Q_t	Total volumetric production of sediment + nodules by mining vehicle	m^3/s
r	Radius (of a particle or pipeline)	m
R_0	Richardson number at (discharge) source	-
R_{sd}	Relative submerged density of solids	-
Re	Reynolds number	-
Re_p	Particle Reynolds number	-
S	Ratio of initial turbidity current and settling velocity of solids	-
S_s	Relative density of solids	-
SSC	Suspended solids concentration	g/L
U_0	Flow velocity at (discharge) source	m/s
U_a	Cross flow	m/s
v	Forward speed of the mining vehicle	m/s
v_{dl}	Deposition limit velocity	m/s
v_m	Mixture velocity	m/s
v_{sm}	Maximum value of deposition limit velocity	m/s
v_t	Settling velocity of a particle	m/s
v_{th}	Hindered settling velocity of particles	m/s
w	Width of a mining vehicle module/Duct width	m

Greek letters	Description	Unit
α_s	Particle absorption coefficient	dB/m
α_w	Water absorption coefficient	dB/m
β	Parameter for determining hindered settling velocity	-
β	Parameter for determining χ_{sv}	m^{-1}
γ	Relative density	-
η_c	Collector efficiency	-
η_k	Dimensionless parameter for determining χ_{ss}	-
η_p	Dimensionless parameter for determining χ_{ss}	-
η_s	Separator efficiency	-
θ	Dimensionless parameter for determining χ_{sv}	-
κ_s	Compressibility of solids	Pa^{-1}
κ_w	Compressibility of water	Pa^{-1}
λ	Wavelength	m
μ	Kinematic viscosity	m^2/s
ν	Dynamic viscosity	Pa·s
ξ_s	Particle attenuation coefficient	m^2/kg
ρ_0	Density of the ambient water	kg/m^3
ρ_a	Density of the mixture at the (discharge) source	kg/m^3
ρ_m	Density of the mixture	kg/m^3
ρ_s	Density of solids	kg/m^3
τ	Dimensionless parameter for determining χ_{sv}	-
χ_s	Normalised total scattering cross section	-
χ_{ss}	Normalised scattering cross section of a solid sphere	-
χ_{sv}	Normalised scattering cross section (viscous) of a solid sphere	-
ω	Agular (acoustic) frequency	s^{-1}

1. Introduction

This chapter has the purpose of giving background information about the emerging deep-sea mining (DSM) industry and its consequences, specifically giving insight into some of its current issues regarding the understanding of the environmental impact. Section 1 explains why this industry is currently emerging, what resources will be mined and what the current concepts for exploiting these resources look like. It will also elaborate on the environmental impacts of DSM. Section 2 will discuss the relevancy of thorough research into the environmental impacts of DSM and identify the knowledge gaps regarding this environmental impact. Section 3 will cover a problem analysis in which the identified knowledge gaps will be further explained, after which the research objective and questions related to this research subject will be stated. Sections 4 and 5 will discuss the research methodology and assumptions respectively.

1.1 Background to deep-sea mining

The availability of resources in the deep-sea is relatively well known for quite some time. Already in the 1960s and '70s there have been evaluations and tests for deep-sea mining operations [1]. After interest declined in the 1980s due to falling prices of metals, it has once again gained interest in recent years, mainly driven by the growing demand for minerals and metals [2][3] [4].
The rising demand and prices of minerals and metals can be attributed to different factors. Land-based resources are depleting while demand keeps growing due to a growing world population and economy [2] [5][4]. Many different kinds of metals and minerals are furthermore increasingly used in manufacturing products related to sustainable energy such as electric cars, wind turbines, batteries and other electrical products [2] [5]. Furthermore, the reserves and production of some metals and rare earth elements (REE) are currently controlled by a small number of countries. Examples of this are Congo, which accounts for roughly 60% of the world's total cobalt production, and China, which holds about 50% of the world's land based REE reserves and currently accounts for over 90% of the total global production. This also increases the volatility of prices because the policy and stability of a single country can shift the balance of demand and supply [2].
To summarize, a combination of rising demand caused by a growing population, economy and number of applications for metals combined with some uncertainty in supply has led to a renewed interest in the exploration of mineral resources in the ocean.

1.1.1 Deep-sea mineral sources

Currently there is a focus on three main resource types for DSM operations: polymetallic nodules, seafloor massive sulphides (SMS) and cobalt-rich crusts [2] [6]. Each of these resources require different mining approaches and contain different minerals [4]. They will be discussed below.

Polymetallic nodules
Polymetallic or manganese nodules are rocks with a potato-like shape, and most commonly sized between 5-10 cm in diameter [2][4]. They are located on the deep-ocean abyssal plains. Nodules have mainly been found in the Pacific where the Clarion-Clipperton Zone (CCZ) currently receives a lot of interest, as well as in the central Indian Ocean [2][5][4]. They are found lying on top of the seabed or partially buried [7]. The nodules form in a process taking millions of years, with growth rates thought to be in the range of 1 mm/million years [8]. They are mainly made up of manganese, copper and nickel, but also cobalt and REE can be found inside [2][4].

Seafloor massive sulphides
Seafloor massive sulphides are formed near hydrothermal vents. These vents are located across different regions of the ocean in areas of tectonic activity, which is mainly near oceanic ridges [2]. These vents are shaped like chimneys and can reach up to several metres in height. The vents eject hot acidic fluids with temperatures of around 250-400° C [4]. They are believed to be rich in copper, zinc, lead, silver and gold [2] [9].

Cobalt-rich crusts

Cobalt-rich crusts, also called ferromanganese crusts, form on rock surfaces on seamounts and ridges at variable depths [4]. Their main constituents are manganese, iron, cobalt, copper and nickel. While the metals which are found here are highly sought after, mining these crusts is typically thought of as being more challenging than nodule harvesting since that crusts are attached to the rock below and will thus require drilling or cutting [2].

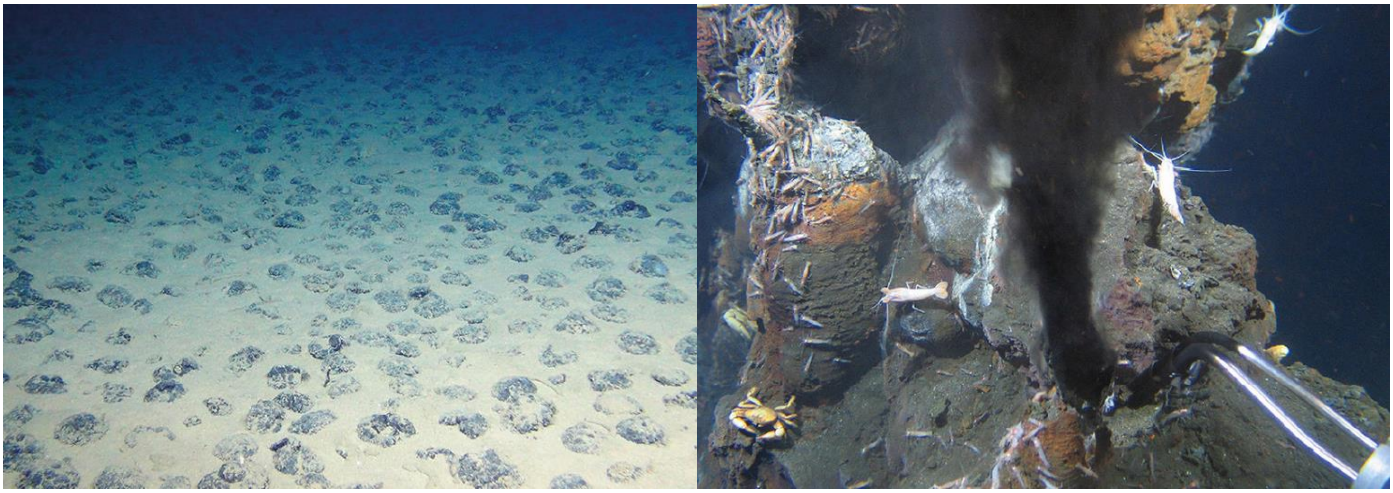

Figure 1.1: Example of manganese nodules (left) and hydrothermal vents (right) [4]

1.1.2 Deep-sea mining systems

All currently proposed concepts for DSM operations follow the same basic design, consisting of a miner/seabed resource collector, a (hydraulic) lift system for transporting the minerals to the surface and a support vessel where the minerals can be collected and transferred to transport vessels [3] [4][8]. All three main components will be briefly discussed below.

Miner/collector

The seabed equipment will consist of a vehicle carrying a collector. These vehicles will range in size, with current estimates ranging between 6 and 16 metres in width, and will most likely be fitted with tracks [7] [1]. The production velocity of the concept vehicles is in the range of 0.5 m/s [10] [8] [11]. Minerals can be removed from the seabed by multiple principles, including hydraulics, mechanical and bucket dredging, drilling and cutting [2][8]. In the case of nodule mining, the miner would collect the nodules by hydraulic or mechanical means [1][8]. In addition, most concepts use water jets to loosen the nodules from the sediment in which they may be partially buried [1][8]. The nodules will be collected together with sediment and water. Miners that are used for the extraction of minerals from the hydrothermal vents will remove those chimneys entirely. The miners will for this purpose be equipped with cutterheads [2][4].
The miners will cause resuspension of sediment by their movement over the seabed and by discharging slurry with hydraulic jets [1] [12] [9]. The slurry will be horizontally discharged at the back of the miners, which result in sediment plumes. The discharged slurry consists of sediment and water that is picked up together with the nodules. Most concepts aim for separating the nodules and sediment at the seabed, after which the sediment will be discharged at the back of the miner using water jets, while the nodules will be transported to the surface [6][8]. The reason for this is because removal of the sediment at this stage results in less total mass and therefore less required energy needed for the vertical transport of the mixture to the surface [7] [13].

Vertical transport system

For transporting the minerals and nodules from the seafloor to the surface multiple concepts have been found in literature. These include continuous-line-bucket-dredging (CLB), wireline basket dredging and hydraulic dredging [1]. Hydraulic appears to be the most effective and thus most concepts make use of hydraulic

transport through a riser pipe [1] [8]. The riser is connected to the miner through a flexible connection and uses centrifugal pumps to transport the minerals to the surface [1] [4] [8].

Surface vessel

The surface vessel provides a platform for the deployment, recovery and maintenance of the seabed equipment, as well as a central point from which the entire mining operation can be (remotely) controlled [2]. It also acts as a temporary storage for the mined materials and is the power supply for the seabed equipment which is connected to the support vessel through an umbilical [2] [8]. The aforementioned separation at the seabed will have a certain efficiency meaning that not all sediment is removed from the slurry and some of it will be transported to the surface. The surface vessel will therefore also be required to separate the mined minerals/nodules from the water and sediment that is transported with it. This waste water will be discharged back into the ocean, either at the surface or at greater depth, resulting in a vertically discharged sediment plume [4] [8].

1.1.3 Environmental aspects

The operations associated with deep-sea mining have been elaborated in the previous section. This section will discuss the environmental effects of these operations and the concerns of environmental organizations and marine biologists.

The main concern related to deep-sea mining is the limited understanding of the effects that deep-sea mining will have on the sometimes unique ecosystems found on the seafloor [2] [4]. Many of these ecosystems took millions of years to develop and it is feared that once destroyed, it will take a long time for them to recover [1]. Especially near hydrothermal vents, where scientist expect that the first life was formed, marine biologists often find unique species and isolated pockets of life, all of which are vulnerable and will be affected by deep-sea mining operations [2] [4].

It is expected that the miners will cause the greatest impact on the deep-sea environment [8]. Mining operations will generate sediment plumes and be the source of noise and artificial light, all of which are expected to severely impact marine life [3] [6]. The miners will also cause a direct physical impact on the seabed. Crusts will be drilled, hydrothermal vents will be completely removed, and the picking up of nodules will leave the areas desolate [4] [8].

Sediment plumes

The formation of sediment plumes is one of the main concerns. The plumes are formed by discharging the picked up sediment, either at the back of the miner or coming from the surface vessel, as well as from the movement of the miner itself [3] [1] [8]. The sediment plumes will have a density higher than that of the ambient water. This results in the plumes sinking to the bottom and impinging at the seabed. Here the slurry will continue spreading as a gravity current. A gravity current is a current driven by density differences between two fluids. In the case of the discharged slurries the emerging gravity current is called a ‘turbidity current’, in which the density difference is caused by the suspended particles. Especially the very fine sediment and dissolved metals can stay in suspension for a very long time. This allows the ocean currents to carry it away over large distances where it will settle [3].

Most deep ocean waters have very low suspended sediment concentrations and the plumes and turbidity currents generated by mining may cause damage to respiratory organs and surfaces of marine life [3] [5]. They can also block and damage feeding systems of seabed organisms [2] [14]. The sediment is eventually deposited away from the mining site, where it can disrupt local ecosystems by covering them beneath a layer of sediment [2] [6] [12]. The sediment plumes may furthermore block bioluminescent light, hindering communication between animals [3] [14].

Noise

Noise will be generated by the miner through the grinding of vents and crusts [3]. Also the pumps that are used for the vertical transportation of the minerals will be a source of noise in the area [3]. The deep-sea is usually very quiet, and the sound generated by the miners could propagate for many kilometres, affecting life in a large area [2]. It is known that some fish and marine mammals communicate using low frequency sounds.

This may be interfered with by the sound generated by seabed equipment [3] [4]. This may cause distress and hinder the communication for several species [3].

Light

Since the deep-sea is pitch black under normal conditions, life here has adapted and depends on bioluminescence for hunting and communications. Miners will likely require artificial light for controlling and monitoring purposes, which will interfere with the bioluminescent light of marine life [2]. This may hinder communication or hunting capabilities for species using bioluminescence [4].

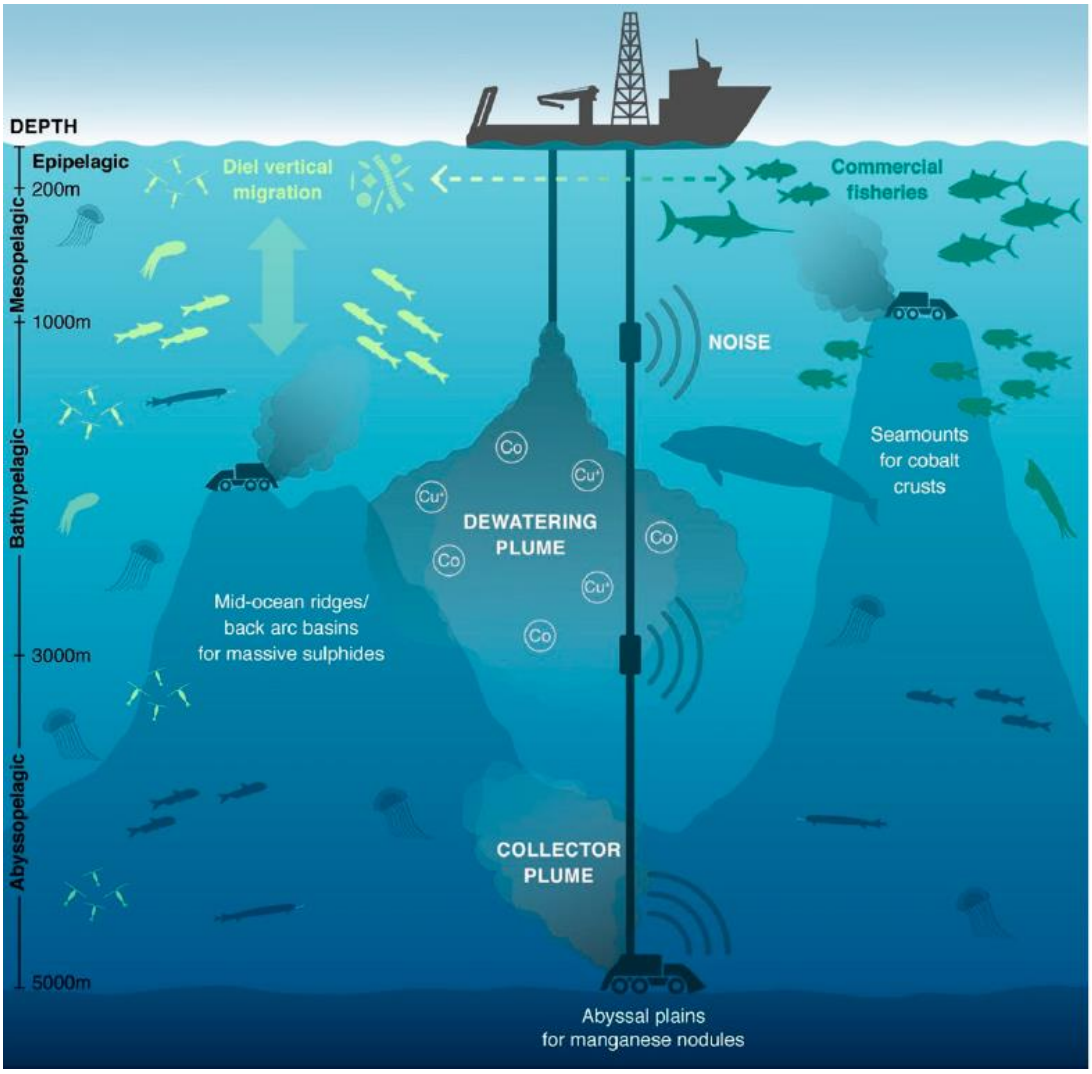

Figure 1.2: Side view showing all the parts in the design: (seafloor) miners, VTS and surface vessel. Also the emission of noise by the miner and pumps as well as the sediment plumes are shown [3]

1.2 Relevancy

Deep-sea mining will affect the ecosystems in and around the mining sites in multiple ways as has been explained in the previous section. In this section the focus will lie on the criticism outed by environmental agencies and the legal implications of deep-sea mining. These subjects show the relevancy of further research into the consequences of deep-sea mining and also show which knowledge is currently lacking.

1.2.1 Criticism from environmental agencies

The environmental issues regarding deep-sea mining have been addressed in the section 1.1.3. As explained, the main point of criticism of environmentalists and marine biologists is the lack of knowledge regarding the effects that deep-sea mining will have on local ecosystems. Not enough is currently known regarding the

impact that the deep-sea mining operations will have on the unique and vulnerable ecosystems of the deep-sea [2] [4]. Furthermore, it is clear that the seabed equipment will generate sediment plumes that have the potential to impact an area many times larger than the mining site alone, and of which the influence on the deep-sea environment is yet unclear [1] [4].

1.2.2 Licensing from ISA

Further research into the environmental effects of deep-sea mining is also required from a legal perspective. In accordance with United Nations laws, each country has the authority over the sea and air up to 12 nautical miles off the coast. In addition, each state has the exclusive rights on all resources up to 200 nautical miles away from the coastline, called the exclusive economic zone (EEZ) [4]. In the EEZ each country has the rights over any resources found there. For deep-sea mining however, the rights over the resources are more complicated. Since deep-sea mining will take place in the deepest parts of the ocean, areas that have been found interesting are regularly located in international waters. According to UN laws, these waters belong to mankind. Because of this, the International Seabed Authority (ISA) was created by the UN with the aim to equally divide the benefits of these international waters as well as preserving its environment for future generations [4]. The ISA is tasked with organizing and regulating deep-sea mining beyond national jurisdiction [3]. They can issue licenses and exploration contracts for specific areas [4]. These allow companies to explore and exploit the deep-sea mineral resources [1]. They are currently developing codes and regulations regarding exploitation of deep-sea mineral resources, because they are also tasked with making sure that the marine environment and deep-sea ecosystems are protected [3] [4]. For this reason, the ISA requires companies that want to acquire licenses to be able to predict the effects of their operations. This is yet another reason why it is important to get a better understanding of the spread of sediment plumes generated by the mining, as well as other adverse effects of deep-sea mining such as the aforementioned noise and light pollution.

1.2.3 Best environmental practices

The environmental concerns and licensing by government agencies as introduced above, can be summarized in the term ‘Best Environmental Practices’ (BEP). This term is a tool used to identify the best environmental management by looking at techniques and measures to minimise the impact on the environment by activities and industries. It aims for using the most appropriate environmental control measures and best available techniques for activities while still taking into account the economic viability. Considered for this are a number of criteria, among which are:

- Saving resources (e.g. energy and water, as well as choosing for renewable sources)
- Limiting the amount of waste material (optimise the disposed quantities)
- Limiting the effect of the disposal of waste material
- Optimise the methods used
- Minimise the effects of contamination by chemicals
- Minimise the impact of the collecting (specific for deep sea mining)

Another term which is often used for this concept is ‘Best Available Technology’ (BAT), which is comparable to BEP and aims to apply the best currently available technology in order to minimize impact to the environment. BAT can be used by legislators and regulators for formulating environmental policies, regulations and industry standards. BAT is comparable to BEP in its aim to reduce environmental impact, but with an emphasis on applying the best and newest technologies following advances and changes in scientific knowledge and understanding.

1.3 Problem analysis

1.3.1 Problem definition

As explained in sections 1.1 and 1.2, DSM is likely to have a significant impact on the environment, leading to the knowledge gaps regarding the risks of deep-sea mining being identified. These include the effects that

it will have on the ecosystems and uncertainty regarding the spatial spread of sediment plumes. More knowledge on the spread of this slurry produced by the DSM processes is therefore required. Both for the sake of the environment, and to be eligible for a license from the ISA [4]. For limiting the effect that the sediment has on the environment the aim should be to decrease the sediment flux inside the aforementioned turbidity currents as quickly as possible [14].
For this research the focus will be on the slurry that is ejected horizontally by the seafloor mining vehicles used for nodule mining. The reasons for this are the following. First of all, it is expected that the greatest impact on the deep-sea will results from the miner itself making it a subject of high importance [8]. The reason for the focus on nodule mining specifically is due to two differences that this resource has compared to hydrothermal vents and cobalt-rich crusts. The first being that the sediment of the abyssal plains on which nodules are found consists of fine-grained particles, which are easily suspended and can stay in suspension for a long time [15]. The second difference between these resources is the scale at which the mining takes place. Due to the nodules being spread out over large areas, the mining sites of nodule mining operations will be significantly larger than those of hydrothermal vents and cobalt-rich crusts [16] [17]. These two factors result in sediment plumes playing a large role in nodule mining. The reason for the focus on horizontal discharge is that most concepts currently in development make use of diffusers discharging the slurry horizontally as was discussed in section 1.1.2. Meanwhile, most research regarding sediment plumes resulting from slurry discharge done so far was mainly focussed on vertically discharging jets [18]. These researches were focussed on the effects of dewatering plumes created by the sediment/water mixture being discharged back into the ocean from the surface vessel. This results in a need for research done into the horizontal discharge of slurry by the mining vehicles.
To analyse this problem, the process of how turbidity currents are generated will be explained. The generation of the turbidity current by the mining vehicle can be subdivided into different stages, which will be discussed below.

Miner

For determining the magnitude of the tailings discharge of the miner, its width, velocity and cutting layer depth are the most important characteristics [7]. Blue Nodules, a research project funded by the EU in which multiple offshore industry companies and research institutes work together, currently mentions 6 cm as the cutting layer thickness [14]. Multiplied these parameters give the total production in m^3/s. Depending on the nodule abundance, collector efficiency and sediment properties at the mining site this production is made up of a mix of nodules, sediment and water [19] [8] [11]. Inside the miners this mixture will be separated and depending on the efficiency of this process a certain amount of sediment will be filtered out and discharged behind the miner as a jet [20] [6] [8]. This leads to an almost constant sediment flux being discharged behind the miner. Because this sediment flux is nearly constant, only the concentration of the discharged mixture can be altered by adding more or less water to the jet. The velocity at which the mixture is discharged depends on the total volume flow and diffuser area. The aim is to discharge the sediment at the same velocity as the miner is moving forward with. Because the discharge velocity is in the opposite direction, this results in the outflow from the diffuser effectively having a relative velocity of zero. This way the least energy is given to the sediment which is expected to help the settling process [21].

Jet and plume

The unwanted sediment picked up by the mining vehicle will be discharged behind it. The discharged slurry initially results in a negatively buoyant jet with a density higher than that of the ambient water. This results in a source of both momentum and buoyancy. A source of momentum results in jet like flow, while a source of buoyancy results in plume like flow [22]. This combination leads to a negatively buoyant jet, which is driven by momentum and buoyancy and in which both can dominate [18].
The main parameters of the flow at the discharge source are the initial volume flow Q_0, initial momentum flux M_0 and initial buoyancy flux J_0. These are given by the following equations [22]:

$$Q_0 = \frac{\pi D^2}{4} U_0, \qquad M_0 = U_0 Q_0, \qquad J_0 = g_0' Q_0 \tag{1}$$

Where U_0 is the exit velocity of the jet and g'_0 is the apparent gravity, given by the following equation:

$$g'_0 = g\frac{(\rho_a - \rho_0)}{\rho_a} \tag{2}$$

Where ρ_a is the density of the ambient water and ρ_0 is the density of the discharged slurry. Further note that $\rho_0 > \rho_a$, so g'_0 and hence J_0 is negative. The above results in a jet discharge with an initial momentum and buoyancy flux that can both be expressed as a function of the volume flow and initial discharge density, which are controllable inputs for both experiments and real mining machines. It should be noted that at the impingement point the flow parameters are generally different from the initial ones, except for the buoyancy flux which is preserved [23].

The impingement location is determined by the jet/plume transition length scale. As stated before, a momentum and buoyancy source gives rise to both jet like and plume like flow. For a horizontal jet as discussed here, the momentum results in the horizontal motion of the slurry, hence the distance travelled, while the negative buoyancy results in the downward motion of the slurry. Which one dominates is determined by their ratio through the so called 'jet/plume transition length scale'. This distance, L_M, determines the length of the jet region, beyond which the flow is more similar to a plume, falling downward towards the bottom under the influence of gravity [24]. During this phase, the negative buoyancy dominates and the flow impinges on the bottom resembling a plume [23]. If momentum dominates, the flow will maintain the jet like flow for a longer distance. This means an impingement location further away from the discharge diffuser and a smaller impingement angle with the horizontal. If negative buoyancy dominates this leads to an almost vertical impingement with the bottom [22]. The angle at which the impingement takes place determines the shape of the outflowing turbidity current. Vertical impingement leads to a circular outflow (also called axisymmetric), while impingement at an angle smaller than 90 degrees (with the horizontal) leads to asymmetric outflow [22] [23].

The aforementioned distance L_M is given by the following equation [22]:

$$L_M = \frac{M_0^{3/4}}{|J_0^{1/2}|} \tag{3}$$

If the equations of (1) are substituted into (3), it becomes clear that this ratio increases with volume flow Q_0 and decreases with the initial discharge density ρ_0.

Impingement and Turbidity current

At some distance from the discharge source the plume impinges the bottom at a certain angle with the horizontal. This angle is important for the shape of the outflow. Most researches done so far focus on vertically upward or downward discharges [18]. This results in a circular and axisymmetric outflow shape. If impingement happens at an angle however, the outflow is not axisymmetric and mostly in the direction of the flow [18] [22].

After impingement, the flow is directed radially outward. This happens initially as a wall jet, which develops into a gravity current. A gravity current is a current driven by density differences between two fluids and is also called a density current for that reason. These can be the result of temperature differences or dissolved substances. The gravity currents occurring when discharging slurry are a particular kind of gravity current called 'turbidity currents' [25]. For these fluids it is the weight of the suspended particles that drives the flow. The emerging turbidity current is fed by the 'outflow source'. This is the wall jet that develops from the impinged plume [18]. The buoyancy flux generated here is what drives the turbidity current, which will propagate outwards. What happens next depends on the bottom characteristics such as sloped or flat, smooth or rough and erodible or non-erodible. In the case of a sloped and erodible bed the suspended concentration

can increase, resulting in a self-accelerating turbidity current [25]. In the case of a flat bed and a decrease in suspended particles due to settling, the driving buoyancy force will eventually decrease causing the turbidity current to die out [18].

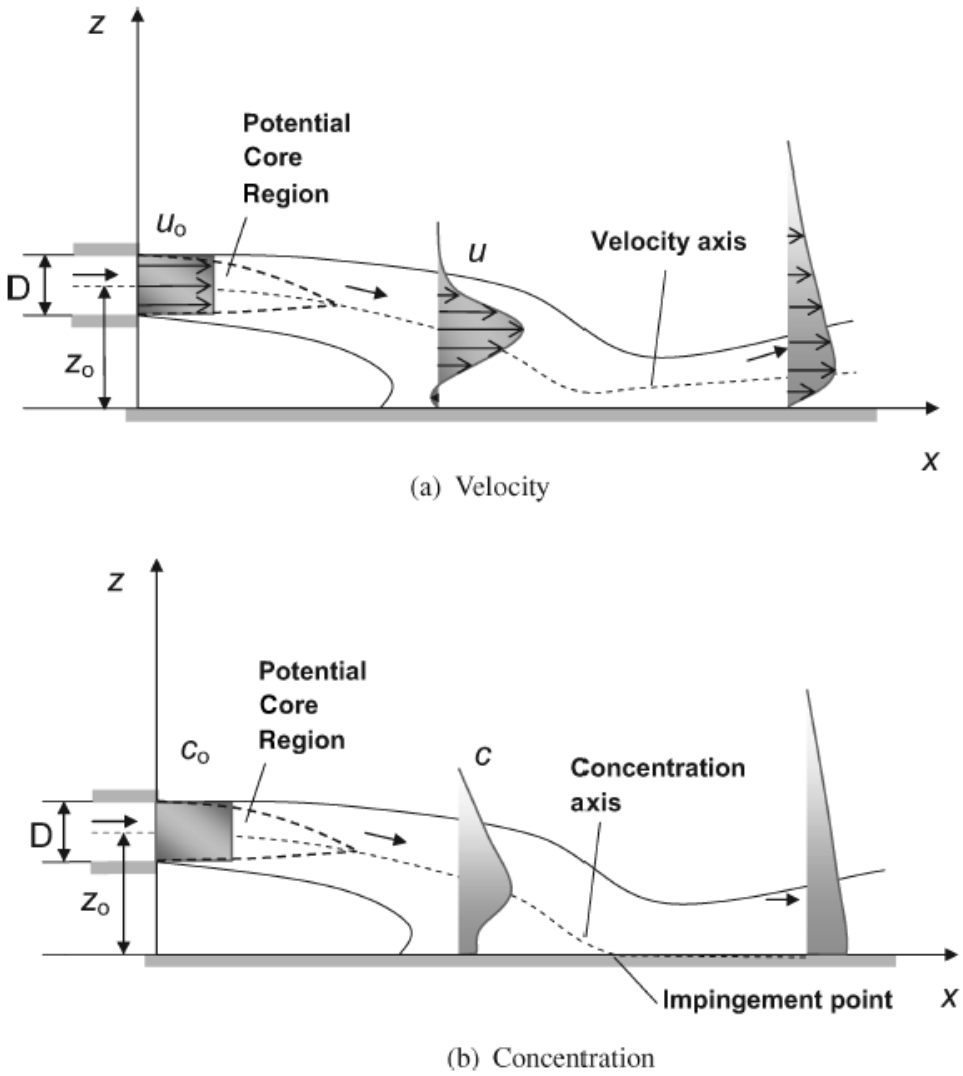

Figure 1.3: A schematic sideview of the velocity and concentration profile development away from the jet. The aim of this research is to find quantitative values for these profiles for different initial concentrations at different distances from the source [28]

Knowledge gaps

The above described situation of a slurry being discharged as a jet, sinking as a plume and spreading out as a turbidity current involves different flow regimes and transitions between these phases. Some of these remain relatively poorly understood.

First of all, most research currently has been done into vertically discharging jets. These result in vertical impingement and circular outflow. Not much is known about the impact of impingement at an angle due to angled or horizontal discharge [24] [18] [9].

Secondly, not much is known about the process at the impingement zone and the development of the turbidity current [24] [18] [26]. The characteristics influencing the transition into a brief wall jet and subsequent turbidity current and the bottom interaction require more research [18].

Thirdly, while it is known that the flow conditions at the diffuser (discharge source) determine the flow conditions at the outflow source, it remains unknown how these are related exactly. Since the flow conditions at the outflow source are the source parameters for the turbidity current, this correlation needs to be understood to be able the determine the influence of the discharge source on spatial and temporal spread of the turbidity current [18] [26].

Finally, it should be mentioned that plume behaviour is currently also simulated using numerical models. This allows for the simulation of sediment plumes with different properties and in different environments. However, these numerical models have to be validated using real data in order to be able to prove that they are correctly modelling the sediment plumes. For this purpose, field measurements and the results of benchmark experiments are required [27].

Conclusion

In this section the knowledge gaps have been identified regarding the influence of the mining operations on the deep-sea environment. It was concluded that there is a lack of knowledge when it comes to the total effect that mainly sediment plumes will have on marine life as well as the recovery rate of the ecosystems. It is however clear that sediment plumes can cause damage to marine life by damaging and blocking respiratory and feeding systems as well as covering them underneath a layer of sediment and hindering communication and hunting. For this reason it seems clear that the spread of sediment as a result from the mining operations should be limited as much as possible [26].

In this section, literature regarding the engineering perspective of deep-sea mining has been analysed. It was found that it is still unclear how changing the flow parameters at the discharge source influences the outflow source and turbidity current that develops after impingement. Also the transition from a plume into a short-lived wall jet and then turbidity current is still poorly understood. It is also clear that the amount of nodules and sediment picked up is mostly predetermined as this is a result of the miners width, velocity and cutting layer depth as well as the pickup efficiency and nodule abundance and sediment properties at the mining site. Combining these findings from both the environmental and engineering aspects of deep-sea mining it has become clear that limiting the spread of the turbidity current is of paramount importance while at the same time it is unclear how this should be achieved.

1.3.2 Research objective

Based on the findings in literature as described in the previous sections it has been concluded that one of the main issues of deep-sea mining is the influence of suspended sediment on marine life and the lack of understanding of the spread of the turbidity current generated by the miner. For this reason, the research objective has been set to the following. The objective is to determine through laboratory measurements how changing the flow parameters at the discharge source, the initial concentration in particular, influences the flow parameters at the outflow source, and subsequently the flow parameters in the turbidity current. The aim is to find a relation between the changing discharge source flow parameters and outflow source parameters. It is believed that when this relation is better understood it can help decrease the sediment flux in the turbidity current generated after impingement. Decreasing the sediment flux in the turbidity current as fast as possible will help in preventing the turbidity current from influencing a large area outside the mining site [14]. This results in the research objective to be defined as follows:

*'Determine how changing the **initial volumetric concentration** of the discharge mixture influences the flow parameters after impingement and sediment flux inside the turbidity current for **a constant sediment flux and discharge velocity** through measurement of velocity and concentration profiles. Subsequently use the findings to **identify how the spread of sediment can be limited** for the benefit of the ecosystems around the mining area.'*

The volumetric concentrations considered in this research are in the range of 1 to 7%, which equals 25 to 175 g/L for the sediment type under consideration. Blue Nodules, which is often taken as an example in this research, assumes a volumetric concentration of 1.3% in their reports. However, they also stated that increasing the concentration might offer advantages when it comes to limiting the plume spread and therefore these higher concentrations require more research. Increasing the density of the discharged mixture is believed to be beneficial for the settling and flocculation rates, and therefore requires further research [27] [5]. For this purpose, experiments will be performed using mixtures with both high and low concentrations in order to compare the different behaviour of their resulting outflow.

1.3.3 Research questions

In order to be able to reach the objective of this research, the following sub-questions have been defined:

- How does the initial concentration influence the impingement location and angle?
- What is the effect of changing the initial concentration on the outflow shape?
- Can the transition from wall jet to turbidity current be observed and if so, what is the effect of increasing the initial concentration on the length-scale at which this transition takes place?
- How does the head velocity change with increasing initial concentration?
- How does increasing the initial concentration influence the concentration profile?
- How does increasing the initial concentration influence the velocity profile?
- How does increasing the initial concentration influence the sediment flux away from the outflow source?

By answering these questions, it is believed by the author that a better understanding can be achieved on the influence of the flow conditions at the discharge source on the emerging turbidity current. This would allow future experiments make better assumptions when splitting the process of the jet to plume to turbidity current process into multiple parts. It also gives insight into how the sediment flux away from the miner can be limited for the benefit of marine life.

1.4 Research methodology

The experiments will be conducted in a modular flume tank. A mixing tank is available in which the slurry can be made and kept at a constant, predetermined concentration. This mixture can then be discharged into the tank at a controllable and constant discharge rate. The resulting jet, plume and turbidity current can be monitored in different ways, as will be explained in the sections below.
In order to answer the research questions the initial concentration will be changed between experiments. As discussed in section 1.3.1, it is assumed that because of the constant miner width and velocity the sediment flux in the discharge flow is also constant. This means that increasing the concentration requires less water to be added to the mixture, resulting in a decrease in mass flow. By changing the concentration and thus mass flow, the initial volume flow Q_0, initial momentum flux M_0 and initial buoyancy flux J_0 are changed between each experiment. The aim of the research is to measure the effect that this changing discharge source has on the outflow source and turbidity current. The discharge velocity will remain constant throughout the experiments in order to make them comparable. In order to achieve a changing mass flow while keeping the discharge velocity constant, 3D printed diffusers with different sizes will be used.

1.4.1 Experimental matrix

Table 1.1 shows the initial experimental matrix. As can be seen, the sediment flux is assumed constant throughout the experiments. This assumption will be explained further in section 2.1. The concentration is the input that will be changed; it will be increased every experiment. As a result of this, the mixture density will also increase since the sediment has a higher density than water. A constant sediment flux combined with an increase in concentration leads to a decrease in added water and hence, a decrease in total mass/volume flow. Since the discharge velocity will be kept constant throughout the experiments this requires a diffuser area that decreases every time the volume flow is decreased.
The chosen concentrations are based on the maximum concentration of 7%. An analysis of available theory showed that 7% is the highest concentration that can be tested in the available setup taking into account all the theoretical and practical limitations. The volumetric concentration of 1% will be tested since this is in the range of concentrations currently mentioned for most deep-sea mining vehicles designs and therefore can serve as a good baseline to which other experiments can be compared. Lastly, the volumetric concentration of 4% was chosen as an intermediate value between the highest and lowest concentration.

Table 1.1: This table shows the intended volume concentrations for the experiments and their corresponding density and concentration (expressed in g/L). For the other parameters this table indicates whether they will decrease or increase in the following experiment. The values of these parameters are yet to be determined.

Experiment	Density [kg/m^3]	Sediment flux [g/s]	Concentration [g/L]	Volume flow [L/s]	Discharge velocity [m/s]	Diffuser area [cm^2]
#3 (C_v = 1%)	1015	Constant	25	Decreases	Constant	Decreases
#2 (C_v = 4%)	1060		100			
#1 (C_v = 7%)	1105		175			

1.4.2 Measurements

The velocity and concentration are two important parameters of the flow. Measured at multiple heights, these can be used to compute the velocity and concentration profiles. By making these profiles at different locations in the current the development of velocity and concentration over distance can be analysed, while at the impingement location the profiles can be used to determine the flow parameters of the outflow source.
The device used to measure the velocity is called an acoustic Doppler velocimeter (ADV). An ADV uses the Doppler shift between transmitted and received signal frequencies to compute the velocity of the particles inside the current [29]. This means that the frequency of the outgoing signal is different from that of the response. This 'shift' in frequency is caused by the movement of the particle and can therefore be used to compute the velocity. Apart from the velocity, ADV probes also measure and record the backscatter intensity, or signal-to-noise ratio (SNR). It is this backscatter that can be used to determine the concentration inside the liquid so that the velocity and concentration profiles can be measured simultaneously [30] [25]. This would allow the velocity and concentration to be measured simultaneously by the same device. The backscatter intensity is dependent on the sediment type, concentration and particle size [31]. For this reason, calibration has to be performed before each experiment in order to find the relation between the backscatter intensity and the concentration for the specific sediment used. This calibration will be performed using samples of known concentration [30] [25] [32]. This way the curve relating the backscatter intensity and concentration can be computed [31].This allows the backscatter intensity measured during experiments to be used to construct the concentration profile of the current [29].

1.4.3 Visual inspection

Cameras will be used to record videos and take pictures. This will allow for further analysis after the experiments. It will show side and top views of the development of the turbidity current and subsequent spread over the table. The recordings can also be used for determining the head velocity of the current. It also allows for comparison between the different experiments by showing the effects of different inputs on the contour, dimensions and outflow shape of the turbidity current.

1.4.4 Scaling

When performing experiments resembling real world operations, it is important that all factors playing a role in the processes are correctly scaled. Two important dimensionless numbers will be discussed in chapter 2. These are the Froude and Reynolds numbers. When scaling, the general thought is that these dimensionless numbers should be equal for the real world and experiment scenarios, the consequences of this will be discussed in chapter 2 as well.

1.5 Assumptions

The experiments will be carried out in a laboratory which means that assumptions and simplifications will have to be made in order to conduct the experiments. The assumptions and simplifications are listed below:

- No salt water. Real mining operations will be conducted in the ocean and thus in a saline environment. The experiments conducted here will be done in tap water. This will need to be taken into account

because it influences the apparent gravity of the mixture as equation (2) shows. Having a different ambient water density therefore results in different buoyancy fluxes for the same volumetric concentration. For this reason calculations will be required to find the concentrations in the lab and the ocean which have the same buoyancy flux and are therefore comparable.

- No initial bottom sediment. The seafloor consists of different types of sediment that may all react differently to an impinging plume. In the experiments the seafloor will be represented by a flat table, which means that the interaction with bottom sediment will initially not be included in this research. The discharged slurry itself will however settle eventually, meaning that during the experiments bottom sediment will develop.
- No ambient current. During mining operations in the deep ocean there will most likely be ambient currents. In the experiments conducted for this experiment the mixture will be discharged into a tank with stagnant water.
- No moving jet. In the experiments conducted for this research the jet will be stationary. The consequence of this is that the mixture will imping the 'seafloor' at a single location throughout the experiment while in reality this location would constantly move forward with the miner. It furthermore means that there will be no wake during the experiments, whereas during mining operations the moving miner would create a wake behind it [8]. This means that the turbulence that is caused by this wake it not taken into account in this research.

  The stationary jet furthermore means that the plume will hit the bottom with a velocity relative to the bottom of non-zero, while for a deep sea mining operations this relative velocity will most likely be equal to zero, as the discharge velocity will be chosen based on the forward velocity of the miner in order to minimize kinetic energy given to the discharges slurry. As a result, the slurry will impinge the bottom with more energy during the experiments, possibly resulting in an overestimation of the spatial spread of the turbidity current.
- Constant sediment flux. The sediment flux and discharge velocity of each experiment will be constant over time. During a real mining operation this most likely would not be the case and deviations will be present.
- Flat bottom only. The experiments will be conducted on a flat table. This means that no sloped surfaces will be taken into account. For the case of seabed equipment this seems acceptable since early assessments have shown that the areas suitable for nodule mining are generally flat with slopes rarely exceeding 2 degrees [1].

1.6 Structure

This first chapter formed an introduction into the background and issues of deep-sea mining operations. It has been identified which aspects play an important role in the adverse effects of sediment plumes. In order to expand the understanding and create an overview of the current development of knowledge of sediment plumes and turbidity current different subjects will be investigated in the following chapter. Chapter 2 will be focussed on the literature study that was conducted in order to gather this background knowledge on different topics that play a role in deep-sea mining and turbidity currents. This literature study is important for the understanding of the processes that will be modelled in the experiments and for analysing the results. Chapter 2 will discuss the following subjects: sediment flux produced by the mining vehicles, buoyant jets, turbulence, gravity currents, turbidity currents, particle settling and the ADV. Chapter 3 will then give an overview of the findings in literature and the discoveries and conclusions of the latest studies. These findings will be combined into conclusions regarding the current state of knowledge on these different subjects. This way it can be identified what aspects and processes of sediment plumes remain not fully understood and as such require more research. The findings in literature will also be used to (partially) answer several the research questions from section 1.3.3.

2. Literature study on horizontal buoyant jet discharges, sediment plumes, turbidity currents and ADVs

This chapter gives the results of the literature study performed to find the current state of knowledge and achieve a better understanding of seafloor miners, negatively buoyant jets, plumes, particle settling and turbidity currents. This knowledge is required in order to fully understand the process of a sediment/water mixture being discharged from the back of a mining vehicle and the subsequent development of a turbidity current, which is necessary for understanding the experiment results and analysis. The literature study furthermore focussed on the scaling required for the experiments as well as the ADV. The goal of the literature study was to expand the knowledge of the author, find the current state of knowledge regarding the subjects discussed and to identify further knowledge gaps.
Section 1 is focussed on the mining vehicle and the parameters determining the near constant sediment flux. After this has been determined, the remaining sections will elaborate on the principles playing a part in the ensuing process. Section 2 focusses on the source of the buoyant jet. Subjects discussed are the diffuser shape, source parameters, characteristic length scales of buoyant jets and the transition into plumes. Section 3 discusses the settling of particles and processes in which this plays a role, being vertical and horizontal slurry transport as well as sedimentation resulting from the horizontal negatively buoyant jet. The impingement of the plume and resulting turbidity current are the subjects of section 4. Finally, section 5 and 6 treat subjects important for experimenting. Section 5 is focussed on the consequences of scaling choices and section 6 investigates the current development regarding velocity and concentration measurement using ADVs. Section 7 will summarize the most important findings from literature and present the resulting conclusions.

2.1 Sediment flux of a deep-sea mining vehicle

In order to perform experiments that sufficiently mimic full-scale operations a realistic estimation of the sediment flux is required. The sediment flux depends on the following aspects: miner width, miner velocity, cutting layer depth, collector efficiency, separator efficiency, nodule abundance and sediment properties. For estimating the sediment flux literature will be used describing miner concept designs. This will mostly be focussed on reports released by Blue Nodules because this company published detailed information regarding their own miner design and production estimations. The sediment flux estimate of a real miner will be scaled down to experiment size.

2.1.1 Miner characteristics influencing sediment intake

The miner as already introduced in sections 1.1 and 1.3 consists of a collector for picking up the nodules, a separator for separating the sediment from the nodules and a flexible hose which connects the miner to the VTS. The miners will have a modular design. This allows for easier maintenance and replacement of parts. During the experiments a diffuser representing one module will be tested. The assumption is made that one module has a width of 1 metre, and therefore this is the width that will be used for scaling and designing the diffusers that will be used in the experiments. More information regarding the scaling and resulting diffuser dimensions can be found in section 2.5. The mining vehicle itself will have a speed of about 0.5 m/s and will most likely be fitted with tracks or Archimedes screws as propulsors [20] [1]. The width of current mining vehicles ranges from 6 to 16 metres and the Blue Nodules miner vehicle will be 16 metres in width [33] [1]. The collector will cover the entire width of the miner in order to prevent the miner from pushing the nodules deeper into the soil with its tracks [34].
The miner will collect the nodules by mechanical or hydraulic means. Both have different characteristics and resulting volume flows. Currently hydraulic dredging seems to be the most effective for commercial mining [1]. The hydraulic collector is also expected to have a much higher total volume flow [7]. Both the mechanical and hydraulic collector will have an expected pickup efficiency of 90% [33]. The hydraulic collector that will most likely be used uses water jets to remove the top layer of the seafloor. This process will cause the sediment to be resuspended after which it will follow the nodules through the collector into the miner. It is after this process that the nodules and sediment will be separated, because the general belief is that the amount of

sediment transported to the surface should be minimised. Minimizing the amount of sediment that is transported to the surface reduces the total required energy for the vertical transport system [8]. The separator efficiency is estimated to be 0.8 for the mechanical collector and 0.9 for the hydraulic collector. Note that these efficiencies are for the separation of the sediment. Also some, mostly smaller, nodules will be separated and discharged with the sediment, although it is expected that this efficiency is rather high [7]. The separated sediment will be disposed at the mining location behind the miner. The discharge velocity at the back of the miner is likely to be equal to the miners forward velocity. This way the least kinetic energy is given to the slurry which is expected to cause the turbidity current to settle faster [21].

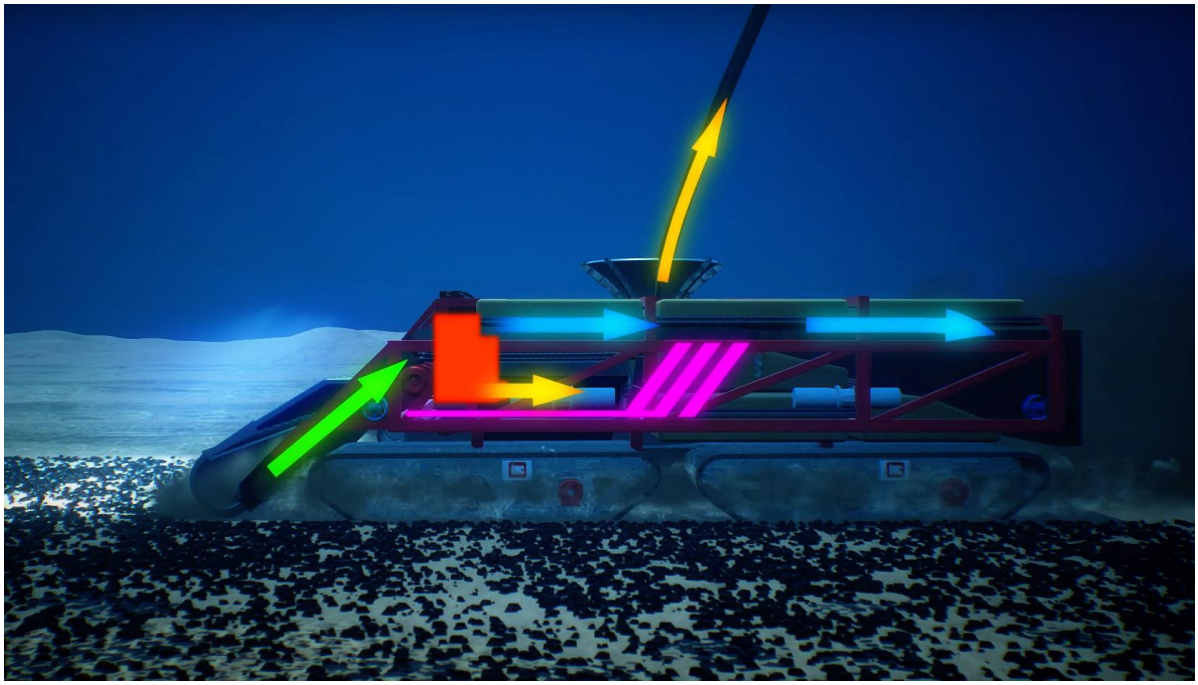

Figure 2.1: Side view of a seafloor miner concept of Blue Nodules. The green arrow shows the inflow of the sand/water/nodules mixture, after which the nodules are send into the riser (yellow arrow) and the water/sediment mixture is discharged at the back (blue arrow). Still from: [35]

2.1.2 Soil properties at the mining sites

Apart from the miner itself, the mining site also influences the sediment flux. While the total volume flow is mostly dependent on the miner width, velocity and cutting layer depth as mentioned previously, the constituents of this mixture depend on the mining site and its soil properties. The number of nodules picked up depends on the nodule abundance, expressed in kg/m^2. The nodule abundance differs per location and estimates of areas receiving interest currently range between 13 and 18 kg/m^2 [11]. The nodule abundance in the area that Blue Nodules has taken interest in is estimated to be 18 kg/m^2 as found in their reports. This is the saturated (wet) density [36]. Another important characteristic is the density of the nodules. Nodules have an in-situ (saturated) density of around 2030 kg/m^3 and a dry density of 1500 kg/m^3 [36]. Combined with the nodule abundance this results in roughly $9 \cdot 10^{-3}$ cubic metres of nodules per square metre of seafloor.
For determining the total sediment being taken in by the miner the soil properties of the sediment are important. The sediment in the mining areas has an in-situ density of 1300 kg/m^3 with the individual sediment particles having a density of around 2500 kg/m^3 [33]. This means that the volume fraction of solids in this sediment is around 0.19 [7].

2.1.3 Resulting sediment flux

As stated in the introduction of this chapter the nodule production and sediment flux of the miner depend on multiple aspects; miner width, minder velocity, cutting layer depth, collector efficiency, separator efficiency, nodule abundance and sediment properties. The miner characteristics and soil properties from the previous 2 sections allow for an estimation of the sediment flux of a typical miner. These can be used to define some more comprehensible factors influencing the production. The first is the mining rate (MR), which is the covered area per second [11]:

$$MR = w * v \quad (4)$$

Where w is the width of the collector in metres and v the forward speed of the miner in m/s. The mining rate can be used to define the nodule production rate which can be defined as follows:

$$P = NA * MR * \eta_c \quad (5)$$

Where NA is the nodule abundance in kg/m^2 and η_c the collector efficiency. The production rate in this equation is the nodule production in kg/s. The total nodule production in m^3/s depends on the density of the nodules. The total volume production of nodules, sediment and water combined would be the mining rate times the cutting layer depth, given in the following equation:

$$Q_t = MR * h \quad (6)$$

Where MR is the aforementioned mining rate and h is the cutting layer depth in metres. This results in the total volumetric production in m^3/s. By using this formula, the total volumetric production of the miner can be calculated. It should be noted however that this is a simplification of reality by assuming that the seafloor is completely flat without irregularities and no nodules are on top of the seabed but all completely buried.
The total nodule production from equation (5) can now be subtracted from the total volumetric production of solids to find the total volumetric production of sediment and water combined. The in-situ density of the sediment from the previous section helps determining the volume fraction of solids in the remaining sediment/water mixture. This way the total sediment flux can be calculated. Because the mining rate will be approximately constant and the cutting depth is assumed constant for simplicity, the total sediment flux of the miner is also assumed to be constant. This is the main reason that for the experiments the sediment flux is kept constant for the different experiments and the total volume flow (sediment + water) is adjusted in order to achieve different concentrations. In reality the sediment flux will be altering over time due to irregularities of the seabed as well as the distribution of the nodules.

2.2 Jets and plumes

The unwanted sediment picked up by the mining vehicle will be discharged behind it as a jet, as was discussed in section 2.1. The slurry will be discharged from a diffuser and this will initially result in a negatively buoyant jet with a density higher than that of the ambient water. The term buoyant jet refers to a flow in which one fluid is driven into another fluid by its momentum and buoyancy, and a negatively buoyant jet is a jet of which the fluid has a density higher than the ambient fluid [18]. In this report the focus will be on these negatively buoyant jets because the slurry discharged by deep sea mining vehicles will have a density which is higher than the ambient water density. Hereafter the negatively buoyant jet will simply be referred to as ‘buoyant jet’. The jets origin is the diffuser at the back of the miner, and this results in a source of both momentum and buoyancy. A source of momentum results in jet like flow, while a source of buoyancy results in plume like flow [22]. This results in the slurry initially resembling a jet, after which it transitions into a plume and starts to settle.

2.2.1 *Diffuser characteristics*

A diffuser is a device causing the expansion of flow and is designed to reduce velocity (kinetic energy) and increase the pressure head of the flow [37] [38]. This is achieved by the diffuser having a larger cross section than the duct or pipeline it receives its flow from. This increase in cross section combined with and equivalent volume flow leads to a reduction in velocity. By examining Bernoulli’s principle one finds that this also leads to an increase in static pressure [39]. A common issue in designing diffusers is how to prevent flow separation or boundary-layer separation from happening, which can occur when flow is slowing down. This can happen for example after passing through a widening section as happens in a diffuser, or when flow crosses the thickest

part of the wing of an aircraft. Flow separation arises when the flow in or around a body is decelerated and the pressure is increased. When this happens, kinetic energy is transformed into pressure. Because the flow also loses kinetic energy due to friction with the wall, particles in the boundary layer lose even more kinetic energy. This then leads to the flow near the wall not being able to advance further into the diffuser because it cannot sustain enough momentum to advance into areas of increased pressure. This leads to standstill or reversal of the flow [40] [41]. As a result of this the flow does not completely fill the widening diffuser, but only a smaller part of it. Because of this it is possible that the flow leaving the diffuser resembles a jet with a much smaller cross section than the diffuser actually has. This results in the flow velocity not being decelerated as intended [39] [42].

Flow separation is directly related to the divergence angle of the diffuser [40]. A too large divergence angle leads to flow separation inducing backflow and increased losses [38]. Schlichting found that it is possible to control flow separation by decreasing the divergence angle [40]. As a result of different researches, stability maps have been created for the flow patterns in diffusers. One study providing these charts for the selection of diffuser dimensions was performed by Reneau et. al [42], which focused on straight, two-dimensional diffusers. They mention that the 'no flow separation' regime is confined to small divergence angles and area ratios. Their charts show allowable divergence angles op to 20 degrees. Despite this high value that is allowable only for diffusers of very small area ratios, most other sources, including Reneau, Johnston and Kline themselves, name a total divergence angle of 7 degrees as the divergence angle offering maximum effectiveness [43] [39] [42].

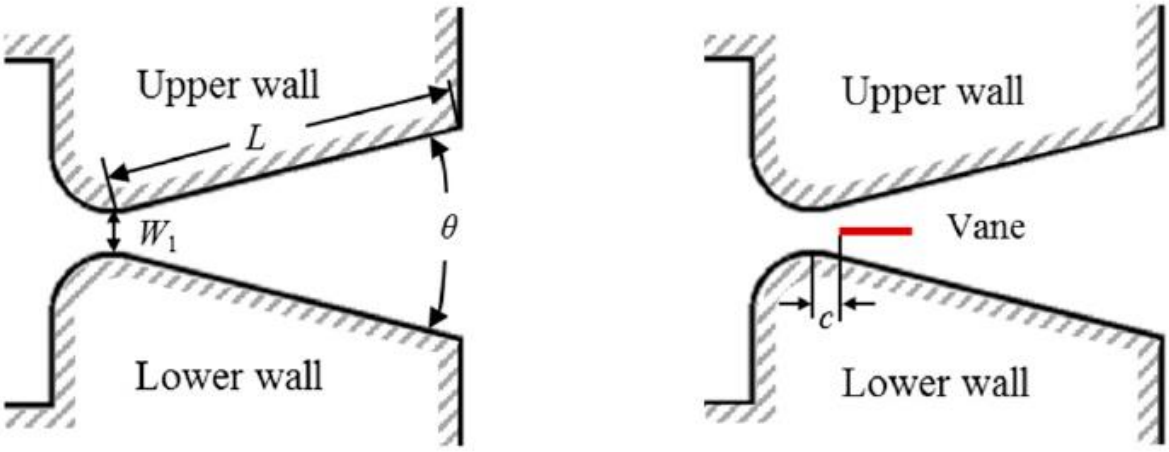

Figure 2.2: Side view of a simplified diffuser. The unvaned diffuser (left) shows how the divergence angle is defined. The vaned diffuser (right) shows schematically where a vane would be located inside a diffuser [44]

It should be taken into account however that a small divergence angle leads to longer diffuser length which might be undesirable. For the experiments for this research, this results in more of the flume tank length being used for the diffuser-pipeline system leaving less length for the jet and sedimentation length, as will be elaborated in section 2.3.2. Also in industrial applications it is sometimes not possible to achieve small divergence angles because space is scarce. If this leads to flow separation the losses in the diffuser increase and the desired pressure recovery decreases [39] [44]. This leads to the need to be able to predict the largest allowable divergence angle of the diffuser in order to ensure no flow separation as well as the shortest possible diffuser length. In order to achieve large divergence angles without flow separation, diffusers can be fitted with a number of active and passive devices to control to flow. Among these are honeycomb structures, mesh screens and vanes [39]. For this research the focus will be on vaned diffusers.
An extensive study into the effect of vanes on flow separation in diffusers which laid the basis for many successive studies including that of Meng et. al was done by Moore and Kline [45]. They performed experiments to determine the effect of the shape, spacing, length and location of vanes. Moore and Kline found that flat vanes proved easier to produce, install and adjust than ones with an air foil profile and were therefore favoured. For the spacing of the vanes, they found that using equally spaced vanes offered the best solutions. For diffusers with total divergence angles of 30 and 45 degrees they found that installing enough diffusers to decrease each individual divergence angle of each passage to 7.5 degrees was enough to eliminate flow

separation altogether. For the length of the vanes no minimum has been found, although it is suspected to very short vanes might not fully prevent flow separation. It was found however that having vanes over the entire diffuser length of the diffuser is less effective than shorter vanes. These vanes effectively split the diffuser into two or more diffuser of equal dimensions. Lastly, regarding the placement of the vanes, Moore and Kline found that the leading edge should be placed slightly downstream of the diffuser throat. A similar investigation into flat vanes was performed by Cochran and Kline [46]. Their work was an extension of the work of Moore and Kline [45], and was found to be in agreement with the latter.
How well a diffuser manages to achieve the wanted pressure recovery can be measured with the pressure recovery coefficient, C_{pr}. A higher value means a more efficient pressure recovery. In one test with a diffuser with a 30 degrees divergence angle, Moore and Kline [45] recorded an increase of the recovery factor from 0.18 to 0.74. Cochran and Kline [46] notice that for diffusers with divergence angles up to 42 degrees the pressure recovery obtained using vanes is equal or greater than the obtained values for vaneless diffusers with optimal divergence angles. A more recent study on applying vanes in order to redirect flow and improve the pressure recovery showed promising results as well. Numerical simulations and experimental results showed a C_{pr} improvement of about 43% [44]. The results of their simulation are in agreement with the findings of Cochran and Kline [46]. While more research is required into the exact shape and dimensions of the vanes, splitter vanes are proven to be able to prevent flow separation at higher divergence angles which in term enables shorter diffuser lengths [45].

2.2.2 Source parameters of buoyant jets

The main parameters influencing the jet, and therefore the subsequent turbidity current, are the dynamic characteristics of the discharge source, which for this research will be a diffuser. The main parameters of the flow at the discharge source are the initial volume flow Q_0, initial momentum flux M_0 and initial buoyancy flux J_0. These are given by the following equations [22]:

$$Q_0 = A_0 U_0, \qquad M_0 = U_0 Q_0, \qquad J_0 = g_0' Q_0 \tag{7}$$

Where A_0 is the cross-sectional area of the discharge source, U_0 is the exit velocity of the jet and g'_0 is the apparent gravity, given by the following equation:

$$g_0' = g \frac{(\rho_a - \rho_0)}{\rho_a} \tag{8}$$

Where ρ_a is the density of the ambient water and ρ_0 is the density of the discharged slurry. Further note that $\rho_0 > \rho_a$, so g'_0 and hence J_0 is negative. The above results in a jet discharge with an initial momentum and buoyancy flux that can both be expressed as a function of the total volume flow and initial discharge density, which are controllable inputs for both experiments and real mining machines. It leads to the conclusion that the discharge parameters are dependent on the cross-sectional area of the diffuser, total volume flow, volume concentration of solids in the slurry and the ambient water density.
Chowdhury and Testik mention the same parameters in their 2014 review paper on buoyant jet discharges, but expand the discharge parameters by also mentioning the densimetric Froude number, which is defined as:

$$Fr = \frac{U_0}{\sqrt{g' D}} \tag{9}$$

Where D is the characteristic dimension of the discharge source. The densimetric Froude number gives the ratio of inertia to gravity. At high ratios the flow typically has a high velocity and enough turbulence to keep the solids in suspension. Studies found that a decrease in the densimetric Froude number results in buoyancy dominating over momentum, resulting in the jet/plume impinging the seafloor at a larger angle with respect to

the horizontal, thus influencing the outflow shape of the turbidity current [23]. This will further be discussed in section 2.4.

2.2.3 *Characteristic length scales of buoyant jets*

The source parameters from the previous section can be used to construct several characteristic length scales which give insight into the ratio of certain source and flow parameters such as momentum, buoyancy and settling velocity. These ratios can subsequently be used to determine the length scale at which their respective influence is dominant.
Jirka and Domeker [22] mention seven characteristic length scale definitions which are useful for an analysis of a momentum jet. For this research three of these length scales are judged to be important. These are the 'discharge (geometric) length scale', L_Q, the 'jet/plume transition length scale', L_M, and the 'jet/cross-flow length scale', L_m. These three length scales are given by the following equations [22]:

$$L_Q = \frac{Q_0}{M_0^{1/2}}, \qquad L_M = \frac{M_0^{3/4}}{J_0^{1/2}}, \qquad L_m = \frac{M_0^{1/2}}{u_a} \tag{10}$$

Where u_a is velocity. Jirka and Domeker [22] define the length scales as follows. L_Q is 'a measure of initial jet size and the length of its establishment'. L_M is 'a measure of the distance at which the transition from jet behaviour to plume behaviour takes place in a stagnant uniform ambient'. Lastly, L_m is defined as 'the distance of transverse jet penetration beyond which the jet is strongly deflected by the cross-flow' [22]. Similar to the discharge parameters, Chowdhury and Testik [18] make mention of these same length scales and describe them as 'important to determine the buoyant jet behaviour' [18].

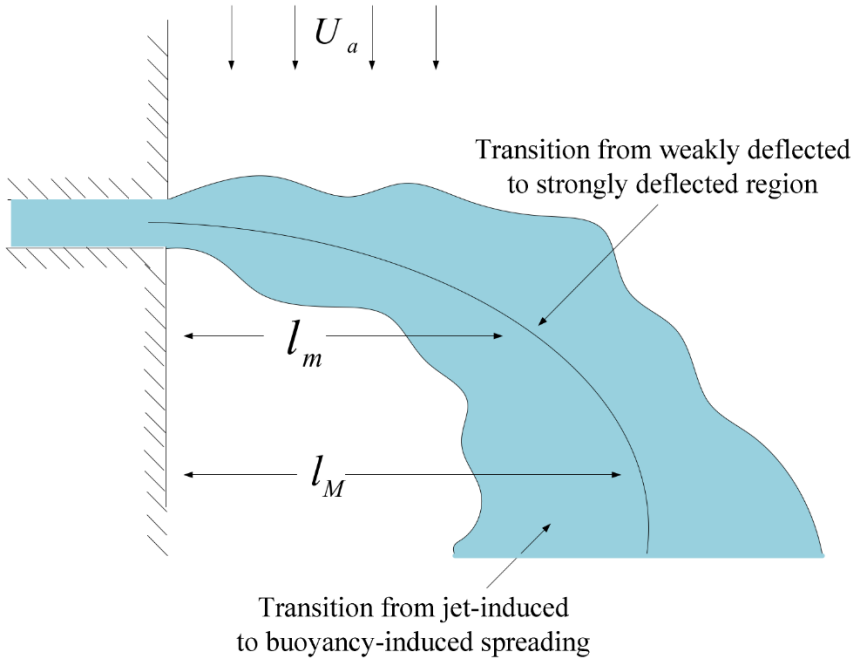

Figure 2.3: Side view of a horizontal negatively buoyant jet with a density higher than the ambient. This figure shows the length scales L_m and L_M as were discussed above. As shown, after a distance L_M the transition is made from momentum to buoyancy dominated flow [47]

The jet/plume transition length scale (L_M) can also be defined as the 'momentum-buoyancy length scale'. This dimension gives the length scale at which the transition from momentum dominated flow to buoyancy dominated flow takes place. For $x < L_M$, momentum dominates and the flow shows pure jet behaviour. For $x > L_M$, buoyancy becomes more dominant and the jet eventually behaves like a plume [48]. Depending on the buoyancy of the jet (positive or negative), the plume is deflected either upwards towards the surface, or downwards towards the bottom. After impinging the surface or bottom, the flow continues as a gravity current. The jet/plume transition length is also mentioned in another study from 2021. This study confirms that beyond

this distance the flow is significantly dominated by buoyancy instead of momentum. It is furthermore suggested that beyond this distance the solids start to settle, while for low concentrations ($C_V < 1\%$) this happens at distances much shorter than L_M [49].
The jet/crossflow length scale (L_m) is also referred to as the 'settling-momentum length scale' in other literature. It gives the ratio of momentum-induced velocity to settling velocity and the equation shows that this length scale depends on the ratio of jet momentum and settling velocity [50] [48]. When $x < L_m$, the sediment transport is dominated by the horizontal jet flow. For $x > L_m$, the sediment transport is dominated by its vertical settling velocity and deposition occurs [50].
Lee, Li and Lee [51] use this length scale for determining the distance at which sedimentation takes place. In their paper, L_m is given by the same equation (momentum flux over velocity) but is called the 'sedimentation length scale'. The settling velocity of the particles involved is used for the velocity in the numerator of the equation, meaning that in their research L_m measures the ratio of momentum-induced velocity to settling velocity. This way the length can be used to determine the distance at which sediment start to fall out and settles. A larger value of L_m means that the particles will settle further away from the source [51]. Because of this it is an important parameter to consider for experiments with sediment-laden jets. The flume tanks in which these experiments are usually conducted are of finite length and it is therefore necessary that the sediment settles before this length is reached. If not, the sediment may be reflected from the back of the tank and influence measurements. In their research they found that sediment first starts to settle at $x/L_m = 0.2\text{-}0.3$, with a peak in sediment deposition rate just before a distance of $x = L_m$. They also observed that at $x = 2.4L_m$ 90% of the sediment mass had settled [51]. Their findings regarding the settling rate of particles in a horizontal sediment-laden momentum jet will be further discussed in section 2.3, which covers the settling of particles.

2.2.4 *The jet to plume transition process*

As a jet advances away from the source its momentum decreases due to decreasing velocity. At the same time buoyancy is preserved. This causes the ratio of momentum and buoyancy to change, resulting in a shift from momentum-driven to buoyancy-driven flow [23]. During the momentum-driven stage the flow exhibits jet-like behaviour, while during the buoyancy-driven stage the flow shows plume-like behaviour. Which one dominates is determined by their ratio through the jet/plume transition length scale, as introduced in the previous section. Initially this jet/plume transition length scale, L_M, can be used to determine the distance at which the transition from jet-like to plume-like behaviour takes place. This definition holds for a stagnant uniform ambient [22]. This distance determines the length of the jet region, beyond which the flow becomes more similar to a plume, falling downward towards the bottom under the influence of gravity [24]. During this phase, buoyancy dominates and the flow impinges on the bottom resembling a plume [23]. Typically there is a region where the flow transitions from a momentum-driven jet to a buoyancy-driven plume before becoming entirely plume-like [52].

The jet/plume transition length scale has been used in different researches to predict the location of the transition region from jet to plume-like flow with more precision. This is typically done by experimentally searching for the dimensionless values of z/L_M and x/L_M where this happens, where z is the vertical distance from the source and x the horizontal distance. This can be used to determine the distance where the transition happens and whether the buoyant jet impinges the bottom as a jet or plume [23]. Researches have been focusing on both vertical and horizontal buoyant jets.
For vertical buoyant jets, experiments showed that for $z/L_M < 1$ the flow behaves like a pure jet and for $z/L_M > 5$ like a pure plume. For $1 < z/L_M < 5$ a transition takes place. [52]. This is in accordance with the definition of L_M, which is said to indicate the transition from a pure jet to plume-like flow. This particular research showed that the transition length equals 4 times L_M after which the flow continues as a pure plume.
For horizontal jets buoyancy first becomes dominant at $x/L_M = 1.5$. Initially the flow behaves jet-like in the horizontal part of the flow, because at this stage momentum is still dominant. Between $1.5 < x/L_M < 5$ the transition takes place from jet to plume, causing the buoyant jet to divert downwards. The flow is considered pure plume-like when $x/L_M > 5$ or $z/L_M > 2$. At this stage the buoyancy flux which acts in the vertical direction has become dominant. This vertical plume-like flow is also characterised by an increase in turbulence when compared to the horizontal jet-like flow. A plume furthermore tends to widen when compared to the jet due to

entrainment of the ambient fluid. This entrainment causes the volume flow, Q, to increase along the length of the buoyant jet. The entrainment of ambient fluid furthermore leads to dilution of the mixture, which decreases the density and thus the apparent gravity. Because the volume flow increases while the apparent gravity decreases the buoyancy flux form equation (7) tends to remain constant [53] [23].

A source parameter that was not yet given in section 2.2.2 is the Richardson number. This is a dimensionless parameter indicating whether the initial flow leaving the source is more jet-like or plume-like. The Richardson number is given by the following equation [52]:

$$R_0 = \frac{Q_0 J_0^{1/2}}{M_0^{5/4}} = \frac{L_Q}{L_M} \tag{11}$$

As shown, it is the ratio of the discharge and jet/plume transition length scales. Equations (7) and (10) show that a large momentum-to-buoyancy ratio leads to small Richardson numbers while the Richardson number increases to above unity for a buoyancy dominated flow. A very small Richardson number therefore indicates initial jet-like behaviour while around unity it indicates plume-like flow leaving the source [53].

2.3 Settling of particles

An important subject for almost every dredging and deep-sea mining research or operation is the settling of particles. Sand, clay, silt and rock all have densities higher than that of water and subsequently sink to the bottom. Being able to predict the (terminal) settling velocity of one or multiple particles is therefore of upmost importance. The settling velocity determines the sedimentation length of a jet, the minimal mixture velocity for vertical transport and the minimal limit of horizontal transport called the deposition limit velocity. When designing pipelines for transporting mixtures of water and solids it is therefore important to first understand the factors influencing a particles' settling velocity, and subsequently be able to apply this to jet and pipeline design.

2.3.1 *Particle settling theory*

This section will discuss the existing theories regarding particle settling as well as well-known equations for calculating the settling velocity for solids. It is divided into the settling of individual particles, the settling of multiple particles resulting in what is referred to as hindered settling, and flocculation. Flocculation is the agglomeration of particles leading to a larger particle, thus increasing their collective settling velocity.

Individual settling

The settling velocity of particles is based on the equilibrium of forces. When a solid with a density higher than water is brought in suspension, it will sink and settle on the bottom after a while. This sinking motion induces a drag force. A solid submerged in a stagnant liquid has 3 forces working on it in total, being gravity, buoyancy and the aforementioned drag. Gravity works in the downwards direction, while the drag force and buoyancy are directed upwards. Buoyancy and gravity can also be combined into what is called apparent gravity (directed downwards). The velocities calculated by the equations for settling velocity are the terminal settling velocities. Different analytical models for calculating this velocity have been proposed in the past. They typically depend on the densities of the water and solids, diameter of the solid, drag coefficient and shape factor. The drag coefficient itself depends on the particle Reynolds number.

Miedema [54] describes different models for calculating the terminal settling velocity. This was done for laminar flow ($d < 0.1$ mm) by Stokes, for the transition zone (0.01 mm $< d < 1.0$ mm) by Budryck and for turbulent flow ($d > 1.0$ mm) by Rittinger. Another equation was proposed by Ruby and Zanke (1977), also for the transitional zone. Figure 2.4 shows the settling velocity in mm/s as a function of particle size in mm. The figure clearly shows overestimations of the settling velocities of very small particles by the model of Rittinger and of large particles by Stokes. Budryck and Zanke both show the same course, with the model of Zanke predicting settling velocities just above those of Budryck.

Hindered settling

The previous theory is applicable on individual settling particles. When multiple particles are present in a liquid, they will influence each other which results in what is referred to as hindered settling. When a particle settles it induces the upwards motion of water. This is caused by the particle taking up the volume that was occupied by the water before. This water has to move somewhere and as a result fills the gap left behind by the moving particle. If multiple particles are present in a volume these together cause an upwards flow of water, which increases the relative velocity of the particles. This increase in velocity increases the drag force and subsequently reduces the settling velocity of the particles. This is called hindered settling. Richardson and Zaki (1954) developed Equation (12) for calculating this hindered settling velocity. This equation is applicable for volume concentrations up to 30%, and depends on the volume concentration and particle Reynolds number [54]:

$$v_{th} = v_t(1 - C_v)^{\beta} \tag{12}$$

Here V_{th} is the hindered settling velocity and β an exponent which depends on the particle Reynolds number. Multiple researchers developed their own equation for calculating β. Richardson and Zaki developed a model with equations and values for β for different ranges of the particle Reynolds number. Their model however does not give a smooth curve and other researchers came up with equations for calculating β for the entire range or particle Reynolds numbers. Rowe (1987) approximated β by the following equation which closely resembles the values as found by Richardson and Zaki:

$$\beta = \frac{4.7 + 0.41 * Re_p^{0.75}}{1 + 0.175 * Re_p^{0.75}} \tag{13}$$

Equation (12) shows that the hindered settling velocity decreases with volumetric concentration. This indicates that altering the initial volumetric concentration of the discharged mixture influences the average settling velocity of the particles and therefore plays a role in the settling rate of a sediment plume.

Flocculation

Flocculation is the process where cohesive particles aggregate to form a larger, heavier particle. Sand is non-cohesive and as such does not flocculate while in suspension. Clay however is cohesive, and as a result forms particles that are larger than the individual clay particles in suspension. Because these flocs are larger and settling velocity increases with diameter as Figure 2.4 shows, this results in larger settling velocities. Because of this, flocculation is believed to reduce the spread of sediment plumes created in deep-sea mining processes [27] [55]. This has led to different researches focussing on the effect of flocculation and ways to stimulate it. Because flocculation in general does not occur in mixtures of non-cohesive material, most modelling approaches separate sand and clay, assuming that no interactions happen between to two. However, experiments focussed on mud-sand mixtures have shown strong evidence for flocculation of these mixed sediments. [56].

Spearman et. al [9] conducted field experiments on which they concluded that the extent of dispersion of sediment plumes is significantly reduced by the effects of flocculation. The experiments, conducted 300 nautical miles from the Canary Islands, involved the formation of actual sediment plumes and concentration measurements at predetermined distances away from the plume origin. The experiment results also posed the basis for validation of numerical models. They mention that earlier studies already noted the importance of flocculation on the settling process of particles and how this reduces the extent of the dispersion. However, these experiments did not assess this effect and used the settling velocities of individual particles which are smaller than the settling velocities of larger flocculated particles. They note that the settling velocities measured in their field experiments are (in most cases) higher than the individual settling velocities of particles. Increasing the mixture density at the miner outlet is expected to be beneficial for settling rates. An increased density and thus volumetric concentration of particles is expected to increase the flocculation rate. This is expected to increase the settling rate by resulting in larger particles [27]. For this reason, it is interesting to

research the effect of higher concentrations than the 1.3% as mentioned in the Blue Nodules reports. Gillard et. al [5] studied this influence of concentration on flocculation. They found that increasing concentration and/or shear rate improved that flocculation efficiency. Discharge simulations involving concentrations between 35 and 500 mg/L showed that the higher concentrations promote the growth of flocs. They also suggest that a further increase in sediment concentration in order to combine the effects of hindered settling and flocculation should be investigated.

Flocculation will not be taken into account during the experiments for this research. The sediment that will be used consists of glass spheres which are non-cohesive. For that reason, only hindered settling will play a role in the settling process. For future research it would be interesting to deploy a sediment mix of sand and clay in salt water to be able to experiment on the influence of flocculation on the settling process of a sediment plume.

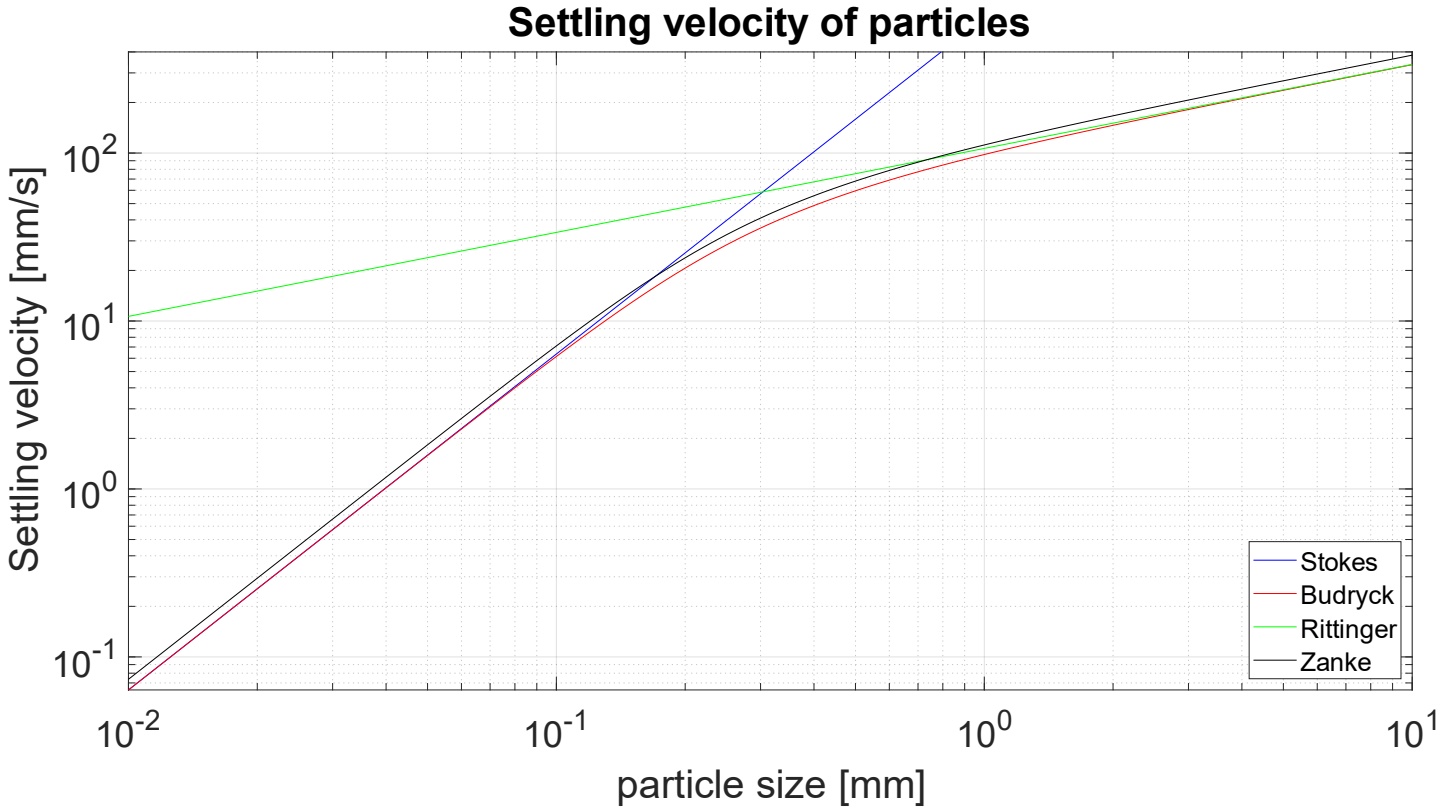

Figure 2.4: Settling velocity of particles for a given diameter according to different models

2.3.2 Sediment deposition rate

In the study of Lee, Li and Lee [51] that has already been mentioned in section 2.2.3, the sediment deposition along the length of the jet is measured. Based on this, a semiempirical equation for the distribution of the deposition rate along the length of the jet could be made. This resulted in the following function [51]:

$$\frac{F_s L_m}{Q_o C_0} = Ae^{-B\left[\ln\left(C\frac{x}{L_m}\right)\right]^2} \tag{14}$$

Where F_s is the sediment deposition rate in g/m/s. The left-hand side in this equation is referred to as the jet sediment flux. The equation involves the three constants A, B and C, which depend on the sediment type [50]. In their 2013 study, Lee, Li and Lee [51] use sand and spherical glass particles. They use the following values for A, B and C: A = 0.702, B = 1.5 and C = 1.19. Since the experiments conducted for this research also make use of spherical glass particles of similar size, the same values will be used for calculations. The function describes the sediment deposition rate based on L_m, Q_0 and C_0. The function can be adjusted to give the sediment deposition rate F_s as a function of x/L_m. If for a jet all the input values are known, the sediment

deposition rate can be plotted as a function of distance from the source in metres. This plot can be used to determine the required length for the jet and whether the modular tank offers enough space for the whole jet to settle before the end of the tank is reached. If not, the sediment might reflect and interfere with the measurements.

2.4 Gravity currents

The previous three sections focussed on how the sediment enters the miner, how the sediment is discharged from the miner as a buoyant jet and transforms into a plume, and on the settling of particles which happens in pipelines as well as in the water column. These sections showed how the mixture forms a sediment plume that sinks to the bottom, due to it having a higher density than the ambient water. This results in the next step of the process, being the impingement of the plume with the bottom and its subsequent spread in the shape of a gravity current. A gravity current is a current driven by density differences between two fluids. This density difference can have different causes, for example differences in temperature or salinity. This difference in density induces a buoyancy flux which is the driving force behind the current. In the case of a discharged slurry the emerging gravity current is called a turbidity current, in which the density difference is caused by the suspended particles [57]. This causes turbidity currents to have complicated fluid dynamics. The dependency of the driving buoyancy force on the suspended solids concentration causes the turbidity current to be influenced by sediment suspension and deposition as well as stratification [58].
The impingement of the discharged fluid and subsequent spread as a turbidity current are among the least understood processes of buoyant jet discharges. Combined with the need for accurate predictions of the consequences of deep-sea mining operations required for ISA licensing, as discussed in section 1.2, this leads to impingement and turbidity currents being among the most important subjects requiring research regarding deep-sea mining.

2.4.1 *Impingement of a plume*

Impingement is the collision of the plume with a surface. In the case of a sinking plume this surface is usually the bottom. Plumes with a density lower than the ambient, for example due to lower salinity or a higher temperature, typically rise and impinge the free surface after which they will also radially spread [18]. For this study the focus will be on plumes with densities higher than the ambient water because the experiments will involve only mixtures with higher densities as well. Impingement occurs at different distances from the source, at different angles (with respect to the horizontal) and with different flow types, with flow showing either plume-like or jet-like behaviour. Especially the angle and the flow type determine the outflow shape. After impingement the flow is redirected along the bottom. This initially happens as a wall jet, after which the height of the current grows and the flow transforms into a gravity current. The subsequent radial spread occurs as a turbidity current, driven by the density differences between the discharged fluid and the ambient water [18]. The transition in the flow that occurs when a plume impinges the bottom and starts spreading as a turbidity current is considered one of the most complicated parts of the flow [59].
The impingement angle depends on the distance given to the buoyant jet before impingement and the ratio of momentum and buoyancy. If buoyancy dominates a vertical or near vertical impingement is more likely. This angle influences the outflow shape of the turbidity current, causing differences between vertical impingement and impingement at an angle. Vertically impinging plumes tend to spread in an axisymmetric, circular way, while angled impingement leads to a non-symmetrical spread of the turbidity current. This causes a more pronounced downstream spreading [23].
As was shown in section 2.2.4, a jet transitions into a plume after a certain distance, depending on the ratio of momentum and buoyancy. It was shown that after a certain distance the flow shows pure plume-like behaviour, resulting in the flow impinging on the bottom resembling a plume. It is however also possible for the buoyant jet to remain in the jet-like behaviour region and imping on the bottom resembling a jet. Being able to predict the regime of the impinging flow is important as it influences the behaviour of the outflowing turbidity current. If the buoyant jet still resembles a jet at impingement this indicates that momentum is still dominant which causes the wall jet to extend for a larger distance, resulting in a larger spread of the turbidity current. Plume-

like impingement on the other hand results in a smaller wall jet and a less energetic spread of the outflowing turbidity current [18].
The impingement point can be assigned the same source parameters as were seen for the discharge source, being a momentum flux, buoyancy flux and volume flow. The buoyancy flux in this case is preserved, but the other parameters are different than the initial ones [23]. The impingement point is also referred to as the outflow source. The source parameters at this location determine the flow dynamics of the outflowing gravity current, just like the source parameters at the diffuser determine the behaviour of the buoyant jet. Studies have found that the distance of the impingement location from the source depends on the value of L_M and the discharge angle. The impingement still requires additional research however, as the impingement point (outflow source) parameters and outflow shape is still poorly understood [18]. Especially the correlation between the discharge source and outflow source parameters is not fully understood as well as the influence of the outflow source parameters on the properties of the turbidity current [23].

2.4.2 Turbidity currents

As explained above, the outflow after impingement first behaves like a wall jet after developing into a turbidity current. This current is being generated from the impingement point and the source parameters at this location determine the properties of the turbidity current [18]. Apart from the buoyancy flux the source parameters at the outflow source are different that those at the discharge source.
The driving force in any gravity current is the buoyancy flux. Turbidity currents differ from other types of gravity currents because they are not buoyancy-conserving. This is due to the fact that in most other gravity currents the density difference, which causes the buoyancy flux, is a result of temperature difference or solvents. For turbidity currents on the other hand the density difference is caused by suspended particles. The deposition or resuspension of this particles results in the density difference with the ambient not being constant. Typically as the turbidity current propagates, its buoyancy flux gradually decreases due to the settling particles inside the current [18]. Lippert and Woods [60] conducted experiments on the sedimentation front in particle-driven gravity currents. In their research they define a variable S, which is the ratio of the initial current velocity and the settling velocity of the particles. Their study showed that for larger values of S the total distance reached by the turbidity current as well as the height of the current increases. They also found that for smaller values of S the height of the turbidity current gradually decreases away from the source. This indicates that sedimentation takes place and results in a decreasing volume, momentum and buoyancy flux. The decrease of the buoyancy flux causes the turbidity current to decelerate which in turn leads to the flow not being able to keep the sediment in suspension [58]. Therefore, on a flat bottom turbidity currents eventually stop flowing due to them being net depositional. Once all the particles have settled meaning that the buoyancy driving force is exhausted, the turbidity current disappears [49] [25].

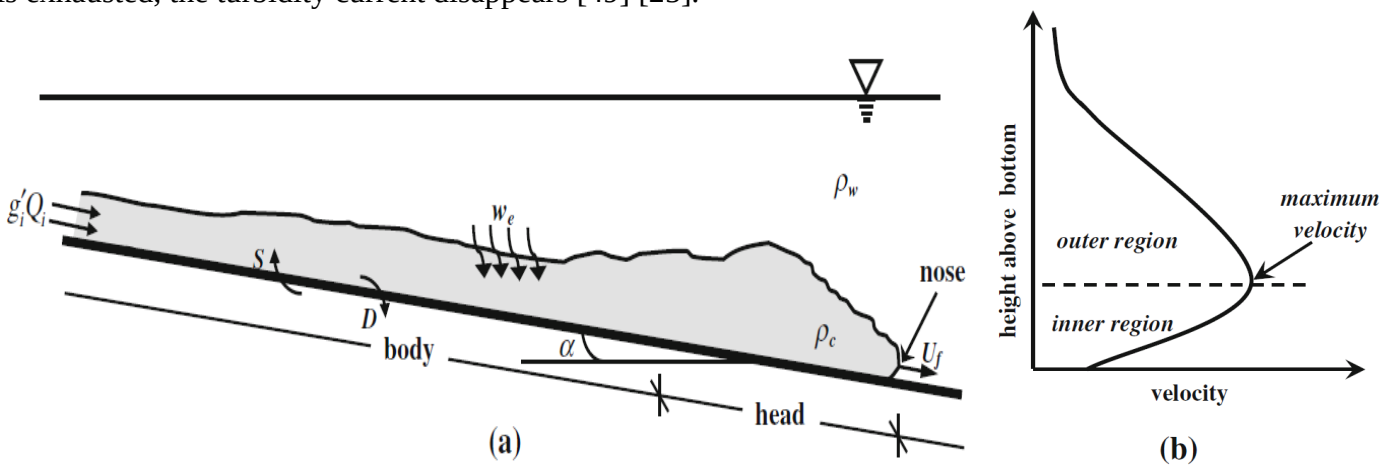

Figure 2.5: Figure (s) shows a schematic overview of a turbidity current divided in a body and head. It shows the entrainment of ambient water and well as the suspension and sedimentation happening inside the body. Figure (b) shows the typical velocity profile of a turbidity currents head [18]

The structure of a turbidity current can be divided into two parts. The front part of the current is called the head and is characterised by having a larger thickness than the body of the current, as well as being highly

turbulent [61]. The shape of the head is related to the friction between the current and the bottom. This leads to the shape of the current head being dependent on the roughness of the bottom, as well as the forward most point of the head usually being just above the bed [18]. The velocity profiles usually show this same maximum just above the bottom due to the lowest layer of the turbidity current experiencing friction from the bottom [58]. The velocity decreases away from the bottom and is usually negative (opposite to the current direction) right above the flow, which is caused by a counter current [25]. The concentration profile is largely dependent on the ratio of particle settling velocity and the upward directed velocity components of eddies. Due to the high turbulence in the current head the concentration distribution in the head is vertically well-mixed. In the body of the current the concentration increases towards the bottom being more stratified due to the settling of particles and limited influence of turbulence [61].
Multiple studies have been performed investigating the time-averaged concentration and velocity profiles of turbidity currents to find the influence of different factors on their shape. Wells and Dorrell [58] summarised this in their 2021 review paper. Here it is mentioned that the height of the velocity maximum is dependent on both drag and the densimetric Froude number. A decrease of the Froude number, which is caused by a decrease in velocity, is assumed to lead to an increase of the height of the velocity maximum. At the same time however a lower velocity leads to more stratification, which is known to lower the height of the velocity maximum. In order to prove this, multiple studies have shown that the velocity profiles of gravity currents with a nonzero settling velocity, i.e. turbidity currents, show a lower height of the velocity maximum than gravity currents with a zero settling velocity.
Tilston et. al [57] aimed on finding the influence of grain size on the velocity and sediment concentration profiles of turbidity currents. They performed multiple experiments with changing grain sizes and (mass) concentrations. Their measurements showed that smaller particles sizes result in less stratification, especially at higher concentrations. They also found that for smaller solids the velocity maximum is positioned higher above the bed, which leads to a reduction of internal shear and mixing. The measurements of velocity profiles also showed an increase in the velocity profiles with concentration. Their reporting however does not state anything about the input of the experiments. Because of this it remains unclear if higher concentrations were achieved by increasing the sediment flux or by decreasing the total volume flow. The author of this report beliefs however, based on the description of the experimental setup, that Tilston et. al [57] achieved the concentration increase by increasing the sediment flux and as such also increased the buoyancy flux at the source. Since the buoyancy flux is the driving force of a turbidity current, increasing this would logically results in an increase in velocity. This choice is important for analysing the results. For the experiments that will be conducted for the study of this report, the sediment flux and discharge velocity will be equal for all experiments. As a result of this, the buoyancy flux is equal for all experiments and only the momentum flux changes. The volume flow decreases for increasing volumetric concentrations, which results in the momentum flux to decrease. As a result of this, the momentum-buoyancy ratio will decrease for higher concentrations without altering the buoyancy flux. The results of the experiments that will be conducted for this report will therefore show the consequence of keeping this driving force constant while changing the momentum-buoyancy ratio by decreasing the momentum flux, which possibly decreases the velocity and spatial spread of the turbidity current [18].

Turbidity currents transport sediment by resuspending sediment from the bottom and depositing it further downstream. The amount of sediment picked up and deposited depends on the particle sizes and the current velocity. A higher velocity increases that maximum concentration capacity of suspended solids. As a result of this a turbidity current propagating over an erodible bed with a high velocity may entrain many particles. This way the buoyancy flux is maintained or even increased, causing the turbidity current to accelerate [18]. In the aforementioned research of Lippert and Woods [60] this was also found. They observed that for large values of S (> 40) resuspension of particles occurs causing the turbidity current to propagate for longer distances. For deep-sea mining applications the ratio S should be kept below the critical value at which resuspension becomes relevant in order to limit the spread of the turbidity current. This means keeping the initial current velocity as low as possible which is in line with the philosophy to discharge the sediment with a relative velocity of zero to the seabed. Apart from the initial discharge velocity the current velocity also depends on the outflow source. As explained in the previous section however this correlation is still poorly

understood. Finding the influence of initial volumetric concentration at the source on the current velocity after impingement could therefore be useful in achieving a better understanding of this connection. Also limiting the discharge height could help in reducing the initial current velocity.
Apart from the roughness of the bottom and initial current velocity, also the slope of the bottom affects the propagation of the turbidity current. This subject will only be described briefly since sloped bottoms are not expected to influence turbidity currents resulting from nodule mining operations too much. This is due to the deep-ocean floor being generally flat and the mining sites only having very small inclination angles [6]. Sloped bottoms influence turbidity currents by resulting in outflow shapes which are all directed downslope. Even initial axisymmetric outflow shapes become directed downstream under the influence of gravity. Researches have shown that increased slope angles increase sediment transport and reduce deposition. This causes the turbidity currents to propagate for larger distances [18]. Sloped beds may also result in self-accelerating turbidity currents. Under the influence of gravity these currents propagate downslope and increase in velocity. Because of this, they experience an increase in suspended sediment concentration entrained from the bed. This increases the buoyancy flux which further accelerates the turbidity current. This results in both velocity and concentration increasing in a feedback loop [25] [58]. This leads to the capability of turbidity currents to transport large amounts of sediment over large distances [62].

2.5 Scaling

When performing experiments resembling real world operations, it is important that all factors playing a role in the simulated process are correctly scaled. Two important dimensionless numbers will be discussed below. These are the Froude and Reynolds numbers. When scaling, the general thought is that these dimensionless numbers should be equal for the real world and experiment scenarios. The consequences of this will be discussed at the end of section 2.5.1. The Froude number can also be used to determine whether the flow is critical or subcritical, which will be elaborated in section 2.5.1. The Reynolds number is used for determining whether the flow regime is laminar or turbulent.
Based on the dimensionless numbers the allowable scale can be determined and the dimensions of the experiment diffusers can be calculated. However, apart from the dimensionless numbers it is also important to look at the factors influencing the flow characteristics inside the scaled pipeline and diffuser. For this reason, literature regarding the rheology of mixtures and the influence of the aspect ratio of a duct on the flow characteristics has been studied. These subjects will be discussed in sections 2.5.2 and 2.5.3 respectively.

2.5.1 Non-dimensional numbers

Froude

The Froude number gives the ratio of inertial to gravitational forces [63]. Therefore it is an indication of the influence that gravity has on the flow. It is given by the following equation:

$$Fr = \frac{U}{\sqrt{gL}} \tag{15}$$

Where U is the velocity, g is the gravitational constant and L is the characteristic dimension. For circular pipeline flow of a mixture, the Froude number is usually rewritten as [23]:

$$Fr = \frac{U}{\sqrt{g'D}} \tag{16}$$

Where D is the inner diameter of the pipe. It should further be noted that not the regular gravitational constant should be used for g, but rather the reduced gravity g', which can be calculated using equation (2). The resulting Froude number is the densimetric Froude number. This results in the Froude number that should be used for the flow of mixtures with density differences. Since the diameter of the experimental discharge pipes will be smaller than that used in real life, it follows from equation (16) that the flow velocity should be scaled

by the square root of the geometrical scaling, given that the reduced gravity of both the real and experimental mixtures is equal. This means that in order to keep de Froude number constant, both velocity and diameter should be decreased in scaled experiments.
It should also be noted that the diffusers and pipe used for the experiments will have a rectangular cross section. This means that the equation needs another change in order to be applicable to a rectangular duct. For this purpose, the length scale in the equation, which was the pipeline diameter before, is replace by the hydraulic depth. The hydraulic depth is the cross section area divided by the top width of the duct, which for a rectangular duct equals the overall width, resulting in the hydraulic depth being equal to the duct height [64]. The resulting equation is the following:

$$Fr = \frac{U}{\sqrt{g'h}} \tag{17}$$

Furthermore, the reduced gravity is not the same for the experiments and real-world operations and should therefore also be taken into account. Equation (2) shows that the apparent gravity depends on the density of both the mixture and ambient fluid. Since the real operations will be conducted at several kilometres depth in the ocean, the ambient water density will be larger than during the experiments. The deep-ocean waters are saline, near freezing temperature and compressed under the high pressure at these great depths. This results in an ambient water density that is higher than the 1000 kg/m^3 for the tap water at room temperature that will be used in the experiments. Equation (2) shows that this results in the apparent gravity being larger for the experiments than it would be at the seafloor. This would lead to a smaller Froude number for the experiments if the hydraulic depth and discharge velocity are scaled by a given value and its square root respectively. In order to keep the Froude number constant, either the velocity has to be larger, or the hydraulic depth smaller than it would be for a constant apparent gravity.
As mentioned in the section introduction, the densimetric Froude number can also be used to determine whether the flow is subcritical or supercritical. Flow is said to be subcritical for Fr < 1, critical for Fr = 1 and supercritical for Fr > 1. Supercritical flow is flow in which inertia dominates over gravity. Velocities are high and the flow is typically turbulent. Because of this turbulence, concentration distributions become uniform and the slurry is accepted as homogeneous [65]. Also, the high velocities allow the solids to stay in suspension and prevent a two-layer flow from developing [66]. To conclude, the experimental duct should be designed such that supercritical flow is ensured and the mixture enters the modular tank as a homogeneous mixture.

Reynolds

The Reynolds number relates the inertial forces and the viscous forces within a fluid [63]. It is given by the following equation:

$$Re = \frac{\rho UL}{\mu} = \frac{UL}{\nu} \tag{18}$$

Where U is the velocity, L is the characteristic dimension, ρ is the density, μ is the dynamic viscosity and ν is the kinematic viscosity. For pipeline flow, the equation is usually rewritten such that the diameter is used as the characteristic dimension, resulting in:

$$Re = \frac{UD}{\nu} \tag{19}$$

The above equation is the commonly used equation for circular pipes. When calculating the Reynolds number for differently shaped pipes and ducts, the hydraulic diameter should be used as the characteristic dimension. The hydraulic diameter is given by the following equation [67]:

$$D_H = \frac{4 * A}{P} \tag{20}$$

Where A is the cross-sectional area of the pipeline or duct and P is the wetted perimeter of the cross section. This is the area of the cross section that is in touch with the flow. For circular pipes this means that total circumference, for rectangular ducts it equals twice the height and twice the width. If h is the height of the duct and w the width, this can be rewritten to:

$$D_H = \frac{4hw}{2(h+w)} = \frac{2hw}{h+w} \tag{21}$$

The Reynolds number for a rectangular duct and diffusers than becomes:

$$Re = \frac{2Uhw}{v(h+w)} \tag{22}$$

This leads to the conclusion that in order to keep the Reynolds number constant, it is required to increase the velocity when the dimensions are reduced. Since the dimensions in the experiments will be smaller than the real-world size, this would mean a significant increase in velocity. Furthermore, since the experiments will be performed in tap water at room temperature and the real operations will take place at the ocean floor at near freezing temperatures, the viscosity of the fluid will not be the same for both situations as it is known that this changes with temperature.
For most experiments the flow is desired to be fully turbulent. For pipeline flow it is generally accepted that flow is laminar up to the value of 2000-2300. Between this lower boundary and 4000, the flow is said to be in the transition phase from laminar to fully turbulent. For Re > 4000, pipeline flow is said to be fully turbulent [68].

2.5.2 *Rheology of the mixture*

Rheology investigates the deformation and flow of matter. The rheology of a fluid describes the interrelation between force, deformation and time. For fluids a distinction can be made between Newtonian and non-Newtonian fluids. Newtonian fluids are fluid that follow Newton's law of viscosity, meaning that shear rate and shear stress are linearly correlated and pass through the origin. This also means that the viscosity of a Newtonian fluid is constant and independent of shear rate. For these fluids the shear stress is equal to the product of the viscosity and the shear rate. Non-Newtonian fluids do not follow Newton's law of viscosity. This means that their viscosity is not constant and changes with shear rate. As a result of this, their flow curve is non-linear [69]. Non-Newtonian behaviour can be exhibited in a number of ways including shear thinning (viscosity decreases with shear rate), shear-thickening (viscosity increases with shear rate) and Bingham plastics, which have a linear shear rate/shear strain relation but does not pass through the origin. In the cases of shear thinning and shear thickening this also means that viscosity respectively decreases and increases with shear rate.
Water is an example of a Newtonian fluid. Other examples of Newtonian fluids are air, oil or alcohol. Under normal conditions these fluids behave like Newtonian fluids and thus follow Newton's law of viscosity. However, the presence of solids changes the way the surrounding fluid deforms and influences the viscosity of the mixture. This can cause their behaviour to change from Newtonian to non-Newtonian at higher solid concentrations [70] [71]. The solids concentration at which the transition from Newtonian to non-Newtonian behaviour happens can be caused by the particle size, composition and particle interactions of the dissolved or suspended solids [72]. Non-Newtonian behaviour is commonly seen by small, cohesive particles present in high concentrations like clay and silt in mining tailings. Sand-clay mixtures already show non-Newtonian behaviour at volume concentrations of 5%. Mixtures with clay mostly show the behaviour of the aforementioned Bingham fluids. At very high volume concentrations this behaviour switches to that of the Herschel-Bulkley model [73] [74].
For this research it is important to know that the solids involved (spherical glass particles) are non-cohesive. For this purpose, literature regarding research into the Newtonian to non-Newtonian transition for water with

suspended, non-cohesive solids was reviewed. Studies describe different solids being used for experimenting. One research was focussed on coal-water. Coal pieces were crushed and grinded before being added to the water. It was observed that the fluid started to exhibit non-Newtonian behaviour at solids concentrations of over 30% [71]. According to a research from the Institute of Hydrodynamics in Prague, a sand slurry starts to exhibit non-Newtonian behaviour at volume concentrations exceeding 20% [72]. Another experiment involving sand particles showed that at concentrations of 9% viscosity is independent of shear rate. At higher concentrations that were tested, being 20, 30 and 40%, viscosity increased with shear rate, thus exhibiting non-Newtonian behaviour [70]. The experiments also showed that the particle size has to be taken into account if the concentration at which the transition takes places needs to be determined with more precision.
To conclude, researches involving solid, non-cohesive particles show that the transition from Newtonian to non-Newtonian takes place between 20 and 30% solids concentration. This will be taken into account when determining the maximum solids concentration to be used during the experiments. It was also found that mixtures involving both sand and clay already show non-Newtonian behaviour at much lower concentrations. While this will not be taken into account in the experiments, it is important to understand that for real mining operations the sediment might also involve clay which will alter the rheology of the mixture. This means that the results of the experiments for this research are not fully applicable to these situations and more research is required involving cohesive material.

2.5.3 *Influence of diffuser aspect ratio*

The diffusers used during the experiments will differ in size as has been explained in section 1.4. Each experiment with an increased solids concentration requires a smaller diffuser area in order to achieve the same discharge velocity for a smaller volume flow. This smaller area can be achieved by decreasing either the height of the diffuser, the width or both.
From a realistic point of view, it can be argued that only the height of the diffuser should be decreased. Since the width of any miner vehicle and module will be determined by the required production, this dimension would not be changed in favour of the sediment plume behaviour [34]. As a result of this, only the height of the diffuser would be decreased in order to decrease the total diffuser area. However, changing only the height of the diffuser would change the aspect ratio (AR) of the diffuser which influences the flow characteristics. Therefore, an analysis of literature regarding this topic is required in order to determine the effects of changing the aspect ratio and to assess whether changing the aspect ratio influences the comparability of the results.

Different researches described in literature show the effects of changing the aspect ratio of ducts or open channels. Firstly, the friction factor increases with aspect ratio, especially as the AR goes over 1 [75] [76]. This increases the total head loss, requiring more power to be delivered to the system, and thus requiring more energy. During a deep-sea mining operation this is something that should be taken into account as it increases energy consumption. However, for the experiments conducted for this research the focus is not on energy consumption, making the increase in friction factor negligible as long as the mixture flow is not affected. It was also found that ducts with a high aspect ratio show a strong increase in velocity away from the wall, and that the velocity profile is strongly dependent on the aspect ratio below an aspect ratio of 12 [77] [76].
Researchers also found that the aspect ratio has a significant effect on the characteristics of the secondary currents inside ducts [78]. Secondary currents are circulations in a flow that are formed because of velocity components in a direction transverse to the flow [79]. They affect the distribution of turbulence intensities across a duct as well as the mean flow characteristics [77]. According to a research from the Laboratory of Hydraulics in Zurich, results showed that smaller aspect ratios lead to an increase in strength of the secondary currents. This causes ‘a significant change in flow patterns’ according to the published paper [80]. A 2016 Swedish research on the effect of secondary currents on particle transport showed that the turbulence caused by the secondary currents also significantly affects the flow characteristics. The secondary currents change the cross-sectional particle distribution and mean velocity. It is also shown that the velocity profile is significantly different in the case of increasing aspect ratios [81]. However, a 2019 study showed that an increase in aspect ratio has no great influence on the stream-wise turbulence intensity pattern and vertical turbulence intensity distribution [82] It should furthermore be noted that the influence of the aspect ratio on flow parameters decreases with the aspect ratio. Results from different studies show that the effect of the aspect ratio on flow

properties is high for low aspect ratios but becomes less significant for higher aspect ratios. This is shown in results of Vinuesa et. al [83] and Noorani et. al [81]. The study of Vinuesa et. al [83] shows that the aspect ratio has little effect on the percentage of shear force acting on the side walls between the tested aspect ratios of 7 and 10, whereas it heavily increases as the aspect ratio is decreased. Noorani e t. al [81] show that the aspect ratio has high influence on the particle concentration in the viscous sublayer between the tested aspect ratio values of 1 and 3, but has little influence above these values.
Apart from the secondary currents, turbulence and particle distribution inside a duct, the aspect ratio also has influence on the jet. The aspect ratio of the diffuser might impact the flow of the jet/plume once parted from the diffuser. A 1992 study found that near field mixing of a jet originating from a rectangular diffuser increases with the aspect ratio. However, in the far field the mixing and turbulence intensity showed not much variation between different aspect ratios [84]. This was supported by a 2008 study which showed that the spread of a jet originating from a rectangular diffuser shows no clear difference at distances more than 10-20 times the equivalent hydraulic diameter away from the diffuser [85]. The equivalent hydraulic diameter of a rectangular diffuser or duct is defined as the diameter of a circular pipe that would result in the same pressure loss for equal flow. Different equations for calculating this equivalent diameter have been found empirically in the past. One study from 2008 found that the equivalent diameter equals 0.955 times the hydraulic diameter, D_H, as defined in section 2.5.1 [86]. These studies thus show that rectangular jets with a different aspect ratio show difference in turbulence intensity in the near field, but no clear difference in spread in the far field.

2.6 Acoustic Doppler velocimeter

The velocity and concentration profiles are important parameters of turbidity currents. As the literature reviewed in section 2.4.2 showed, these profiles can be used to visualise the effects of changing a turbidity currents input parameters, as well as their development over distance. Therefore being able to accurately determine these profiles is an important aspect of experimenting with turbidity currents. In order to create velocity and concentration profiles the velocity and concentration need to be measured at multiple heights. Combined these measurements make up the velocity and concentration profiles. By performing these measurements at different locations in the flow (different distances from the source), the development of velocity and concentration inside turbidity currents can be recorded. Especially around the impingement location the profiles together with visual recording can help acquire a much better understanding of the transition from an impinging plume to a turbidity current.
A device that is commonly used to measure the velocity is called an acoustic Doppler velocimeter. These devices are capable of recording the instantaneous velocity at a single point. To do this, an ADV uses the Doppler shift between the transmitted and received signal frequencies to compute the velocities of particles in the flow. Apart from the velocity, ADV probes also measure and record the backscatter signal, or signal-to-noise ratio [29]. It is this backscatter that can be used to determine the concentration inside the liquid. This can be done by coupling the backscatter signal that the ADV measures to a known solids concentrations through calibration [31]. If this is done for multiple known concentrations a calibration curve can be made that can be used to determine the concentration based on measured backscatter signals in mixtures of unknown concentration. This way the velocity and concentration profiles can be measured simultaneously [30] [25].

2.6.1 *Velocity measurement*

An ADV uses the Doppler shift between transmitted and received signal frequencies to compute the velocity of the particles inside the current [29]. This means that the frequency of the outgoing signal is different from that of the response. This shift in frequency is caused by the movement of the particle and can therefore be used to compute the velocity. This way ADV probes have the ability to measure the 3D flow velocity in liquids [30]. An important assumption that is made here is that the fluid flows at the same velocity as the suspended sediment [31]. The ADV measures the velocity for a predetermined period of time at multiple heights. These measurements are then averaged and combined. This way a velocity profile of a specific location in the current can be constructed. This profile gives the average current velocity over the height of the current.

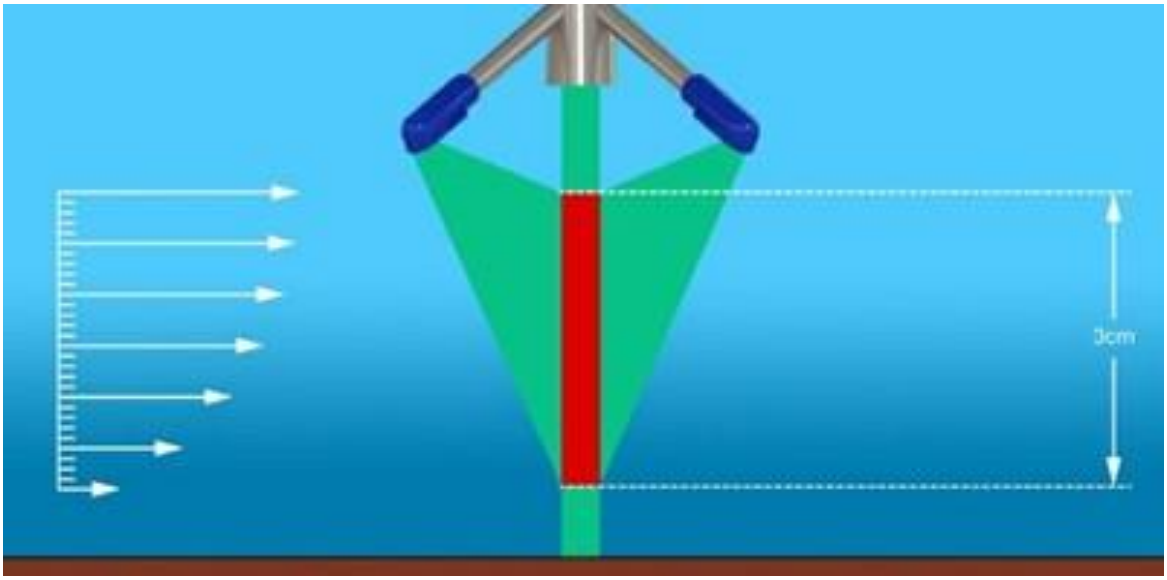

Figure 2.6: Schematic showing the 30 mm profile over which the Nortek Vectrino Profiler measures velocity. This ADV measures at 1 mm intervals, meaning that with one measurement a 30 mm profile of both the velocity and SNR can be created [87]

2.6.2 Concentration measurement

An advantage of using the ADV for both velocity and concentration measurements is that this way the velocity and concentration profile can be simultaneously recorded which allows them to be constructed for the exact same flow conditions and location. ADVs do not directly measure the concentration, however. It is the backscatter that the ADV measures that can be used for predicting the concentration. The backscatter combined with the noise gives the signal-to-noise ratio (SNR). Noise is the ambient sound which is not related to the ADV. Through calibration a correlation can be found between the SNR of an ADV and the suspended solids concentration [30].
The backscatter intensity is dependent on the sediment type, concentration and particle size [31]. For this reason, calibration has to be performed before each experiment in order to find the relation between the backscatter signal and the concentration for the specific sediment type and size used. This calibration is performed using samples of known concentration [30] [88] [25]. Through this calibration, the curve relating the backscatter and concentration can be computed, which allows the backscatter that is measured during experiments to be used to construct the concentration profile of the current [29]. Furthermore, the sediment size must be known in order to use the backscatter signal for estimating the concentration profile [31].
As the backscatter intensity depends on sediment type, size and concentration as well as properties of the ambient water and the signal of the ADV, finding the relation between the backscatter and concentration of a specific set of sediment requires careful preparations, and multiple studies have pointed out that this method does have its limitations. Experiments have shown that at a certain concentration, dependent on the sediment type and size used, the backscatter starts to decline for increasing concentration values [30] [18]. As a result of this, the relation between the backscatter and the concentration is no longer log-linear. This decreases the accuracy of the concentration profiles determined by the backscatter [31]. Furthermore, Hosseini et. al [31] found that above sediment concentrations of 50 g/L acoustic waves are almost completely absorbed in the flow. This resulted in the ADV not being able to operate properly at higher concentrations.

In order to get a better understanding of the limiting factors for using ADVs to predict the suspended sediment concentration, it is important to understand what factors influence the backscatter signal as received by the ADV. The backscatter signal that is received by the ADV is the backscatter intensity minus transmission losses. The backscatter intensity is the backscatter signal in the direct vicinity of the particles. On the way back to the ADV this backscatter experiences losses which cause the backscatter as received by the ADV to be less than the original backscatter intensity [30]. The backscatter intensity increases with the total scattering cross-section. The total scattering cross-section increases with concentration as well as particle size. As a result of this, the backscatter intensity is a function of particles type, size and concentration. This means that calibration

curves are only applicable for determining concentrations in mixtures with a similar sediment type and particle size [30] [31].
Based on the above, it is clear that the backscatter intensity increases with both concentration and particle size. As stated earlier however, there is a difference between the backscatter signal as received by the ADV and the backscatter intensity in the vicinity of the particle. This difference is caused by transmission losses of the signal on the way towards and back from the particle. Transmission losses are due to scattering and absorption of the signal. Together this is referred to as attenuation. Scattering is mainly dependent on the distance between the ADV and the particle. Absorption depends on the properties of the sediment and the ambient water, and can be expressed with the absorption coefficient, α. This coefficient is found by combining the water absorption coefficient (α_w) and the particle absorption coefficient (α_s). The water absorption coefficient is dependent on temperature, depth and salinity and can therefore be assumed to be constant during experiments. The particle absorption coefficient is not, as it increases with concentration [30] [32]. Apart from concentration, the particle absorption coefficient is also dependent on the particle size and type. Small particles are dominated by viscous absorption, whereas larger particles (> 20 um) are dominated by scattering absorption [88]. Lastly, particle absorption is also related to the signal frequency. This can be explained by looking at what is called Rayleigh scattering, one of the principles behind ADVs. This occurs when the diameter of the particle is much smaller than the wavelength of the emitted signal. In the case of Rayleigh scattering, the energy transfer towards the particle can be neglected. This is checked by inspecting the product of the wave number of the signal and the radius of the particle, resulting in the following condition [30]:

$$k * r < 1 \tag{23}$$

Where 'k' is the wave number and 'r' the particle radius. The wave number is given by $k = 2\pi/\lambda$, where lambda is the wavelength. Because the wavelength decreases with increasing frequency, the wave number increases with frequency, causing the left-hand side of equation (23) to increase with frequency as well. This shows that the condition for Rayleigh scattering is more likely to be exceeded for higher frequency, indicating that absorption by particles increases with the emitted signal frequency.
It has now been shown that both the backscatter intensity and transmission losses increase with concentration. Because of this, the calibration curves giving the correlation between the backscatter signal and the concentration all show the following same trajectory. For low concentrations of up to 1 g/L, earlier research has shown that there is a log-linear relation between the backscatter signal and the concentration. For higher concentrations however, this relation becomes non-linear. Eventually the curve flattens, before a decrease in the backscatter signal is measured for increasing concentrations [31]. This maximum and subsequent decrease in the backscatter signal for increasing concentration can be explained by looking at the influence of concentration on both the backscatter intensity and the transmission losses. As explained above, the backscatter intensity increases with the amount of particles, causing an increase in the backscatter signal. However, increasing the particle concentration also leads to an increase of the sound absorption caused by the particles, which causes a decrease of the backscatter signal. While at low concentrations (< 1 g/L) the particle absorption can be neglected and only water absorption plays a role, the absorption by particles increases for higher concentrations. As a result, the increase in absorption by the particles overcomes the increase in backscatter intensity at a certain concentration. This causes the total backscatter signal as received by the ADV to decrease with concentration once that concentration is exceeded [30]. Because of this, most current models relating the backscatter signal to concentration only work for concentrations up to 50 g/L. For higher concentrations absorption becomes too dominant causing the signal to become too weak. This resulting curve also means that for every backscatter signal value there are two possible concentration values: one before, and one after the curve's maximum. During experiments this has to be taken into consideration as it could lead to uncertainty as to which concentration is being measured. Based on initial concentration, knowledge of concentration decay in turbidity currents and visual observation it should however be able to determine the right value.
One of the recent models that correlates the backscatter signal and the suspended solids concentration was presented by Chmiel et. al [30]. It is based on the acoustic sonar theory and has proven to work for several sediment types. They extended the widely used log-linear relation between the SNR and concentration to a higher concentration regime than usual, leading to their model being applicable up to 50 g/L, which amounts

to a volume concentration of 2%. The model of Chmiel et. al [30] has been applied to different sediment types, both natural and artificial. Their results have shown that the relation between the backscatter intensity and sediment concentration is dependent on the type of sediment.
Another study performed by Sahin et. al [88] focussed on the effect of sediment size on the applicability of the SNR measurement of ADVs for determining the concentration of suspended solids. Here it was found that the absorption losses depend in both sediment size and concentration. They too concluded that it becomes especially important at high concentrations. They furthermore found that for the smaller particle sizes used in their research the acoustic attenuation is higher than for larger particles. Their results already show a decrease in the backscatter signal at values of 0.3 and 0.8 g/L for certain particle sizes, far below those reported by Chmiel et. al [30]. This difference can be explained by looking at the size of the used sediments. The sediment experimented with by Chmiel et. al [30] had d_{50} values between 9 and 20 µm. Sahin et. al [88] however experimented with larger particles sizes, having a d_{50} ranging between 77 and 428 µm. The plot shown in Figure 2.7 shows the difference in scattering cross-section for these sizes. This figure shows that especially between solid sizes of about 70 and 220 µm the particle absorption is very dominant. The particle sizes experimented with by Sahin et. al [88] lie exactly in this range of high absorption. For the range of particle sizes used by Chmiel et. al [30] the absorption is very low, explaining why their results show an increasing backscatter signal up to higher concentration values. This explains why the backscatter signal increases up to higher concentration values in the study of Chmiel et. al [30]. A similar plot as seen in Figure 2.7 can also be created for different concentrations, as Sahin et. al [88] have done. Figure 2.8 shows that the absorption coefficient increases with concentration in accordance with equation (24).
The study of Sahin et. al [88] shows that for certain ranges of particle diameters, the correlation between backscatter signal and concentration can only be used up to a very limited concentration. In order to increase the concentration range for these particle diameters, they provide a set of equations that can be used for correcting the backscatter signal for transmission losses. By calculating the transmission losses and adding them to the backscatter signal received by the ADV, the calibration curve can be extended and will show a log-linear relation up to higher concentration values. After the backscatter signal was corrected for water and sediment attenuation, it was found that the backscatter-concentration relation increases for all particle sizes used in their study.

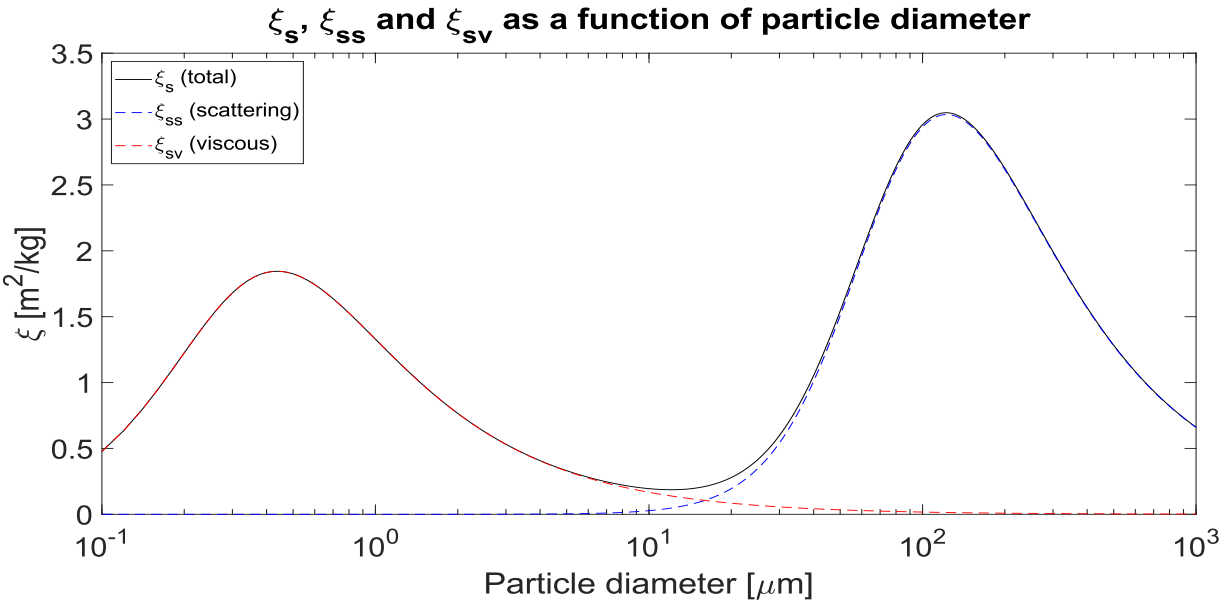

Figure 2.7: Particle attenuation coefficient for different particle diameters. The values given here are for an acoustic frequency of 10 MHz. The red and blue dashed lines show the influence of viscous scattering for smaller diameters and of solid scattering for larger diameters respectively.

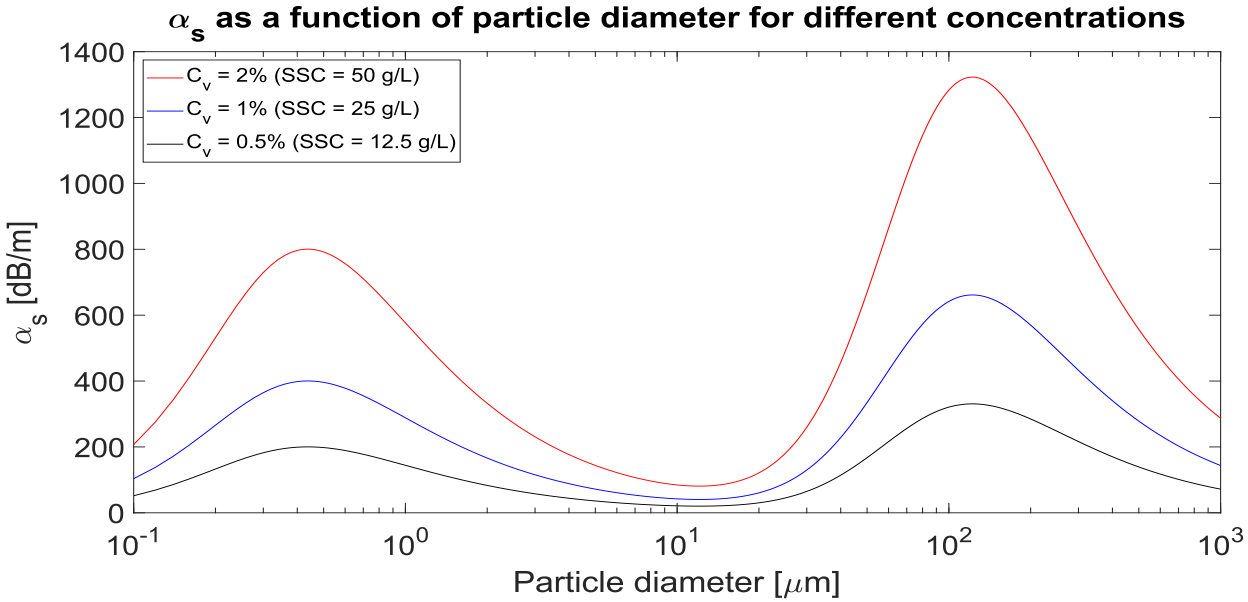

Figure 2.8: Particle absorption coefficient for different particle diameters. The different curves show the effect of increasing concentration on absorption.

Another solution to decrease the absorption losses and thereby increase the concentration range for which the concentration can be measured can be found by inspecting Rayleigh scattering and the equations for calculating the absorption by particles. Thorne et. al [89] give a set of equation to formulate the attenuation (scattering and absorption) of particles. These equations can be used to calculate the normalised total scattering. Sahin et. al [88] used several data sets of suspensions to fit these equations. The result is the following equation for the particle absorption coefficient:

$$\alpha_s = 8.68 * \xi_s * SSC \tag{24}$$

Here 8.68 is a conversion factor to dB, ξ_p is the particle attenuation coefficient in m^2/kg and SSC is the suspended solids concentration in g/L. The particle attenuation coefficient can be calculated with the following equation:

$$\xi_s = \frac{3\chi_s}{4r\rho_s} \tag{25}$$

Where 'r' is the particle radius in metres and χ_s is a dimensionless parameter quantifying the scattering cross-section, which consists of two parts. The first part, χ_{ss}, represents the scattering and dominates the attenuation for larger particles. The second term, χ_{sv}, accounts for frictional losses due to viscosity and dominates for smaller particles. Combined they form the total scattering cross-section, $\chi_s = \chi_{ss} + \chi_{sv}$. These parameters are given by the following equations [88] [89]:

$$\chi_{ss} = \frac{k_{s\alpha} x^4}{1 + x^2 + 0.9 k_{s\alpha} x^4} \tag{26}$$

With

$$k_{s\alpha} = \frac{4}{3}\left(\frac{\eta_k^2 + \eta_p^2/3}{6}\right), \qquad \eta_k = \frac{\kappa_s - \kappa_w}{\kappa_w}, \qquad \eta_p = 3(\rho_s - \rho_w)/(2\rho_s + \rho_w) \tag{27}$$

And

$$\chi_{sv} = \frac{2}{3} x (\gamma - 1)^2 \frac{\tau}{\tau^2 + (\gamma + \theta)^2} \tag{28}$$

With

$$\tau = \frac{9}{4\beta r}\left(1 + \frac{1}{\beta r}\right), \qquad \theta = \frac{1}{2}\left(1 + \frac{9}{2\beta r}\right) \tag{29}$$

In these equations 'x' is equal to the Rayleigh scattering condition as given in equation (23) and γ is the relative density of the solids. The parameters τ and θ are influenced by the particle's radius and β, which is given by $\beta = \sqrt{\omega/2\nu}$, where ω is the angular acoustic frequency of the ADV signal and ν is the kinematic viscosity of the ambient water. Lastly, κ_s and κ_w are the compressibility of the solids in suspension and the ambient water respectively.

By combining these equations and the Rayleigh scattering condition the following can be found. Equation (23) which gives the Rayleigh scattering condition shows that for higher frequencies the left-hand side increases, indicating that the condition being smaller than 1 is met for a smaller range of particle sizes. As explained above this condition is also incorporated in equation (26). By examining this equation it is found that for increasing the frequency and thus the value of 'x', the scattering cross section parameter χ_{ss} increases, which ultimately leads to an increase of the particle absorption coefficient as equations (25) and (26) show. However, by inspecting the equation (26) it is also found that χ_{ss} eventually reaches its maximum value. The flattening of this curve is caused by the fact that 'x' initially has very small values of $<< 1$ for very small particles, but eventually increases to value of > 1 for larger particles. Because of this, the 1 in the denominator of equation (26) is dominant for small particle diameters leading to small values of χ_s. As the diameter increase however, the 'x^4' term becomes dominant, which is both in the nominator and denominator of the equation, leading the value of χ_s to eventually flattening. The numerical value of this maximum depends, among others, on the frequency of the acoustic signal. The most important finding, however, is that by increasing the frequency the particle diameter for which this maximum value of χ_s is reached, is decreased. Because for higher frequencies the maximum χ_s value occurs at smaller diameters, the particle attenuation coefficient of equation (25) also reaches its maximum value for smaller diameters. This equation shows for a continually increasing particle diameter in the denominator and a flattening numerator the maximum value is reached for the smallest diameter at which this maximum value of χ_s occurs. It is then found that this results in the peaks of Figure 2.7 to shift to the left.

Combining the knowledge that increasing the frequency leads to both an increased absorption as well as the peak shifting to the left, towards smaller diameters, can be used during ADV selection and the calibration process as it means that also the opposite is true. By decreasing the signal frequency both the peak shifts to the right (towards larger particles) and the total absorption decreases. As a result, the particles diameters for which the absorption is the most severe can be altered by using an ADV with a different acoustic frequency. ADVs available on the market have acoustic frequency of typically 5, 10 and 16 MHz. Figure 2.9 to Figure 2.11 show the particle attenuation coefficient from equation (25) for these three frequencies. These figures show both the increase of the peak value and shift to the left for higher acoustic frequencies that has been elaborated above. The dashed lines give the diameters of the smallest and largest particle considered for use during the experiments for this research, being 65 and 105 μm respectively. The figures indicate that using an acoustic frequency of 5 or 10 MHz is preferable compared to 16 MHz.

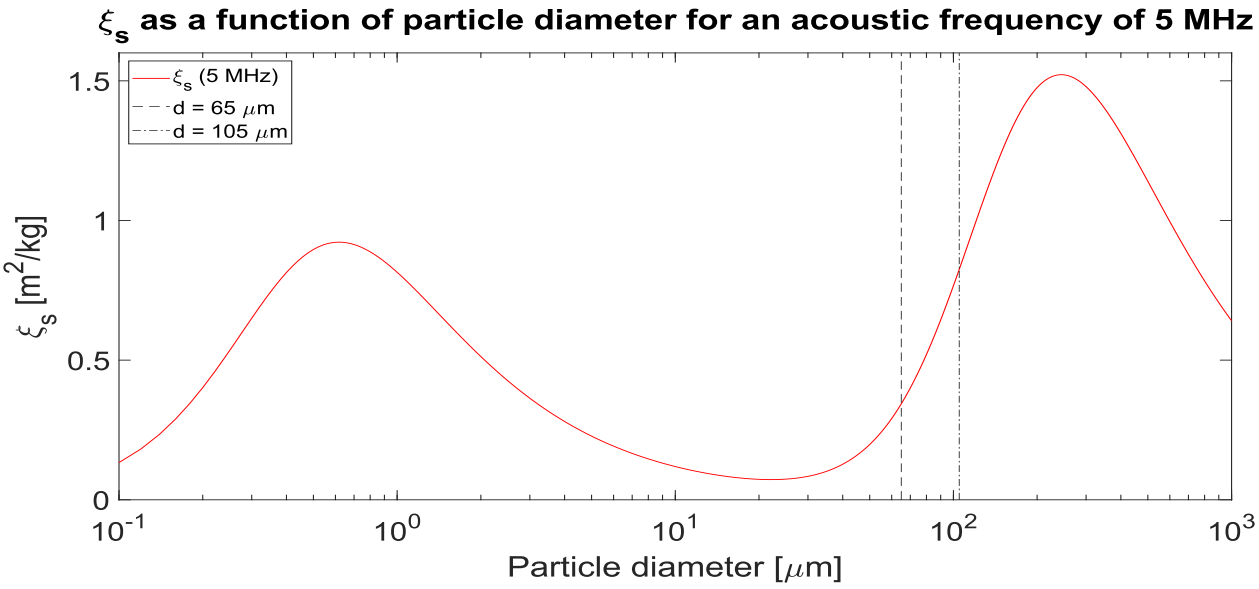

Figure 2.9: Particle attenuation coefficient for an acoustic frequency of 5 MHz

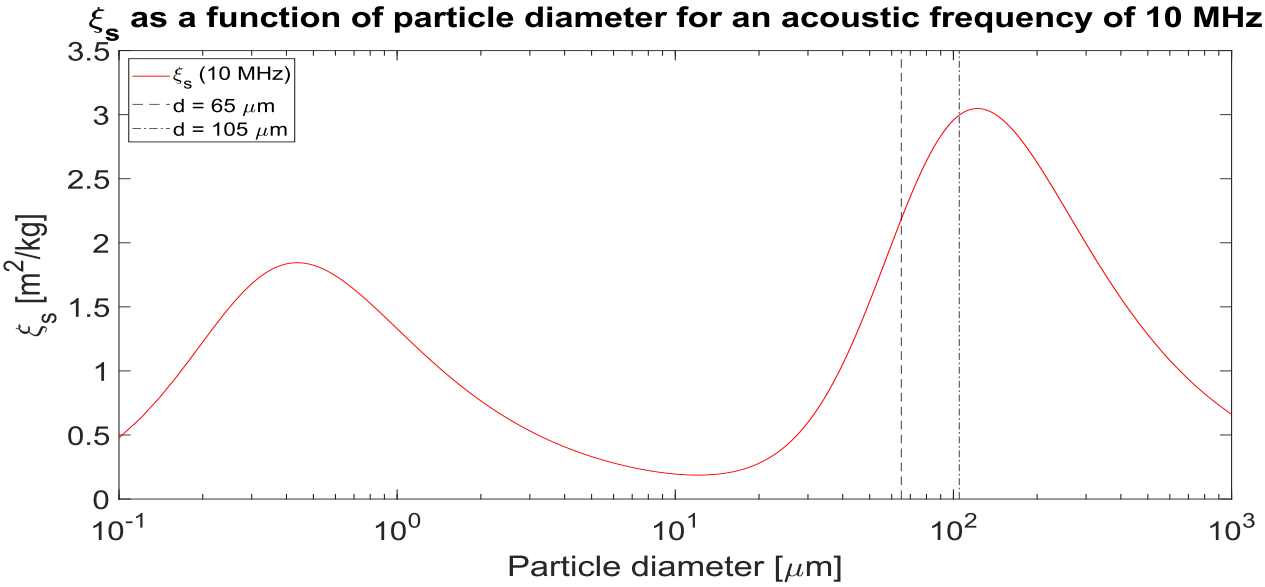

Figure 2.10: Particle attenuation coefficient for an acoustic frequency of 10 MHz

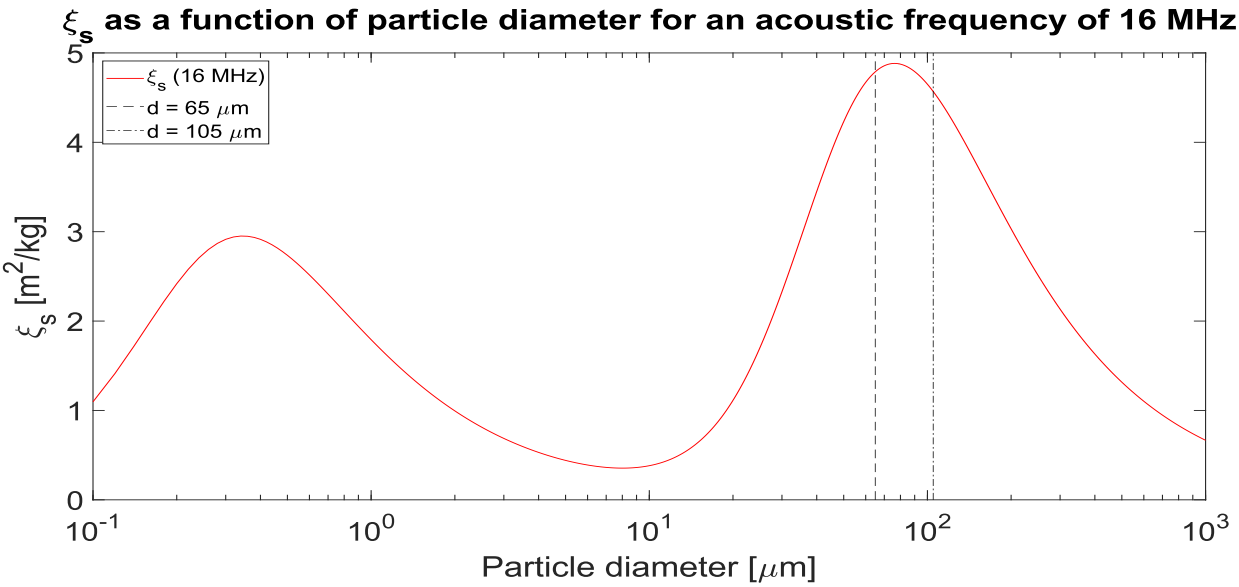

Figure 2.11: Particle attenuation coefficient for an acoustic frequency of 16 MHz. The sediment diameters between 65 and 105 μm are exactly located at the absorption peak for this frequency, indicating that the backscatter intensity will most likely start to decrease for small concentrations.

2.7 Overview and conclusion of literature review

The literature that was reviewed in the previous sections regarding different topics showed the current state of knowledge on these subjects. It was found that some subjects are well understood, while others involve less researched or even poorly understood processes. Section 2.7.1 will give an overview of the findings and discuss the conclusions that were drawn based on these findings in literature. Section 2.7.2 will then elaborate on how these findings help answering a part of the research questions from chapter 1.

2.7.1 Overview and conclusion

The literature study has been sorted to discuss every process influencing the generation of a sediment plume and the subsequent turbidity current by a deep-sea mining vehicle, in the order in which they influence the total process. As such the first section focussed on the sediment intake by a mining vehicle. It was found that the sediment intake is influenced by the velocity, width and cutting layer depth of the mining vehicle, as well as by the nodule abundance, soil properties at the mining site, and efficiencies of the pickup and separation processes. It is important to note that only the first three can be chosen freely while the other factors influencing the intake are mostly independent on design choices. It was found that ultimately the velocity and width, which make up the mining rate, are most likely to be chosen based on economic feasibility of the operation and as such the sediment flux is predetermined and cannot be changed for the benefits of the sediment plume. This is important to take into account when researching the influence of volumetric concentration on the spread of the sediment plume and subsequent turbidity current, since it has to be understood that the sediment flux will be a constant as a result of economical choices. As a result of this, the only way to change the volumetric concentration at the miner's discharge source is by adding a different amount of water to the sediment flux. This means that the total volume flow will change based on the desired initial volumetric concentration which will ultimately influence the diffuser area.

After being picked up, the sediment will be discharged through diffusers at the back of the miner and enter the water column as a buoyant jet. Important aspects for understanding the ensuing process include the diffuser shape and size, the source parameters, characteristic length scales of buoyant jets and the transition from a jet into a plume which will eventually impinge at the bottom. The source parameters are the volume, momentum and buoyancy fluxes, whose ratios give the characteristic length scales L_Q, L_M and L_m. These length scales are important for research into jets and plumes and are commonly used to describe points in the flow where changes occur in the flow regime.
The length scale L_M can be used to determine the region where the flow is dominated by momentum (pure jet-like behaviour), buoyancy (pure plume-like behaviour) or to pinpoint the transition region from jet to plume for different jets. This allows better predictions to be made regarding the trajectory of the buoyant jet which is important for the impingement process. The transition from jet to plume occurs due to a shift in dominance between momentum and buoyancy. Because momentum continually decreases while buoyancy is preserved, buoyancy gains dominance at some point in the flow resulting in the initial jet flow to become pure plume-like. This phase is characterised by an increase in turbulence and entrainment. For horizontally discharged buoyant jets recent research has shown that the transition from jet to plume takes place between a horizontal distance of $1.5 \cdot L_M$ and $5 \cdot L_M$ from the source. Also after having descended for more than $2 \cdot L_M$ the flow typically behaves pure plume-like. These findings can be used for predicting the behaviour of the flow at the impingement point. This gives insight into the influence of different input variables on the impingement angle, impingement location, outflow shape and wall jet phase. In section 2.7.2 these findings will be used for answering a number of the research questions from chapter 1.
The length scale L_m has been used in recent studies to predict the sedimentation length of buoyant jets and the sedimentation rate at different locations from the source. This allows predictions to be made regarding the amount of sediment expected to be in suspension at a given distance from the source.

The next step in the process is the impingement of the sediment plume and its subsequent spread as a turbidity current. Different recent sources comment on the impingement being among the least understood processes

regarding the spread of sediment plumes. Especially the prediction of the outflow source parameters remains difficult and there is no clear correlation between the discharge and outflow source parameters. This leads to the need of more research into the plume impingement. Being able to predict the outflow source parameters based on the discharge source parameters would allow for a better prediction of the flow characteristics of the ensuing turbidity current. Especially the momentum and buoyancy flux which drive a turbidity current are important. This has been confirmed through the recent study of Lippert and Woods [60], in which they found a correlation between the parameter 'S' (the ratio of the initial current velocity and the settling velocity) and the current height and the extent of the spatial spread of the current. It was shown that for higher values of 'S' the height and spatial spread of the current increases. For the research of this report into the influence of the initial volumetric concentration on the spread of a sediment plume and turbidity current this finding can be used as well. By recording the velocity of the current, the influence of the initial volumetric concentration (for equal sediment fluxes) on the initial velocity of the current can be found. If the influence of the initial volumetric concentration on the current velocity is understood, this knowledge could be combined with the findings of Lippert and Woods to find the concentration for which S and therefore the spatial spread of the turbidity current is minimised.
Other important aspects of the impingement influencing the spatial spread of the turbidity which ultimately needs to be reduced for deep-sea mining operations are the impingement angle and flow regime. An impingement angle of 90 degrees with respect to the horizontal is known to result in an axisymmetric, circular outflow. Such an impingement is more likely if the distance between the discharge source and impingement point allow for a transition from a momentum dominated jet to a buoyancy dominated plume to take place. If the flow regime at the impingement point is more jet-like, a smaller impingement angle with respect to the horizontal can be expected. This results in an asymmetrical outflow with a more pronounced downstream spread. Research into the impingement has pointed out that a more jet like impingement also causes a more energetic impingement leading to a higher velocity and larger spatial spread of the turbidity current. For this reason, it is concluded that for deep-sea mining operations a vertical, plume-like impingement is preferred.

In order to understand the settling of a sediment plume and the particle deposition and resuspension inside turbidity currents, as well as being able to prepare experiments, another subject of importance is the settling of particles. Research into the settling velocity of particles has been conducted for decades now and most methods are well established. This is true for both individual and hindered settling. However, the effects of flocculation on the settling mechanism of mixtures is less well understood as multiple sources point out. Flocculation is expected to be an important aspect for deep-sea mining as it is known to increase settling rates which is desirable for deep-sea mining operations. It is also a process that occurs for cohesive sediment like clay which will be present at the deep-sea mining sites. For this reason, more research into the initiation of the flocculation process and how to speed up the process deserves more attention as it is believed to be crucial for deep-sea mining. Flocculation will however not be further researched in this study because as stated in section 1.5, it lies outside the scope of this study.

The literature discussed in section 2.5.2 showed that the rheology depends on both the volumetric concentration and the properties of the solids. For non-cohesive material different experiments have shown that the transition from Newtonian to non-Newtonian behaviour takes place at volumetric concentrations between 20 and 30%. Slurries with cohesive material such as clay already show non-Newtonian behaviour from volumetric concentrations of 5% and upwards. It is concluded that for the experiments that will be conducted for this research, it is unlikely that the mixture will show non-Newtonian behaviour. This research aims at experimenting with mixtures of volumetric concentrations between 1 and 7%, far below the found transition values of 20 to 30%, which leads to the conclusion that non-Newtonian behaviour will play no role in the experiments.
Literature covering the influence of the aspect ratio of ducts and diffusers on the flow showed that the aspect ratio has influence on the secondary currents, concentration profile, velocity profile, turbulence intensity and friction factor. Different sources pointed out that especially at lower aspect ratios the influence is high. Studies focussing on the jet originating from diffusers with different aspect ratios have shown that the aspect ratio does have influence on the turbulence intensity in the near-field but shows almost no difference in the far-field.

Because this research mainly focusses on the influence that the volumetric concentration has on the resulting flow, this will be taken into account. The ultimate decision on how to scale the diffusers will need to be made taking into account the actual aspect ratios of the diffusers, as it was found that the value of the aspect ratio heavily influences the effect of changing the aspect ratio.

Findings regarding the use of an ADV for experiment measurements mainly focussed on concentration measurements as velocity measurement with ADVs is a well understood and widely used application of ADVs. Concentration measuring with an ADV is however a newer application which requires more considerations. It was found that through relatively simple calibration a correlation can be found between the backscatter signal and the suspended sediment concentration. There are however many factors influencing the strength of this signal, which is determined by the backscatter intensity and the attenuation. This causes the range of sediment types and sizes to which this method is applicable to differ quite dramatically for different inputs. The most important conclusions which have to be taken into consideration when using an ADV for concentration measurement are the following. Calibration curves show a decrease of the backscatter signal at some concentration. This means that for this high concentration values the measured backscatter signal also correlates to a lower concentration. This means that if this calibration data is used, the backscatter signal measured during experiments might refer to two concentration values. The method can however still be used in the analysis, as it can be reasoned whether the concentration that is being measured is the one before or after the peak, based on other measurements, knowledge about the initial and expected decay of concentration and visual observations. Recent studies have also shown that the usability of this method is highly dependent on the combination of the particles in suspension and the acoustic frequency of the ADV. For particle diameters of around 100 µm, the study of Sahin et. al [88] has shown that attenuation plays a big role. This could lead the backscatter intensity to decrease at very low concentration values. In order to prevent this from happening their results have shown that a correction can be applied to the measurements. Perhaps the most important conclusion is that also using an ADV with a lower frequency than the 10 MHz as used by Sahin et. al helps decreasing the total absorption. It also causes a shift of the absorption peak to the right, resulting in the 65-105 µm particle range (the particle sizes to be used for the experiments of this research) to not be located in the peak region anymore. In conclusion, through calibration it needs to be found what the resulting curve looks like for a specific ADV and sediment set. Based on this either the frequency can be changed, or a correction can be applied.

2.7.2 *Answers to research questions*

Another important objective of this literature review was to work towards finding the answers to the research questions of chapter 1. Findings in literature have led to the first three questions being (partially) answered. These questions are repeated below and could be qualitatively answered based mainly on findings in sections 2.2 and 2.4. Experimental results could help confirm these conclusions.

- How does the initial concentration influence the impingement location and angle?
- What is the effect of changing the initial concentration on the outflow shape?
- Can the transition from wall jet to turbidity current be observed and if so, what is the effect of increasing the initial concentration on the length-scale at which this transition takes place?

Increasing the concentration for a constant sediment flux leads to a decrease in volume flow. Equation (7) shows that this leads to a decrease in momentum flux, while equation (7) and (8) show that the buoyancy flux remains constant for changing concentrations (given a constant sediment flux). Inspecting equation (10) shows that a constant buoyancy flux and a decreasing momentum flux lead to a decrease of L_M with concentration. As a result, the jet/plume transition length decreases, which decreases the distance from the source at which the behaviour of the flow is changed from pure jet-like to pure plume-like. This indicates that increasing the concentration leads to plume-like impingement being more likely than for lower concentrations. It is also known from section 2.4.1 that if buoyancy becomes more dominant than momentum vertical impingement is likely, while momentum being dominant leads to a more jet-like, angled impingement. Based on the above the first research questions can be answered by concluding that increasing the initial concentration leads to a more

vertical impingement, so close to a 90 degree angle with the horizontal, while decreasing the initial concentration leads to a smaller impingement angle. The finding that increasing the concentration leads to a decrease in momentum, and more importantly a decrease in momentum-buoyancy ratio also shows that increasing the concentration leads to the impingement location being located closer to the source. Section 2.4.1 furthermore showed that the outflow shape is mostly influenced by the impingement angle. Vertical impingement, which is more likely for high concentrations, leads to axisymmetric outflow, while angled impingement leads to a more pronounced downstream outflow. It is important to note however that apart from the momentum-buoyancy ratio (L_M), also the height of the source above the bottom plays an important role in the impingement. As discussed in section 2.2.4, the transition from jet to plume behaviour takes place between $1.5 \cdot L_M$ and $5 \cdot L_M$ in the horizontal direction and up to $2 \cdot L_M$ in vertical direction. This indicates that given enough distance, plume-like impingement will eventually happen for all buoyant jets. If the height above the bottom is less than $2 \cdot L_M$ however, the difference between plume-like and jet-like impingement is important and influenced by the initial concentration.
The same theory applies to the influence of initial concentration on the wall jet region. It was found that the flow regime and the impingement location influences the spatial extent of the wall jet. An angled jet-like impingement is more energetic than a vertical plume-like impingement. As a result, jet-like behaviour of the buoyant jet at the impingement location leads to the wall jet phase being maintained for a longer distance. This increases the momentum flux at the outflow source which is thought to increase the spatial spread of the ensuing turbidity current. The theory above leads to the conclusion that increasing the concentration leads to a decrease of the wall jet region.

The remaining four research questions, which are focussed on the effect that changing the initial concentration has on the velocity and concentration inside the turbidity current, cannot be answered yet. Results of the planned experiments combined with existing knowledge from earlier studies should allow these questions to be answered.

3. Experiments

This chapter discusses all parts of the experimental setup as well as the necessary preparations. The experimental results are at the core of this research and therefore preparing the experiments well is of upmost importance. Section 1 gives a detailed description of the experimental setup. Section 2 focusses on the selection of the sediment type used during the experiments. Section 3 describes the choices made regarding scaling based on literature and practical limitations. Furthermore, the iteration process to determine the dimensions of the diffusers and the pipelines is discussed in this section. These results have been used for shaping the experimental matrix, which can be found in section 4. Section 5 explains the measurements that will be performed for gathering data, continuing on the information given in section 2.6. Finally, section 6 and 7 will give a detailed overview of the experimental procedure and adaptations made to the experiment matrix due to practical limitations found during experimenting.

3.1 Experimental setup

The setup used during the experiments consists of different parts. These are the mixing tank in which the mixture that is to be discharged is prepared, the pipelines connecting the mixing tank to the modular tank, the diffusers, the modular tank itself and the pump for transferring the slurry from the mixing tank through the pipeline into the modular tank. The sections below give a detailed description of each component.

3.1.1 Mixing tank

For the experiments it is important to ensure a constant, homogeneously mixed slurry. For this purpose, the mixture will be prepared in a mixing tank. Two tanks are available, having capacities of 800 and 2000 litres. Using a larger tanks allows for a longer experiment duration. The required tank depends therefore on the required experiment duration and predicted total volume flow. The mixing tank will be placed next to the modular tank and will be connected through pipes made from PVC. Inside the mixing tank two submersible pumps will be placed to keep the sediment in suspension. The submerged pumps are the Einhell GE-DP 6935 A ECO, which has a capacity of 17,500 L/hour. Both submerged pumps are placed on the bottom of the mixing tank ensuring a continuous rotation of the mixture and prevent the sediment from settling. Steel weights are used to keep them in position. To ensure the concentration can be kept constant during experiments the ADV has been used to measure to concentration inside the mixing tank at different points in time. These tests have shown that the concentrations used during the experiments can be kept in suspension for at least the running time of the experiments.
For delivering a steady supply of the mixture into the modular tank, a centrifugal pump is connected to a valve on the bottom of the mixing tank, which makes the connection between the mixing tank and the modular tank. The centrifugal pump used is a Marina SM98/5 CR with a capacity of 100 L/min. The centrifugal pump has a bypass system consisting of two ball valves. One valve is connected to a flexible hose which is connected to the PVC pipe leading to the modular tank. The other valve is also connected to a flexible hose, but this one is led back into the mixing tank. These two valves can be adjusted during experiments in order to achieve the desired volume flow into the modular tank, measured by the flowmeter attached to the PVC pipes.

3.1.2 Pipeline and diffuser

The connection between the mixing tank and modular tank is made through PVC pipes. In order to keep the sediment in suspension and prevent it from settling during transportation, certain velocity thresholds need to be met in the horizontal and vertical sections. For this purpose the inside diameter of the pipeline is chosen to be 20 mm, based on the volume flows as calculated in section 3.3.2. This pipeline is connected to the 3D-printed parts. These printed parts are a transition piece, a 90-degree bend part and the diffuser, of which three different ones will be used. The transition section is a 3D-printed pipeline with a circular entrance and rectangular exit. This part is connected to a 3D-printed pipeline with a rectangular cross section and 90-degree bend. The three different diffusers will be connected to this bend pipe using bolts.
A flowmeter (Katronic KATflow 200) is connected to the pipeline outside the modular tank in order to monitor the flow rate inside the pipeline. This instrument uses acoustics to measure the velocity of the mixture inside

the pipe. Together with the pipeline dimensions this can be used to compute the total volume flow. The measurements of the flowmeter have been verified by collecting water from the diffuser in a bucket. The total mass of the collected water as well as the total time it took have been measured which gave the volume flow in L/s. The measurements using the bucket for different volume flows were within a 10% error range of the KATflow measurements, leading to the conclusion that the KATflow delivered correct measurements. Differences between the KATflow and the collected water measurement are believed to be due to uncertainty in the timing as well as a 0.05 kg precision of the scale that was used.
The KATflow can also be connected to a laptop to record the volume flow over time. This has been done during multiple experiments to check the consistency of the volume flow. It was found that the maximum deviation from the targeted flux was 0.01 L/s, which is an error of between 0.7 and 5%, depending on the target flow rate.

3.1.3 Modular tank

The tank in which the experiments take place is a modular flume tank. Its dimensions are 5 metres in length, 2.25 metres in width and 2 metres high. It consists of steel frames with transparent panels to allow for visual observations. Inside the tank a table is placed which has to represent the seabed. This table has a height of 0.50 metres measured from the bottom of the tank. Its width and length are 1.95 and 4.5 metres respectively, leading it to be slightly smaller than the tank itself. This allows the sediment to fall off the table, preventing it from reflecting against the back wall and influencing the measurements. The table is also fitted with LED lights. These lights span the entire width and length of the table and are placed underneath plexiglass plates. This allows for a better visibility of the plume and turbidity current during experiments.

Figure 3.1: The left panel shows the mixing tank (white) and the modular tank (blue), connected by a flexible tube. The right panel shows diffuser 1 installed in the modular tank at a height of 30 cm above the table

3.2 Sediment type

Two sediment types were available for the experiments, both consisting of spherical glass particles. The first set has particles with diameters between 65 and 105 µm, hereafter referred to as sediment set 1. The second set consists of particles ranging from 40 to 70 µm, hereafter referred to as sediment set 2. The choice on which to use will be based on their influence on the resulting sedimentation length scale (L_m), the deposition limit velocity and the velocity for safe vertical operation. Larger particles have a higher settling velocity and thus

require a larger mixture velocity to stay in suspension during transport. This results in the required flow velocity inside the pipelines to be higher. However, their higher settling velocity also causes them to settle faster in the modular tank resulting in a smaller sedimentation length scale. The latter has to be taken into account as the modular tank has a finite length of 5 metres and thus poses a physical limit to the experiments.

3.2.1 *Sedimentation length scale (Lm)*

The theory regarding the sediment deposition rate was discussed in section 2.3.2. The semi-empirical function of Lee, Li and Lee [51] was given to calculate the deposition rate along the length of the jet. This function has been used to calculate and plot the sediment deposition rate for jets with different volume flows, initial volumetric concentrations and dimensions (based on the different experiment scales under consideration). Figure 3.2 and Figure 3.3 show the resulting plots for concentrations of 7 to 10%, the highest concentrations under consideration during preparation. The horizontal axis gives the distance from the source in metres while the vertical axis gives the deposition rate in $gm^{-1}s^{-1}$.

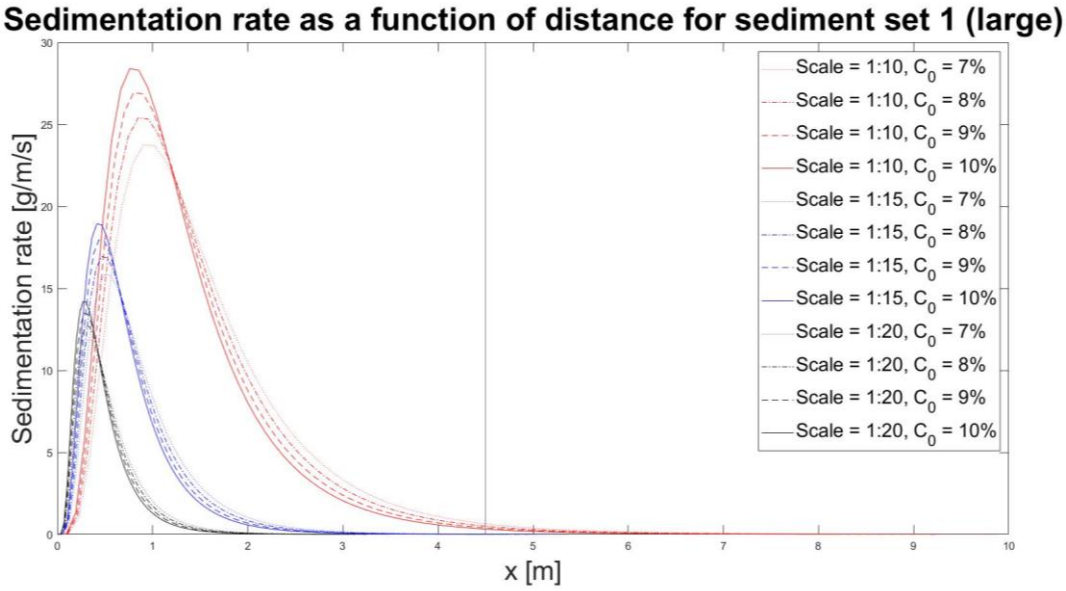

Figure 3.2: Sedimentation rate of particle diameters between 65 and 105 μm for different initial concentrations and experiment scales. The plots show how for higher initial concentrations the peak in sedimentation is higher and located closer to the source. Buoyant jets with lower initial concentrations show a lower peak but a larger reach.

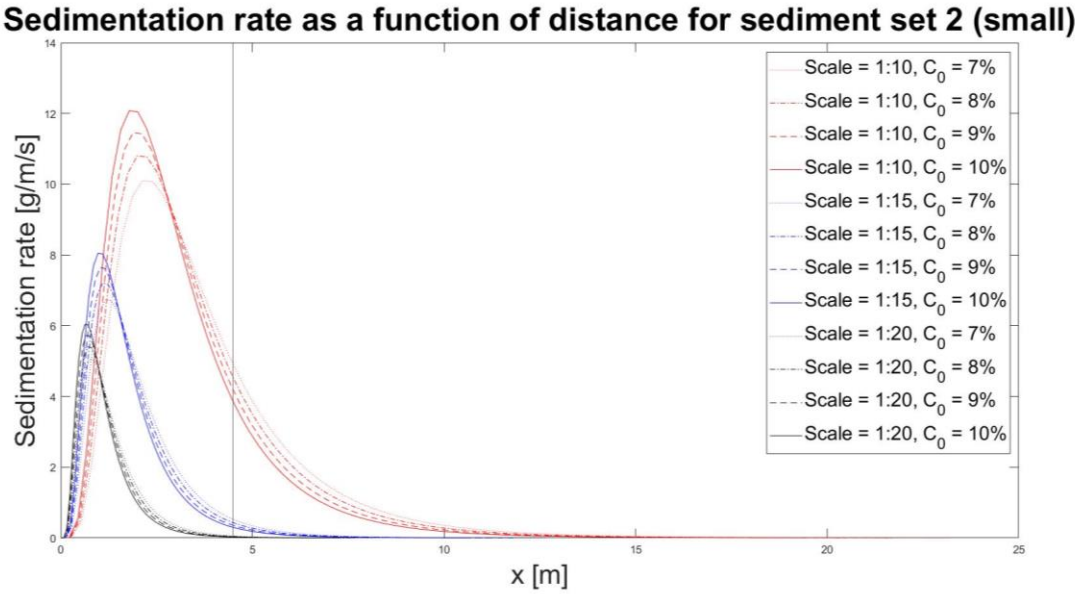

Figure 3.3: This figure shows the same plots as shown in figure 3.1, but for a smaller particle diameter (40-70 μm). By comparing the plots one clearly sees the effect that using particles with a smaller settling velocity has on the sedimentation rate away from the source. The peak value of the sedimentation is less than half for the smaller particles, while the total length required for settling is about twice as large.

These plots have been made for the initially considered experiment scales of 1:10, 1:15 and 1:20. The discharge velocity considered in these plots is the Froude scaled full-scale discharge velocity of 0.5 m/s, resulting in 0.16, 0.13 and 0.11 m/s for each experiment scale respectively.

$$\frac{F_s L_m}{Q_o C_0} = 0.702 e^{-1.5\left[\ln\left(1.19\frac{x}{L_m}\right)\right]^2} \tag{30}$$

The plots clearly show that the distance from the source at which deposition still takes place is larger for sediment set 2 (40-70 microns). This is caused by their smaller size and hence, smaller settling velocity. This smaller settling velocity results in a larger sedimentation length scale as can be seen by inspecting equation (10). The importance of this distance is caused by the limited size of the modular tank. This finite length means that the solids inside the jet either need to settle before the end of the tank is reached or have their forward velocity reduced to a negligible magnitude in order to prevent reflection of the back wall which might interfere with measurements. It is furthermore desired that the plume settles not too far from the source in order to let the turbidity current develop itself. Choosing the sediment that settles far away from the source limits the distance available for measurements and video recordings.
Both plots include a vertical line at 4.4 metres. This is the distance available for settling, taking into account the pipeline and diffuser length. It can be concluded that sediment set 2 settles too slow and requires too much space. It should also be noticed that the experiments will be conducted at 1, 4 and 7 percent initial concentration and that the sediment deposition length scale increases for smaller concentrations. For sediment set 1 the plot shows that only for the 1:10 scale some sediment will still be in suspension at the back wall of the modular tank. It should however also be taken into account that the table on which the solids will settle does not span all the way to the end on the tank, meaning that particles which settle at the back of the tank will fall down instead of reflecting and not end up on the table as long as their forward velocity is low. For this it should be taken into account that the centreline velocity of the jet after multiple metres has decreased to only a few millimetres per second. This results in a negligible forward velocity of the particles still in suspension [90]. To conclude, based on the information and plots above, sediment set 1 is the preferred sediment size.

3.2.2 Deposition limit and safe vertical operation velocities

In order to ensure a homogeneous mixture being discharged from the diffusers the flow velocity inside the pipeline between the mixing tank and modular tank needs to be high enough to keep all sediment in suspension. The minimum required flow velocity depends on the settling velocity of the sediment as well as the pipeline dimensions. For horizontal slurry transport multiple models exist for calculating the flow velocity which prevents a sliding bed from developing, called the deposition limit velocity (V_{dl}). For the calculations in this report, the MTI Holland model was used [91]. For the vertical transport, a flow velocity of four times the settling velocity of the largest particle involved is assumed as the velocity for safe vertical operation, based on findings by Sellgren [92] and van Wijk [93]. This safety factor is required because the drag coefficient of particles can momentarily drop in turbulent flow, which causes the settling velocity to increase [92]. A flow velocity of multiple times the settling velocity is therefore required for upwards vertical transport to prevent the particles from dropping downwards in the flow.
Computing the deposition limit velocity and the velocity for safe vertical operation for both sediment sizes shows that the larger particles require a larger velocity in the pipelines. It should also be noted that the deposition limit velocity reaches values multiple times higher than the velocity for safe vertical operation, meaning that the deposition limit velocity is governing for the minimum required mixture velocity, which is constant in every part of a pipeline for constant dimensions.

3.2.3 Relating lab to field sediment

Another important aspect of the sediment is the influence of using a different sediment during the experiments when compared to the ocean floor. Because the CCZ is one of the most promising areas for nodule mining, the data from this area will be used for comparison. There are three main differences between the sediment in

the lab and at the CCZ. These are the sediment type, size and density, the latter of which is important for scaling purposes. The result of the first difference, sediment type, is that flocculation which is likely to occur in the CCZ will not be taken into account during the experiments. The difference in size translates to a difference in settling velocity. The particles used during the experiments are sized between 65 and 105 μm. The sediment found at the CCZ is much smaller, having a median particle diameter of 20 μm [5]. The resulting difference in settling velocity is a simplification of reality for practical purposes. Using particles with a particle diameter similar to the ones found at the CCZ would result in a significantly longer waiting time between experiments and would therefore decrease the efficiency at which data can be gathered. This lower settling velocity would furthermore lead to a longer runout length of the experiments as shown in Figure 3.2 and Figure 3.3. This distance has to be kept to a lower value than the total tank length. The last difference is the density of the sediment, which is a difference that can be corrected for. The sediment density difference results in a different relative submerged density (R_{sd}) in the lab when compared to the CCZ. Scaling this R_{sd} correctly is especially important for the plume phase of the buoyant jet, because as explained in chapter 2, buoyancy is the dominant force during the descend of the flow as a plume. As equations (7) and (8) show, the R_{sd} heavily influences the buoyancy flux of the buoyant jet. Because of this, scaling the R_{sd} correctly is important for analysing the results and relating this to the behaviour of mixtures in the CCZ.
A relation has to be found between the lab and CCZ conditions. The sediment and ambient water densities of both situations need to be compared in order to determine which mixture concentration at the CCZ leads to the same R_{sd} as the 1, 4 and 7% mixture concentrations in the lab. Table 3.1 gives the (dry) sediment and ambient water densities of both the lab and the CCZ. It shows that especially the ambient water density differs between the two locations. For the experiments in the lab freshwater around room temperature will be used. At the CCZ the water will be just above freezing point and saline, resulting in a higher density. Because of the lower ambient water density in the lab, mixtures that are prepared there will have a higher R_{sd} than mixtures at the CCZ for the same volumetric concentration. It should be noted that as discussed earlier, increasing the volumetric concentration for a constant sediment flux leads to a decrease in volume flow. Combining equations (7) and (10) shows that for an equal R_{sd} and discharge velocity, a decrease in volume flow leads to a decrease in jet/plume transition length (L_M). This means that while it is achievable to find for what concentration a mixture has the same R_{sd} for both CCZ and lab conditions, there will still be a difference between the behaviour of the two buoyant jets as solving for both the R_{sd} and L_M cannot be achieved. Table 3.3 shows for which volumetric concentration a mixture under CCZ conditions has the same L_M as the experiment mixtures in the lab. This table shows that for equal L_M the concentration differences between lab and CCZ are slightly less than for equal R_{sd}.

Table 3.1: The differences in sediment and ambient water densities between the lab and the CCZ.

Location	**Sediment (dry) density [kg/m^3]**	**Ambient water density [kg/m^3]**
Lab	2500	998.2
CCZ	2475	1046.5

Table 3.2: Shown in this table are the CCZ mixture concentrations that result in the same relative submerged density as the mixtures in the lab.

ρ_m lab [kg/m^3]	**C_m lab [g/L]**	**C_V lab [%]**	**R_{sd}**	**C_V CCZ [%]**	**C_m CCZ [g/L]**	**ρ_m CCZ [kg/m^3]**
1015	25	1	0.017	1.2	29.7	1064
1060	100	4	0.062	4.5	111.4	1111
1105	175	7	0.12	7.8	193.1	1158

Table 3.3: Shown in this table are the CCZ mixture concentrations that result in the same jet/plume transition length as the mixtures in the lab

ρ_m lab [kg/m^3]	**C_m lab [g/L]**	**C_V lab [%]**	**L_M [m]**	**C_V CCZ [%]**	**C_m CCZ [g/L]**	**ρ_m CCZ [kg/m^3]**
1015	25	1	0.18	1.1	27.2	1062
1060	100	4	0.064	4.3	106.4	1108
1105	175	7	0.042	7.5	185.6	1154

Table 3.2 shows the volumetric concentrations for CCZ conditions that result in the same relative submerged density of the mixtures as the lab mixtures. The third column shows the volumetric concentrations that will be experimented with in the lab, being 1, 4 and 7%. Column 1 and 2 give the resulting mixture density and mass concentration. On the right side of the table the volumetric concentration, mass concentration and mixture density is given for slurries at the CCZ with the same relative submerged density.

3.3 Scaling

The following dimensions and decisions are based on findings in literature, practical limits and an iterative process taking into account all the threshold values that have to be met. These are the densimetric Froude number of > 1, the Reynolds number of > 4000, the mixture velocity being more than the velocity for safe vertical operation and the mixture velocity being more than the deposition limit velocity. The sedimentation length scale is monitored as well but due to the very small velocity of particles at the back wall of the modular tank, this length scale is of smaller influence.
In the iterative process, the initial considered scales were 1:10, 1:15 and 1:20 and for the first estimate of the dimensions the discharge velocity was a Froude scaled 0.5 m/s. The Froude and Reynolds numbers were plotted for the diffusers for each scale, as well as for the pipelines. The circular pipeline was initially assumed to have an inner diameter of 25 mm, but later adjusted to 20 mm to ensure a higher flow velocity. Apart from the dimensionless numbers also the mixture velocities for each scale were plotted for both the circular and rectangular pipelines along with the deposition limit velocity and velocity for safe vertical operation to check whether the mixture velocity was high enough to prevent the particles from settling in the pipelines.

3.3.1 *Scaling of the diffusers*

The diffuser dimensions are based upon the required discharge velocity, sediment flux and volumetric concentration. As explained before, the total volume flow decreases with an increasing volumetric concentration for a constant sediment flux and discharge velocity. This results in a decreasing diffuser cross section. After determining the experiment scale and diffuser dimensions, section 3.3.2 will focus on checking the velocity thresholds in the circular and rectangular pipelines because the velocities depend on the pipeline dimensions and the volume flow, the latter of which is a result of the experiment scale.

Constant aspect ratio vs. constant width

The goal of this research is to find the influence of the volumetric concentration of solids on the behaviour of sediment plumes discharged by a miner. In order to compare the results and make conclusions regarding the influence of the volumetric concentration, it is important that all other factors are the same or as similar as possible. However, as explained in chapter 2, choices have to be made on how to scale the diffusers for different volume flows. This can be done by either keeping the aspect ratio constant, or by keeping the width constant. A constant aspect ratio ensures that any influence that a changing aspect ratio has on the flow is removed from the experiments. A constant width has the advantage that this gives a more realistic prediction of what might be expected for the discharge from real miners as it is to be expected that their width will be constant and only their diffuser height can be adjusted in order to accommodate a smaller or larger cross section. Findings in literature which were discussed in section 2.5.3 pointed out that the aspect ratio influences the secondary currents, concentration profile, velocity profile, turbulence intensity and friction factor inside the pipeline/diffuser. Different sources also pointed out that especially at lower aspect ratios this influence is high. Studies focussing on the jet originating from diffusers with different aspect ratios have shown that the aspect ratio does have influence on the turbulence intensity in the near-field, but shows almost no difference in the far-field. Because the research in this thesis mainly focusses on the influence that the volumetric concentration has on the resulting flow away from the source, this latter is of higher importance than the aspect ratios influence on the flow inside the diffuser itself.
The assumption that only adjusting the diffuser height gives a more realistic view of the problem combined with the small influence that it has on the flow away from the diffuser, results in the decision to keep the width of the diffusers constant. While it can be argued that keeping the width of the diffusers constant is bad for

comparing the influence of C_v only, it is a more realistic way of scaling the diffuser and therefore results in data for more practical use. This is confirmed in Blue Nodules reports stating that the vehicle width is determined by the collector width, which depends on the required production, and therefore stays constant [34].

Diffuser cross section dimensions

As explained at the beginning of this section the first step in the iterative process was using a Froude scaled discharge velocity. This results in discharge velocities of 0.16, 0.13 and 0.11 m/s for each experiment scale respectively. The graphs that were plotted for this first step showed that for the 1:20 and 1:15 scale the Reynolds number drops below 4000 for concentrations above 1.8 and 2.1% respectively. For the 1:10 scale the Reynolds number eventually also became less than 4000 at a concentration of 6.2%, which meant that an increase in velocity was necessary. The Froude number is above 1 for all considered concentrations and scales for this discharge velocity and will thus not pose a problem. In order to increase the Reynolds number the discharge velocity had to be increased in the next iteration steps, resulting in the experiments being no longer Froude similar. Further iteration steps resulted in the following conclusion. Increasing the velocity with 1.15 times the initial values resulted in all thresholds being met for the 1:10 experiment scale. However, the limited capacity of both the mixing tanks and pump posed practical limitations. The maximum experiment duration for this scale was 18 minutes for the experiment with the largest total volume flow. This was deemed too short to gather data effectively. For this reason the experiment scale was lowered to 1:15, requiring a discharge velocity increase of 2.1 times the initial values, resulting in a discharge velocity of 0.27 m/s. This resulted in all the thresholds being met, as well as a minimum experiment duration of 30 minutes.
Figure 3.4 shows the plot for the Reynolds number of the final iteration step. Table 3.4 shows the resulting diffuser dimensions and aspect ratio for each volumetric concentration. The dimensions stated in Table 3.4 are that of the diffuser exit. The diffuser entrance dimensions will be equal to that of the rectangular pipeline, which are dependent on the deposition limit velocity. This will be discussed in section 3.3.2.

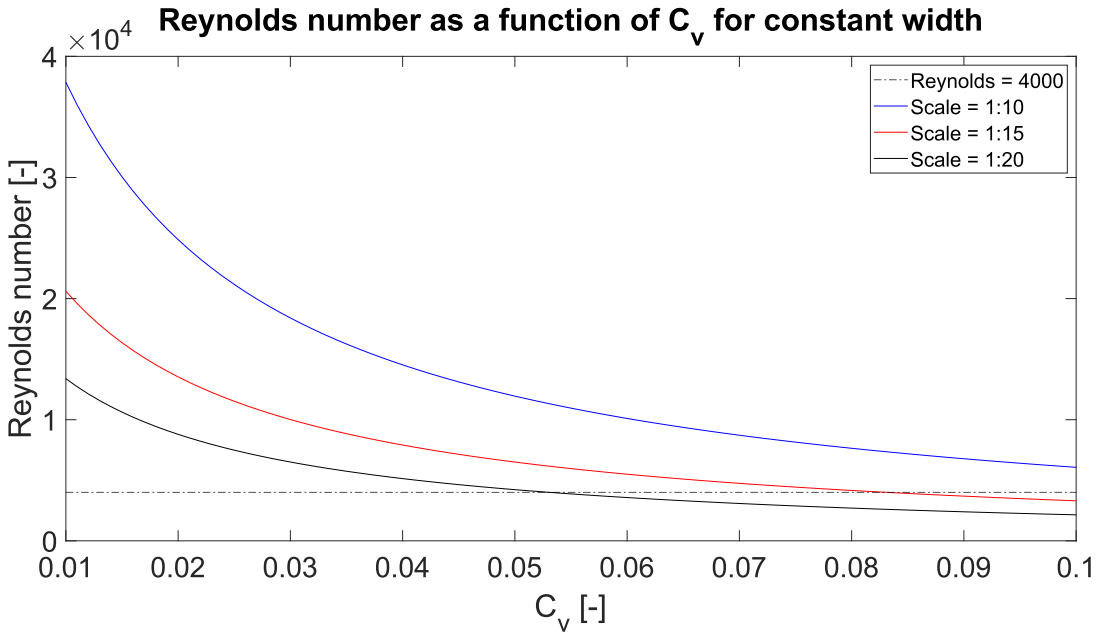

Figure 3.4: The 3 lines show that Reynolds number of the flow at the diffuser exit for all three scales under consideration as a function of volumetric concentration. For the 1:15 scale the Reynolds number has a value above the threshold of 4000 up to volumetric concentrations slightly higher than 7%.

Table 3.4: Table summarizing the diffuser exit dimensions for all three experiments.

Experiment	Height [mm]	Width [mm]	Aspect ratio [-]
#3 (C_v = 1%)	65	66.7	1.0
#2 (C_v = 4%)	16.3	66.7	4.1
#1 (C_v = 7%)	9.3	66.7	7.2

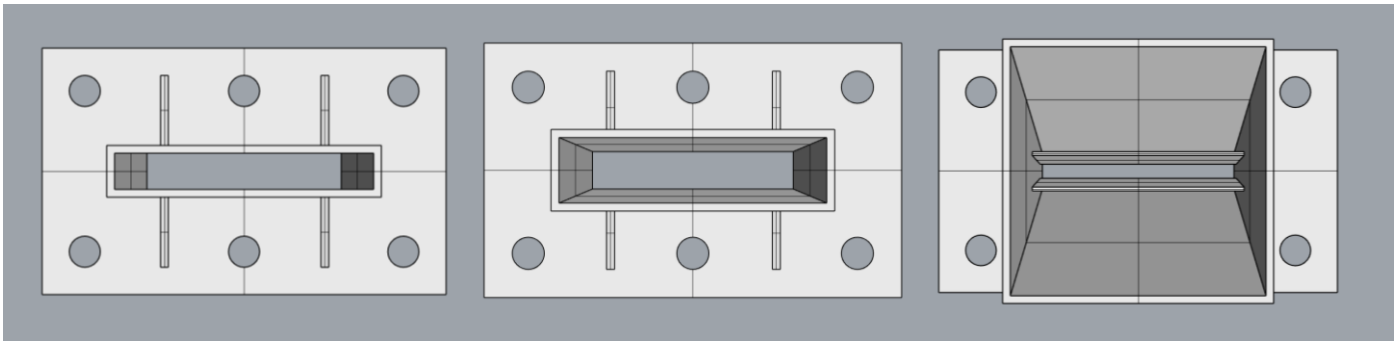

Figure 3.5: Shown are the front views of the three diffusers. The diffusers as depicted are for the 7, 4 and 1% volume concentration experiments from left to right, hereafter referred to as diffusers 1, 2 and 3.

Diffuser length

The theory discussed in section 2.2.1 showed that an important parameter of diffusers is their divergence angle. It has been found that in order to prevent flow separation this angle should be kept below 7 degrees. For the diffuser and pipeline dimensions given in Table 3.4 and Table 3.7 respectively, the diffusers require a minimum length of 13.6 cm in order to ensure a divergence angle of less than 7 degrees in horizontal direction. For the smallest two diffusers this length also results in a divergence angle of less than 7 degrees in vertical direction, thus requiring no vanes. The largest diffuser however would require a total length of 45 cm to prevent having a divergence angle of larger than 7 degrees. Because this is considered too space consuming in the modular tank the decision has been made to apply vanes in this diffuser. It is furthermore desired that all diffusers have the same length, as it allows for a better comparison between the experiment results as well as the same setup being applicable to all experiments. It should furthermore be noted that since the diffusers all have the same width, the divergence angle in width direction will be equal for all diffusers. Since the vanes will be placed horizontally to prevent flow separation at the top and bottom plates of the diffuser, the length of the diffusers has to be chosen such that flow separation at the diffuser side walls is prevented without the need of vanes. This results in a minimum required length of 13.6 cm, which gives a divergence angle of 7 degrees.

For a diffuser length of 13.6 cm it can be shown that the divergence angle of the largest diffuser equals 23.2 degrees. A diffuser with a total divergence angle of 23.2 degrees would require 3 vanes, resulting in four individual passages of 5.8 degrees each. However, the limited height of the diffuser throats due to the small height of the rectangular pipeline leads to a smaller number of vanes being more desirable. Having too many vanes in a compact space limits the maximum achievable thickness and decreases the spacing between the vanes. For this reason the diffuser length has been extended to a length for which the largest diffuser has a total divergence angle of just below 21 degrees. This allows for this diffuser to be fitted with only 2 vanes instead of 3. It was found that this holds for a diffuser length of 15.1 cm. The resulting divergence angles and number of vanes for each diffuser can be found in Table 3.5. The decisions are in accordance with the findings of Moore and Kline [45] and Cochran and Kline [46], results which have been confirmed in a recent study [94]. The location of the vanes will be in the vicinity of the diffuser throat. Regarding the length of the vanes, Moore and Kline [45] were unable to precisely define a best value, as discussed in section 2.2.1 They however found good results with the vanes having ¼ of the diffuser length. For this case this would result in a length of 3.8 cm.

Table 3.5: Table summarizing the diffuser length, divergence angles and number of vanes (n).

Experiment	Length [mm]	Divergence angle (height) [°]	Divergence angle (width) [°]	Number of vanes [-]
#3 (C_v = 1%)	151	20.9	6.3	2
#2 (C_v = 4%)	151	2.6	6.3	0
#1 (C_v = 7%)	151	0	6.3	0

Diffuser height above bottom

Apart from the diffuser dimensions, another important parameter of the diffusers is the height at which they are installed. Existing concepts and designs can be used to estimate a realistic diffuser height. Oebius et. al [8] mention a German mining concept having a total height of 3 metres. Blue Nodules also released details on their miner dimensions and their full-scale miner called Apollo III, is expected to have a height of 5 metres including equipment [34]. Expected is that the Apollo III will discharge from 4.5 metres height [21]. It is however unclear from which point (centreline or top of the diffuser) this is measured. Except for the values given above, not much more information is publicly available on the intended height of miner concepts.

For the diffuser height of the experiments it has been decided to follow the diffuser height of 4.5 metres as mentioned by Blue Nodules. Given the experiment scale of 1:15 this results in a discharge height of 0.30 metres for the experiments. This height will be measured from the top of the table to the centreline of the diffusers. The calculation in the previous paragraph shows that this height means that the buoyant jet of the 1% volume concentration experiment will impinge before it has developed into a pure plume. It is expected that this will result in an increased range of the turbidity current as discussed in section 2.4.1. For the other experiments this height ensures pure plume-like behaviour at the impingement location, which is believed to be desirable because it helps limit the spread of the turbidity current as was explained in section 2.4.1.

3.3.2 Scaling of the pipelines

The pipeline dimensions will depend on the aforementioned velocity thresholds. The vertical ascending pipeline requires the fluid velocity to be above the value that ensures safe operation, being 4 times the hindered settling velocity of the largest particle diameter. For the horizontal pipeline sections the focus will be on the deposition limit velocity as calculated with the MTI Holland model. The velocities in the pipeline depend on the pipeline dimensions and the required volume flow, the latter of which depends on the scale of the experiments.

The deposition limit velocity will be calculated and checked for both the circular and rectangular pipeline sections as they both have a horizontal part. The velocity threshold for safe vertical operation will only be tested for the vertical section of the circular pipeline. The rectangular pipeline's vertical section is descending and as such not prone to blockage due to mixture velocities being too low.

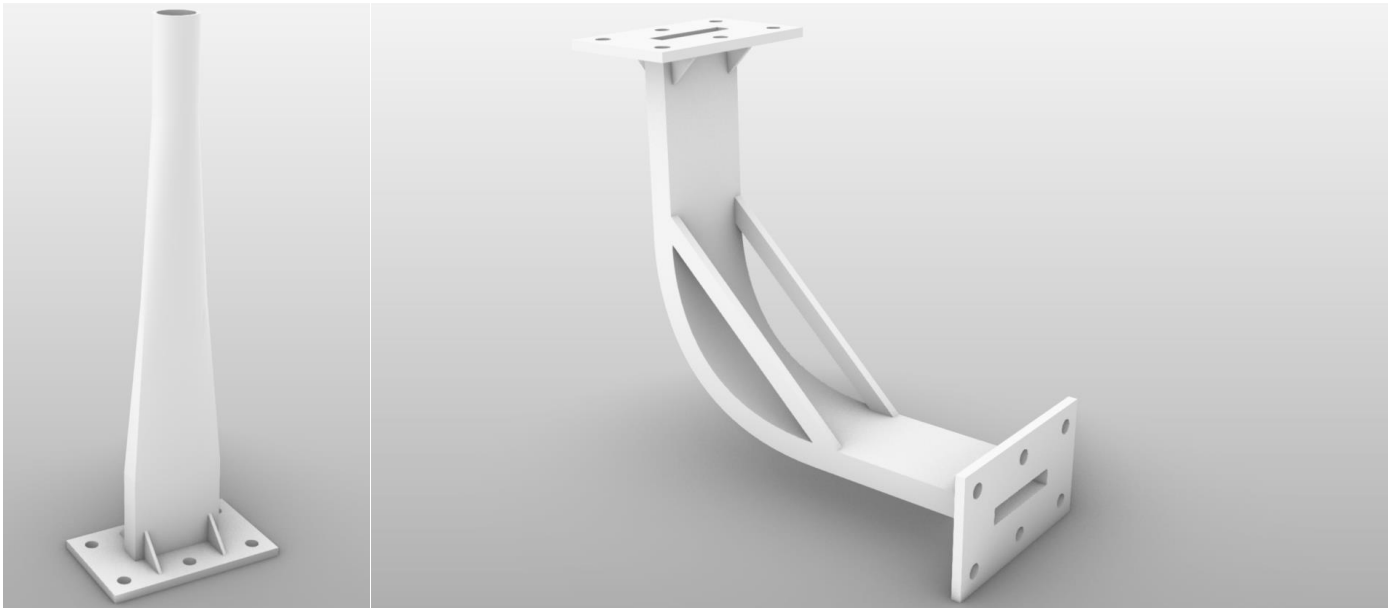

Figure 3.6: This figure shows the transition (left) and bend (right) parts of the pipeline as have been discussed in section 3.1.2. The circular entrance of the transition part has the same inner diameter as the other circular piper, being 20 mm. The exit of the transition piece and the bend part have the same dimensions as given in the table below.

Horizontal slurry transport

For the experiments that will be conducted it is deemed important that all particles remain in suspension. The MTI Holland model uses the definition for the deposition limit velocity that is required for this research, being

the threshold between partially-stratified and fully-suspended flow. For calculating the deposition limit velocity with the MTI Holland model the diameter of the largest available particles will be used. For the rectangular pipeline section the pipeline diameter in the equation will be replaced by the hydraulic diameter D_H, which is also used in the calculations of the Reynolds number. Equation (31) shows the deposition limit velocity as calculated using the MTI Holland model [91].

$$V_{dl} = 1.7\left(5 - \frac{1}{\sqrt{d_{mf}}}\right)\sqrt{D}\left(\frac{C_{vd}}{C_{vd}+0.1}\right)^{\frac{1}{6}}\sqrt{\frac{S_s - 1}{1.65}} \tag{31}$$

Vertical slurry transport

For determining the velocity threshold for safe operation it has been decided to calculate the settling velocity of the particles with size d_{100}, meaning that the particles with the largest diameter will be used to calculate it. The decision to use the largest particle diameter for the calculations is based upon conservatism. It is believed by the author that using the largest particle, which results in the largest settling velocity, leads to the highest threshold value and thus to the most certainty of ensuring safe operation. The decision has also been made to multiply this calculated settling velocity by a factor of 4 as advised by Sellgren [92] instead of the factor 2 as applied by Van Wijk [93]. The reason for this is that van Wijk designed a vertical transport system for nodules which are shaped irregular and non-spherical, and therefore have a higher drag coefficient than spherical particles. For this reason they are likely to have a settling velocity lower than that of spherical particles of similar size and density, resulting in a multiplication factor of 2 being sufficient. The particles that will be used during this research however will be spherical and will therefore have a settling velocity very close to the calculated value.

Circular pipeline

The experiment scale and discharge velocity have been determined based on the diffusers. The next step was to check whether the mixture velocity in the circular pipeline is high enough to ensure a fully-suspended flow. The initial considered inner pipeline diameter was 25 mm. It was found that for the volume flow resulting from the diffuser scaling and a diameter of 25 mm the mixture velocity would drop below the deposition limit velocity. For this reason the diameter of the pipeline was decreased to 20 mm, ensuring high enough mixture velocities for all concentrations. Decreasing the diameter both decreases the deposition limit velocity and increases the mixture velocity (for an equal volume flow). For this diameter the mixture velocity is above the deposition limit velocity for the 1-7% volumetric concentration range for the considered 1:15 scale and thus no further alterations of the circular pipeline are required. Also the Froude and Reynolds numbers are above 1 and 4000 respectively ensuring supercritical turbulent flow.

Table 3.6: Table summarizing the pipeline diameter, volume flow and resulting mixture velocity for all three experiments on a 1:15 scale.

Experiment	Diameter [mm]	Volume flow [L/s]	Mixture velocity [m/s]
#1 (C_v = 7%)	20	0.17	0.53
#2 (C_v = 4%)	20	0.29	0.94
#3 (C_v = 1%)	20	1.2	3.74

Rectangular pipeline

The dimensions of the rectangular pipeline/duct could be freely chosen. The dimensions were initially chosen to be equal to that of the lowest diffuser, being 9.3 mm in height and 66.7 mm in width. The reason for choosing the height equal to the smallest diffuser is based on two arguments. Firstly, the height of the rectangular pipeline should not be larger than the of the smallest diffuser because that would lead to the diffuser actually being a nozzle. Secondly, choosing the pipeline height as large as possible helps in bringing the velocity down before entering the diffuser which could further help prevent flow separation in the largest diffuser. It was found however that the dimensions as given above resulted in mixture velocities below the deposition limit velocity for the volumetric concentration of 7%. The only way to increase the mixture velocity for a given

volume flow is decreasing the cross section of the pipe. The width would be decreased until a mixture velocity above the deposition limit velocity was reached. This resulted in the rectangular pipeline having a total width of 50 mm. Table 3.7 shows the final rectangular pipeline dimensions.

Table 3.7: Table summarizing the pipeline height and width, volume flow and resulting mixture velocity for all three experiments on a 1:15 scale.

Experiment	Height [mm]	Width [mm]	Volume flow [L/s]	Mixture velocity [m/s]
#1 (C_v = 7%)	9.3	50	0.17	0.36
#2 (C_v = 4%)	9.3	50	0.29	0.63
#3 (C_v = 1%)	9.3	50	1.20	2.53

3.4 Experiment matrix

Table 3.8 below is the same as given in section 1.4.1. The completed scaling calculations result in all the table inputs being known. The table shows the concentration and mixture density increasing each experiment. The sediment flux and discharge velocity stay constant and the total volume flow and diffuser area decrease. The experiment scale is 1:15. The larger scale of 1:10 could not be achieved due to the large volume flows involved and the capacity of the available pumps. A smaller scale would require discharge velocities of above the full-scale discharge velocity in order to remain in the turbulent mixing regime.
Table 3.9 shows that the buoyant jets for all experiments have a Richardson number well below unity. This means that it is to be expected that these jets will show jet-like behaviour at the source. The table furthermore shows that the ratio of momentum flux and buoyancy flux at the source is much higher for a volumetric concentration of 1% than it is for 4 or 7%. This is caused by the much larger volume flow required for the volumetric concentration of 1%. This will results in a buoyant jet having a much larger range than that of the 4 and 7% experiments.

Table 3.8: Table summarizing the important parameters of the three experiments. Increasing the volumetric concentrations leads to a larger density and a smaller volume flow and diffuser area

Experiment	Density [kg/m^3]	Sediment flux [g/s]	Concentration [g/L]	Volume flow [L/s]	Discharge velocity [m/s]	Diffuser area [cm^2]
#1 (C_v = 7%)	1105	29.4	175	0.17	0.27	6.2
#2 (C_v = 4%)	1060	29.4	100	0.29	0.27	10.9
#3 (C_v = 1%)	1015	29.4	25	1.20	0.27	43.4

Table 3.9: Table summarizing important source parameters for all three experiments. Increasing the concentration results in a smaller momentum flux while the buoyancy is preserved.

Experiment	Momentum flux [m^4/s^2] (*10^{-5})	Buoyancy flux [m^4/s^3] (*10^{-4})	L_m [m]	L_Q [m]	L_M [m]	R_0 [-]
#1 (C_v = 7%)	4.55	1.73	1.30	0.025	0.042	0.59
#2 (C_v = 4%)	7.97	1.73	1.72	0.033	0.064	0.51
#3 (C_v = 1%)	31.9	1.73	3.43	0.066	0.18	0.36

3.5 Measurement techniques

During the experiments data is gathered in a number of ways. In the subsections below, each measurement technique is described in detail.

3.5.1 Flow velocity and concentration profiles

During the experiments the ADV will be used for measuring the velocity and SNR. As explained before, the SNR can be used to determine the sediment concentration and requires calibration in order to do so. The ADV performs 30 simultaneous measurements over a 30 mm profile, leading to a spacing of 1 mm between each

data point. The accuracy however is not the same across the entire measuring volume. The boundaries of the profile are known to have a lower correlation and SNR value. This could lead to wrong velocities being measured and wrong concentrations being calculated.

Profile stacking procedure

This lower accuracy of the profile boundaries has consequences for the measuring procedure. As explained before, the ADV measures velocity and SNR values over a 30 mm profile as stated before. As it is expected that the actual turbidity current during the experiments will exceed this height, it will be necessary to perform measurements at different heights and combine the results in order to construct a complete velocity and concentration profile for that specific location.

For making the profiles, a measurement will be performed for a predetermined amount of time, after which the results will be averaged over time. Afterwards, the ADV will be relocated to a higher position for the next measurement. It should be noted that after the relocation of the ADV, the flow should be given some time to recover from this disturbance. Each relocation will be a 15 mm increase in height. The reason for this is the higher accuracy that the centre of the profile offers [95]. By having multiple 30 mm profiles overlap this way, the inaccurate measurements at the profile boundaries can be omitted. Afterwards a velocity profile can be constructed containing a value at every millimetre.

The SNR values that will be used for calculating the concentration are measured simultaneously with the velocity, but the concentration profiles will be constructed differently. As mentioned above, the measurements at the profile boundaries are inaccurate and this is especially true for the SNR, which has a parabolic shaped profile. This results in significantly lower SNR values at the boundaries compared to the profile centre. For this reason, only the SNR values of the 'high accuracy' region of the ADV will be used, laying between 5 and 20 mm [95] [96]. Furthermore, because the parabolic shape of the SNR profile is still visible in this region, even for homogeneous mixtures, it has been decided that the concentration can be calculated more accurately by taking the average SNR value over this 15 mm 'high accuracy' region. This way a single, time averaged SNR value is found for 15 mm intervals over the total concentration profile. The calibration curve, relating SNR values to concentrations, has been constructed using this same method as can be found below. This results in concentration profiles with less data points than the velocity profiles, but a higher certainty than otherwise would be the case.

Figure 3.7: This schematic gives an impression of the overlap the will be applied to the measured profiles. The green area being the 'high accuracy' region, located between 5 and 20 mm as measured from the top of the profile, and the red being the area of which the values will be discarded

ADV calibration

The calibration was performed using a bucket, a mixer and an ADV. The bucket was filled with 6 litres of water, after which sediment was added step-by-step. Beforehand calculations were made regarding the amount

of sediment to add to acquire certain concentrations. Between 1 and 10 g/L steps of 1 g/L were taken. From 10 g/L to 50 g/L, steps of 5 g/L were taken and from 50 g/L onwards, steps of 10 g/L were taken up to a maximum of 180 g/L. The reason for the smaller steps at lower concentrations is because the concentration at which the maximum SNR value occurs had to be found, and relatively high changes in the measured SNR values were found at low concentrations when compared to the SNR differences measured between higher concentrations.
The resulting plot of the concentration as a function of the SNR (Figure 3.8) shows an increase in SNR values up to a concentration of 6 g/L. For higher concentrations the SNR decreases. Measurements have been performed up to concentrations of 180 g/L, corresponding to a volumetric concentration of 7.2%. It was found that for higher concentrations the SNR drops below 30 dB. Since the manufacturer recommends not to work with SNR values of below 30 dB, it has been concluded that for this sediment type this method is only applicable up to a concentration of 180 g/L. Because the highest initial concentration that will be experimented with equals 7% and is expected that the concentration only decrease after leaving the diffuser due to dilution, this method will be applicable throughout the experiments. The literature reviewed in section 2.6.2 mentioned a maximum concentration of 50 g/L for this method, far lower than the maximum concentration in this calibration. Those reports state that measurements have been performed for higher concentrations but this data showed low correlation. During the calibration it was found that the correlation of the signals drops below 40 for concentration above 50 g/L, or a volumetric concentration of 2%, as reported by literature. After that the correlation decreases with increasing concentration to a minimum of 25 for the highest concentration (180 g/L). The Nortek manual states that the correlation as measured by the velocimeters should be above 70% for generating good quality data, and above 40% for average data [95]. This has to be taken into account during the data analysis of the experiments, as it implies that the data might be unreliable. It is however expected that the initial concentration decreases quickly due to dilution allowing accurate concentration measurements further downstream. During the initial phase of the plume however this might result in inaccurate measurements. This should be taken into account during the data analysis.

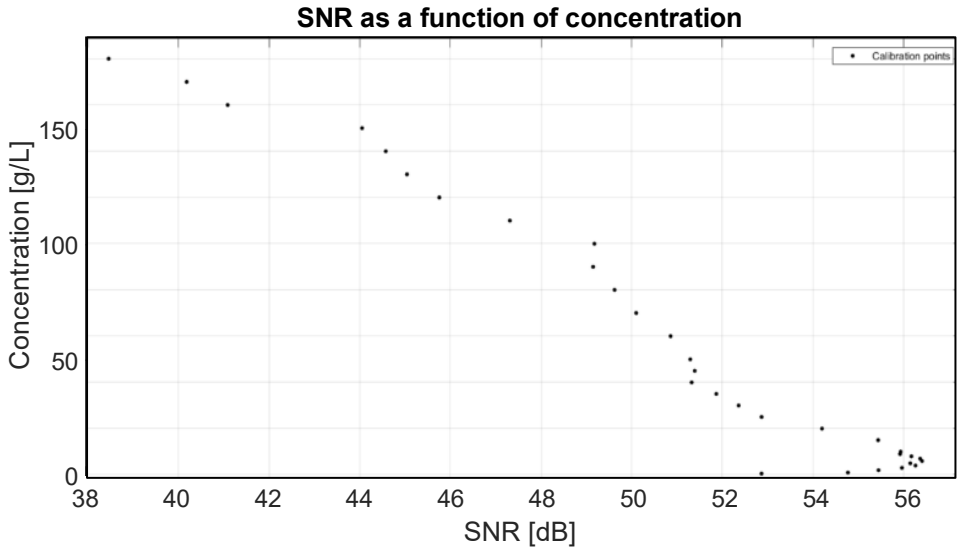

Figure 3.8: This figure shows all the collected SNR values plotted for their respective concentration. For the low concentrations (0.5-6 g/L) a quick increase in SNR value with concentration can be observed. For concentration higher than 6 g/L the SNR value decreases.

To get a better understanding of the effect the concentration of suspended solids has on the correlation, a measurement has been performed which was started at the instant the mixer was taken out. At this point the water kept flowing in the bucket but in a less chaotic and turbulent way. It is assumed that from the moment the mixer is taken out, the homogeneous concentration starts to become more stratified as particles start to settle, resulting in a continuously decreasing concentration at the location of the ADV. The SNR data measured during this experiment confirms this and shows first an increase in SNR values after which it decreases again to the 'clear water' values. During the individual concentration measurements it was found that the concentration related to this 'turning point' is 6 g/L. More importantly, the correlation of this data shows much higher values than that of the individual measurements. The correlation was shown to be consistently above

70 for all data except for the first few seconds of measuring. During this instance the velocity data is still fluctuating heavily, but after 10 seconds the velocity became constantly positive or negative. The SNR values at which this correlation became higher than 70 correspond to about 130 to 140 g/L. Because of this observation, it was suspected that the low correlation that was observed during some of the calibration measurements is due to the heavily chaotic mixing and turbulence, and not because of the high concentrations. Manuals of NORTEK and SonTek (another manufacturer of ADVs) confirm this finding by stating the low correlations can be caused by turbulence [95] [97]. The NORTEK manual furthermore states that the SNR is not necessarily affected by this, again confirming the findings of the calibration, which found a continuous decrease of the SNR for high concentrations, which could be reproduced in a separate calibration despite the correlation being low.

Calibration curve for spherical glass particles

The averaged SNR values could be used in a fitting tool in MATLAB to find a function representing the curve. The y-axis shows the concentration in g/L and the x-axis shows the total SNR in dB. This way the computed function can be used to calculate the concentration as a function of the SNR. After analysing the data it was found that two separate calibration curves had to be created. The reason for this is the SNR value reaching its maximum at a concentration of 6 g/L (C_v = 0.22%). Because of this, certain SNR values correspond to two concentration values, and no function can be found that fits all the data points. This resulted in one calibration curve for a high range of concentrations, being 6-180 g/L (0.24-7.2 %), and one calibration curve for all lower concentrations, being 0.5-6 g/L (0.02-0.24 %). Because more precision was required, it was ultimately decided to split the high concentration regime into two, resulting in a medium and high concentration regime. These cover 6-50 g/L and 50-180 g/L respectively. Figure 3.9 shows an example of one of the resulting plots, in this case for the high concentration range. During the creation of the plots, the data points of the measured SNR corresponding to the concentrations of 5, 9 40 and 100 g/L were discarded due to them being outliers.

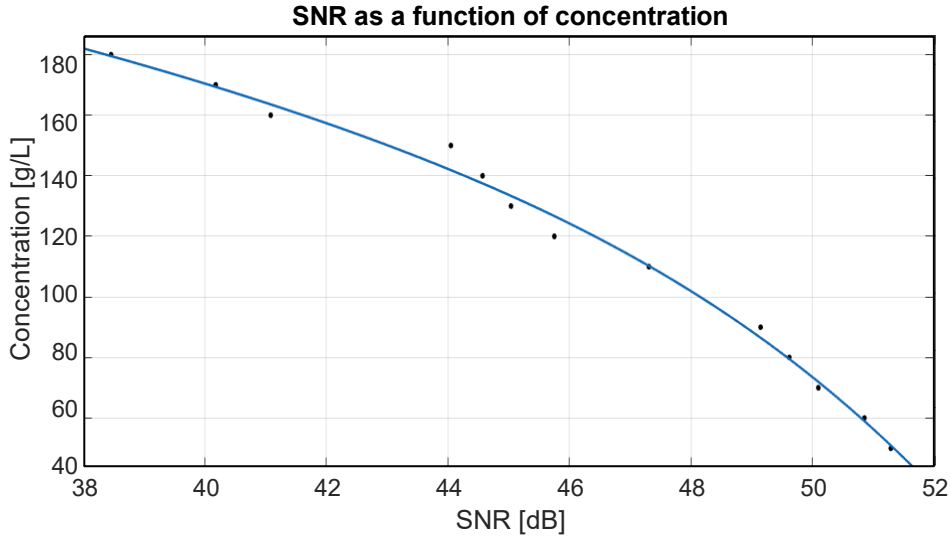

Figure 3.9: This figure shows the data point as seen in Figure 3.8 for concentrations of 50 g/L and above. This resulted in the possibility to find a function that fits the data points and is applicable for calculating the concentration based on measured SNR values for the range of high concentrations. The x-axis shows the SNR in dB and the y-axis shows the concentration in g/L

The fitting tool resulted in the following equations for the high, medium and low concentrations respectively:

$$Conc = -0.001096 * SNR^4 + 0.1691 * SNR^3 - 9.944 * SNR^2 + 258.5 * SNR - 2274 \quad (32)$$

$$Conc = 1.07 * 10^5 * e^{-\left(\frac{SNR-27.15}{8.687}\right)^2} + 14.34 * e^{-\left(\frac{SNR-54.4}{2.05}\right)^2} \quad (33)$$

$$Conc = \frac{39 * SNR^2 - 1872 * SNR - 68.12}{SNR^3 - 225.1 * SNR^2 + 9566 * SNR + 348.1} \quad (34)$$

All curves show a high correlation with the R^2 being between 0.985 and 0.994. Furthermore, both curves have been used to calculate concentrations based on SNR values measured in known concentrations and showed good results.

Calibration curve for clay

The same calibration procedure as for the glass particles has been performed with clay mixtures. The results of this are however very different. Three separate calibrations have been performed using clay mixtures of known concentrations. It was found that all three calibrations resulted is highly varying SNR values. The overall shape of the SNR as a function of concentration graphs were similar, and maxima in terms of SNR values were found in the same 5-10 g/L region, but the magnitude of the SNR values differed highly between the experiments.

Looking into this problem by analysing the known theoretical background as discussed in section 2.6 as well as looking into literature regarding acoustic measurements in clay has resulted in the following conclusions. First of all, by examining the theoretical background, it is believed that due to aggregation the particle size distribution is highly alternating between different mixtures as well as over time in the same mixture. As can be seen in section 2.6.2, the particle diameter has a significant impact on the characteristics of the mixture regarding its absorption, which could explain the different SNR values being measured by the ADV. As Figure 2.9 to Figure 2.11 show, an increase in particle size due to flocculation can lead to the attenuation factor being multiple times higher or lower than before flocculation occurred. The clay particles used have individual diameter of between 20 and 25 microns. It can be seen in the graphs that this corresponds to a region of low attenuation. Further investigation of the graphs shows that aggregation of these particles will most likely lead to higher attenuation factor and hence, a lower SNR.

Experiments described in literature showed similar observations and conclusions when performing concentration measurements in clay mixtures using ADVs. It has been found that the scattering properties of cohesive sediments, such as clay, are greatly affected by aggregation [98]. A series of laboratory experiments have shown that the acoustic properties of aggregated particles are not solely controlled by the primary particles. It was concluded that the structure of the flocs influences the scattering characteristics of the mixture involved. It was also found that an empirical relationship can be fitted, but still holds uncertainties due to a limited theoretical understanding of how aggregated particles interact with acoustic signals [89] [98]. Furthermore, measurements performed in the Yangtze Estuary also found errors in SSC estimates using both optic and acoustic sensors. The size of the flocs showed strong variations over time and are believed to be the source of the errors in SSC estimates, as the influence of grain size on the acoustic response of mixtures is also acknowledged here [99].

To conclude, it has been shown that the structure of the flocculated particles influences the scattering properties of the mixture. Furthermore, based on the known dependency of the scattering characteristics on the diameter of the particles involved, it has been concluded that also the effective diameter of the different particles and the changing PSD over time plays a part in the highly fluctuating SNR values measured in mixtures of the same concentration expressed in g/L.

3.5.2 Video recordings

Video recordings will be captured from a side and top view. The side view will be captured using a FASTEC IL5 high speed camera. This camera has been setup to have a resolution of 1920 x 810, a frame rate of 120 fps and a shutter speed of 1/250 second (4 ms). The frame rate is chosen such that the video can be slowed down up to 5 times and still be played at 24 fps, a regular frame rate for videos. A higher frame rate and resolution allow for more detail and slow motion, but at the cost of a larger file size.

For the top view video recordings, a GoPro HERO 7 will be used. The goal of the top view is to capture the outflow shape and deposition pattern of the turbidity current. In order to capture usable videos of the turbidity currents the table on which the current flows is fitted with LED strips. In order to diffuse the light from these sources, polyethylene (PE) plastic sheets were applied to plexiglass plates to cover the LED lights. Some distance was kept between the plastic and the lights which increases the diffusing of the light. It was found that one layer was required to sufficiently diffuse the LED light. The light from below allows for post video

processing during which the contour lines of the bed shape can be identified. This way the different shapes and dimensions of the resulting sediment bed can be compared. The side view of the turbidity current can be used to identify the front velocity of the current during the initial phase, as well as its height. It furthermore allows for a comparison of the jet/plume trajectory and impingement angle of the different experiments.

3.6 Experimental procedure

All the experiments have the same basic steps that have to be taken in order to complete them successfully.

Preparations

Step 1 Fill the modular tank with tap water to the required height

Step 2 Install and check the KATflow meter

Step 3 Install the correct diffuser

Step 4 Start the mixing pumps and prepare the water-sediment mixture in the mixture tank to acquire the desired concentration

Step 5 Fix ADV position
Fix camera settings and position (if applicable)

Step 6 Cover modular tank with blackout curtains (if applicable)

The experiment

Step 7 Start the KATflow meter
Start the camera recording (if applicable)

Step 8 Start the centrifugal pump
Regulate the flow to a uniform and constant flow rate as desired for the experiment
Wait till steady state is reached

Step 9 Start velocity and SNR measurement of ADV
Stop ADV measurement

Step 10 Relocate ADV for next measurement (adjust height by 15 mm)
Start velocity and SNR measurement of ADV
Stop ADV measurement

Step 11 Repeat step 10 until a full profile has been measured

Step 12 Stop the camera recording (if applicable)
Stop the KATflow meter

Step 13 Stop the centrifugal pump
Stop the mixing pumps

Step 14 Removing sediment of table

End

4. Experiment results and analysis

This chapter displays and explains the results of the experiments. Actions performed for visualising the results are explained and shown for one of the experiments, with the remaining velocity, correlation, SNR and concentration profiles being shown in the appendices.
The first section elaborates on changes that were made to the experiments resulting in alterations from the initially planned experiments. These changes were due to physical limitations of the experiment setup. Sections 2 and 3 discuss the velocity and concentration data respectively, also elaborating on the statistical analysis. Section 4 focusses mainly on the characteristics of the plume and turbidity current around the impingement region. Lastly, section 5 discusses the results found during an experiment that has been performed using clay as a sediment instead of the spherical glass particles that have been used for all other experiments.

4.1 Adjustments to experiments

During initial tests of the experimental setups two flaws have been discovered which led to an alteration of the experimental matrix. These flaws are fall-out of sediment at the diffuser outlet and the inability to keep a volumetric concentration of 7% (175 g/L) in suspension. As a result, the volume flow of each experiment was increased and the concentration of each experiment was decreased, the reasons for which will be explained below.

Increase in volume flow

The first experiments were performed with the smallest diffuser and thus the highest concentration. The reason for this is the expectation that if any problems would arise regarding the setup it would be most likely to happen during the high concentration experiments as this gives problems with keeping everything in suspension.
During these initial tests it was found that at the intended discharge velocity of 0.27 m/s, corresponding to a volume flow of 0.17 L/s for this smallest diffuser, sediment fell out of the diffuser underneath the buoyant jet. Based on the visual observations this seems to be due to sediment not being in suspension but sliding over the bottom of the diffuser, otherwise known as a sliding bed. During earlier research in the TU Delft dredging lab using the same setup, this phenomena was also observed. Tests during this earlier research ruled out that the fall-out is caused by alignment of the diffuser, the valves or the diffuser surface. One solution to stop the sediment from falling out is to increase the flow rate and thus discharge velocity. For the experiments in this report it was found that the flow rate needs to be increased to at least 0.24 L/s to prevent the sediment fall-out from occurring. Due to a limited pump capacity however, ultimately the decision was made to increase the flow rate to 0.20 L/s, corresponding to a discharge velocity of 0.315 m/s. The reason for this is the maximum pump capacity of 1.4 L/s, which therefore served as the maximum achievable flow rate value for the experiment with the largest flow rate and diffuser. Ultimately this has led to an increase of the discharge velocity and flow rates for each experiment of 16.5%. At these new flow rates sediment fall out only occurred for the smallest diffuser/largest concentration experiment and concentrations measurements using the ADV pointed out that the amount of sediment falling out was negligible.

Decrease in concentration

Another alteration to the experiments was made because the maximum concentration that could be kept in suspension in the mixing was lower than the intended 7%. During tests it was found that the maximum concentration that could be kept in suspension for a longer period of time was 5.6%, corresponding to 140 g/L. This led to a 20% decrease in concentration for each experiment.

Adjusted experiment matrix

Table 4.1 and Table 4.2 below shows the new experimental matrix, resulting from the changes described above. The main differences are the increase in discharge velocity and decrease in concentration. Due to the opposite effects that decreasing the concentration and increasing the flow rate have on the sediment flux, this value only slightly decreased. The combined effect of the decrease in concentration and increase in discharge velocity results in the momentum/buoyancy flux ratio to increase for each experiment. It is expected that as a

result the plumes will impinge the bed further away from the diffuser than otherwise would have been the case. The changes are expected to have no further impact on the scientific value and comparison of the results.

Table 4.1: Table summarizing the important parameters of the three experiments. Increasing the volumetric concentrations leads to a larger density and a smaller volume flow and diffuser area

Experiment	Density [kg/m^3]	Sediment flux [g/s]	Concentration [g/L]	Volume flow [L/s]	Discharge velocity [m/s]	Diffuser area [cm^2]
#1 (C_v = 5.6%)	1084	28	140	0.20	0.32	6.2
#2 (C_v = 3.2%)	1048	28	80	0.34	0.32	10.9
#3 (C_v = 0.8%)	1012	28	20	1.40	0.32	43.4

Table 4.2: Table summarizing important source parameters for all three experiments. Increasing the concentration results in a smaller momentum flux while the buoyancy is preserved.

Experiment	Momentum flux [m^4/s^2] (*10^{-5})	Buoyancy flux [m^4/s^3] (*10^{-4})	L_m [m]	L_Q [m]	L_M [m]	R_0 [-]
#1 (C_v = 5.6%)	6.2	1.62	1.51	0.025	0.049	0.51
#2 (C_v = 3.2%)	10.8	1.62	2.00	0.033	0.075	0.44
#3 (C_v = 0.8%)	43.4	1.62	4.00	0.066	0.21	0.31

4.2 Turbidity current velocity

The velocity profiles have been created using measurements performed by the ADV. The data was processed in ways that will be explained in the next subsection. This section will only give a few examples of the created velocity profiles for the purpose of explaining the data processing as well as showing the key observations. For the complete collection of created velocity profiles one should consult Appendix A.

4.2.1 *Velocity profiles*

The velocity profiles have been created using the stacked profiles measured by the ADV as explained in the previous chapter. For most measurements the ADV was first placed 6 cm above the bottom. As explained in section 3.5.1, this allowed for a measurement in the high accuracy region of the ADV, being located between 4.5 and 6.0 cm away from the ADV itself. Measurements were performed for a period of 30 seconds before the ADV was relocated to a position 1.5 cm higher. This process was repeated until a height was reached at which the ADV showed low correlations, a velocity of around zero and/or an SNR of below 30. Profiles have been made for six different horizontal distances from the diffuser mouth. The first measurement (1A) was performed directly in front of the diffuser, at 3.3 cm. This distance equals two times the hydraulic diameter of the smallest diffuser. The next three measurement locations were determined based on the observed impingement distance. One profile was measured at the identified impingement point (3A), and two others were measured at 10 cm before and 20 cm after the impingement point (2A and 4A respectively). The last two profiles have been measured at a constant distant from the diffuser, being 100 (5A) and 150 cm (6A). The three constant measurement locations have the purpose of being a direct comparison between the profiles of the different diffusers. The three varying locations have been chosen to acquire insight into the velocity changes in and around the impingement point, which differs between diffusers, an automatic result of this being that these locations change per diffuser. Per diffuser also one profile was measured in the lateral direction, 20 cm to the side at the impingement distance (3B). It should be noted that for the experiment using the largest diffuser the impingement distance is significantly larger than for the first two diffusers. As a result an additional measurement location (7A) was added at 200 cm from the diffuser.
The time averaged value over the 30-second measurement period have been calculated to create the velocity profiles. In the profiles, the x-axis shows the velocity in m/s and the y-axis shows the height above the bottom in millimetres. The diffuser heartline is located at a height of 300 mm and is indicated by the horizontal line in the plots. Figure 4.2 below shows an example of one of the velocity profiles resulting from the experiments. Figure 4.1 shows the six (normalised) velocity profiles of each diffuser in one image. The horizontal axis shows the distance of the profile from the diffuser.

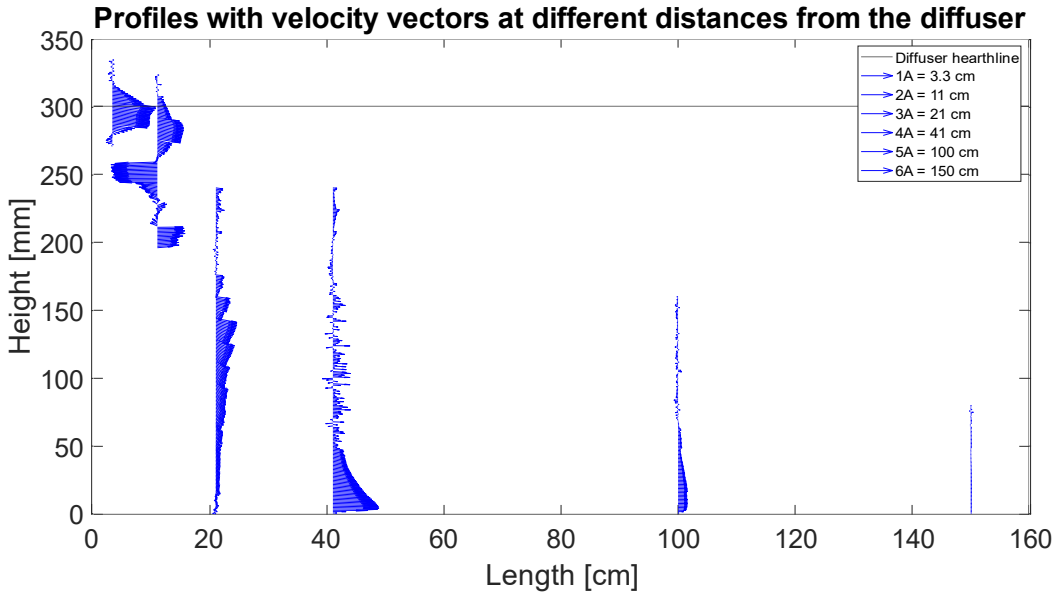

(a) Velocity vectors for diffuser 1 (concentration of 140 g/L)

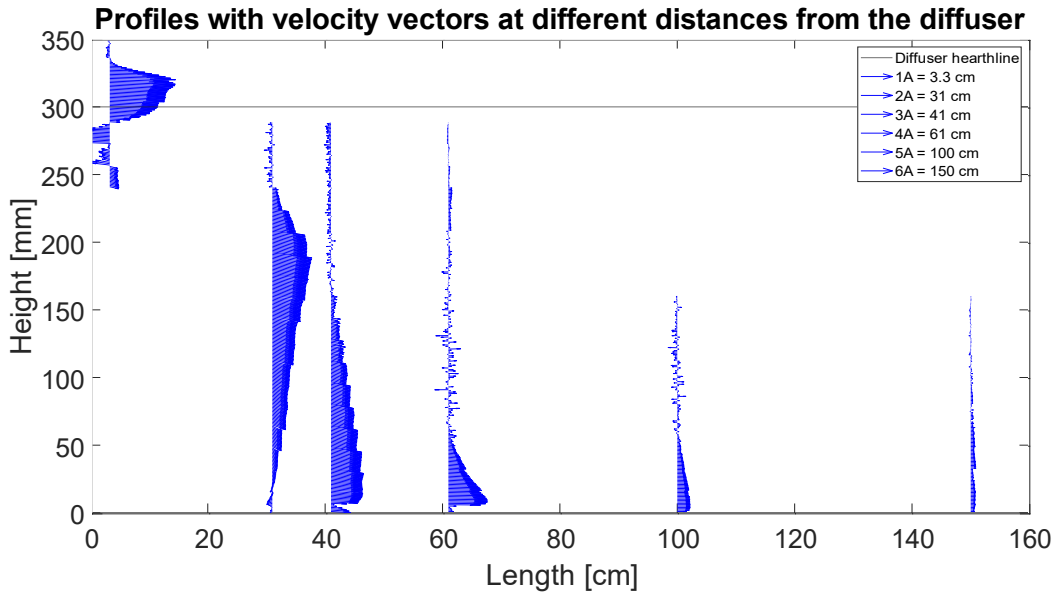

(b) Velocity vectors for diffuser 2 (concentration of 80 g/L)

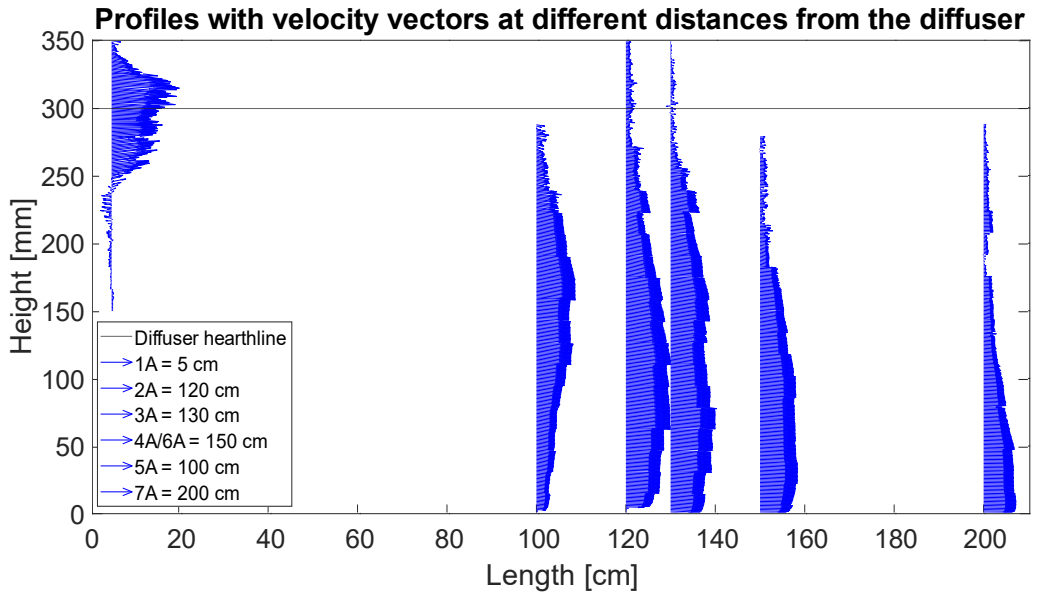

(c) Velocity vectors for diffuser 3 (concentration of 20 g/L)

Figure 4.1: (Normalised) velocity profiles (vectors of the velocity in x and z direction) at different distances from the diffuser mouth

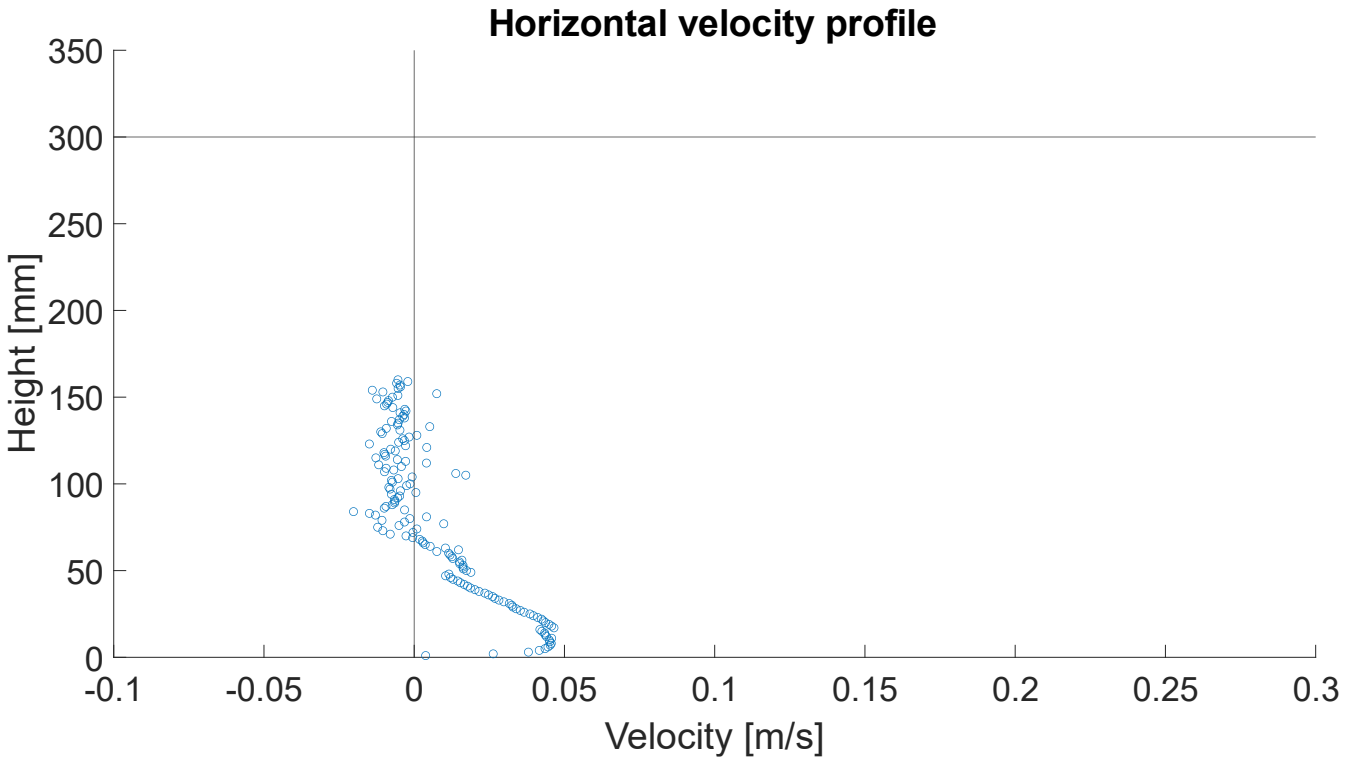

Figure 4.2: Zoomed in velocity profile of diffuser 1 at location 5A (100 cm from the diffuser mouth)

4.2.2 Analysis of velocity profiles

Analysing the data involves both comparing the results of different diffusers to find the effect of different initial concentrations on the velocity away from the diffuser, as well as a statistical analysis of the data to make sure the right conclusions can be drawn. Visualising the data after statistical analysis can furthermore reveal properties of the velocity signal and processes inside the turbidity current which before where hidden. For analysing the data a Fourier transform has been used to plot the data points into the frequency domain. This allows to identify the presence of peaks in the signal at certain frequencies, which indicate a certain periodicity in the signal. An example of what can cause periodicity in the velocity signal are turbulent phenomena such as eddies. If peaks are found in the signal at certain frequencies a filter can be applied to the data which isolates that data points corresponding to the dominant frequencies. This allows for the filtered data to be plotted as a function of time to visualise the periodicity. The individual data points were also plotted into a histogram to see how the data is distributed around the mean. This way it can be determined whether the mean value is a good estimate for the velocity, which can be shown by having a normal distribution. Also the correlation data measured by the ADV can be used for analysing the velocity data. As mentioned before a correlation of above 70 corresponds to good data and a reliable velocity measurement. The correlation as a function of profile height can be found in Appendix B.

The results of the statistical analysis of the velocity data have shown no clear periodicity in the signal. Plotting the velocity data in the frequency domain has led to the conclusion that there is no clear dominant frequency in the velocity signal, as panel (a) of Figure 4.3 shows. The histograms that were created using the individual velocity signal data points of a single height of the profile showed a normal distribution around the mean, indicating that the time averaged value is a good indication of the velocity inside the turbidity current, as can be observed in panels (b) and (c) of Figure 4.3.
Looking into the measured correlation data, it was found that some measurements show a low correlation at certain parts of the profile. It is known from the manufacturer that this can be caused by both a low amount of scatterers or turbulence, the latter of which has also been confirmed in earlier researches [100] [101]. In combination with the SNR the cause of the low correlation can be determined. A low correlation and low SNR most likely is the result of a very low concentration, causing the signal of the ADV to be not reflected properly.

Situations in which this occurred were when measuring in a tank of clean water, or far above the turbidity current during experiments. If a low correlation is found in combination with a high SNR (> 30) however, the cause is most likely a highly turbulent flow. This combination of low correlation but a sufficiently high SNR occurred during multiple measurement, especially for the locations 4A and 5A, upstream from the impingement point. Figure 4.4 shows one of these profiles. It can be observed that at the heights where the correlation drops below 70, the time averaged velocity heavily fluctuates between positive and negative values, with magnitudes that are larger than that of the velocity above and below this region. Visual observations of the experiments have led to the conclusion that these low correlations are indeed the result of turbulence in the flow. Figure 4.5 shows a still from the captured video, with the red lines approximating the height at which the correlation drops below 70. The videos have shown vortices being active in this region of the turbidity current. These large eddies appear to be Kelvin-Helmholtz instabilities. These instabilities occur at the interface between two fluids with different velocities, as is the case for the moving turbidity current and almost static fluid above it. This phenomenon is present at all the experiments performed for this research and is believed to be the cause for the unreliable velocity measurements at the interface between the turbidity current and clear water above it. The presence of eddies in the flow can also be observed in velocity profile 2A of diffuser 1, shown in Appendix A and Figure 4.1, by observing the negative velocity components.

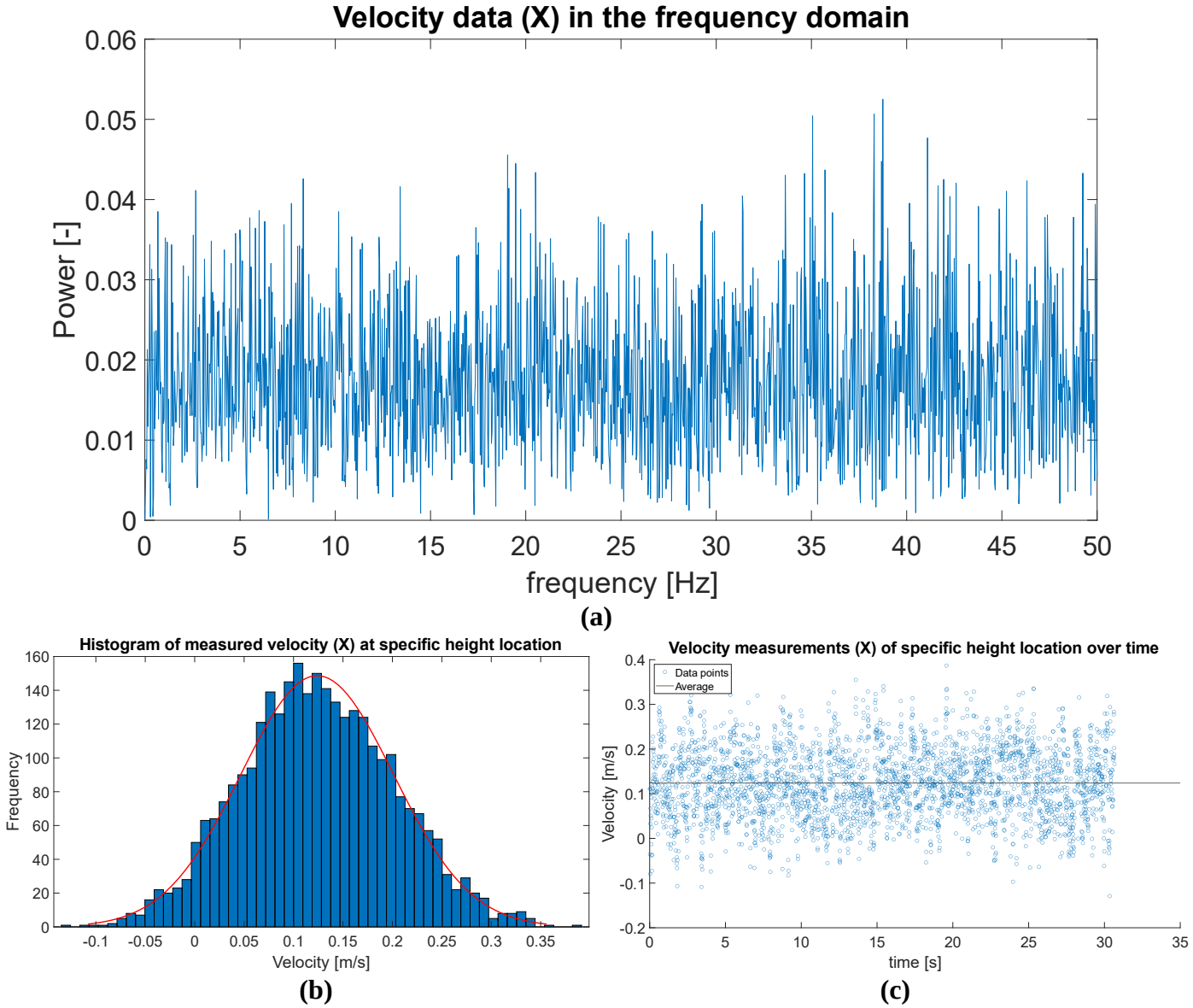

Figure 4.3: Statistical analysis of one of the velocity profiles (diffuser 1, location 2A). (a) data points of 1 specific height location of the profile in the frequency domain. (b) Histogram of the data with in red a normal distribution as reference. (c) measured velocity over time

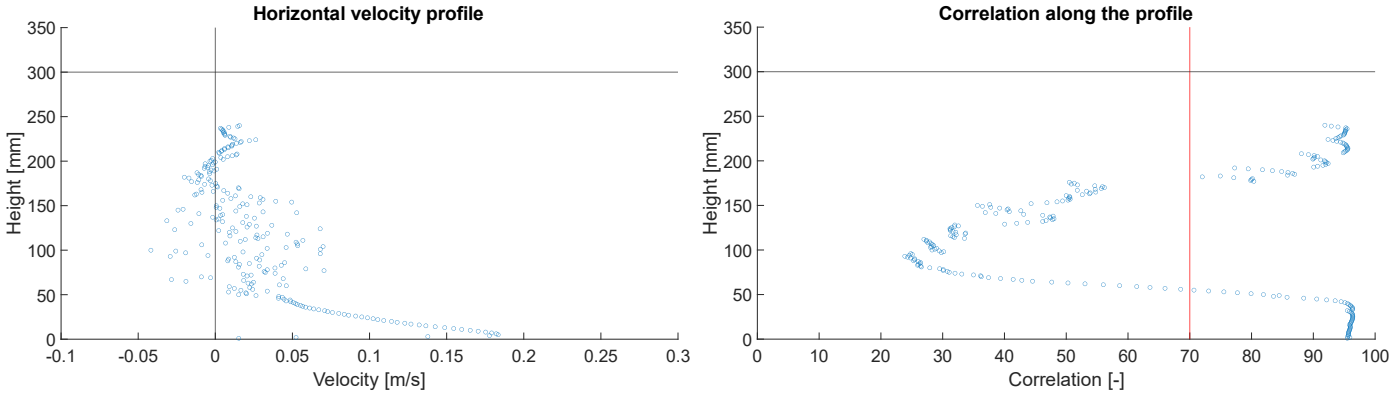

Figure 4.4: Velocity and corresponding correlation profile measured for diffuser 1 at location 4A. The correlation profile shows that at the height at which the correlation is below 70 (indicated by the red vertical line), the velocity in the profile starts fluctuating heavily

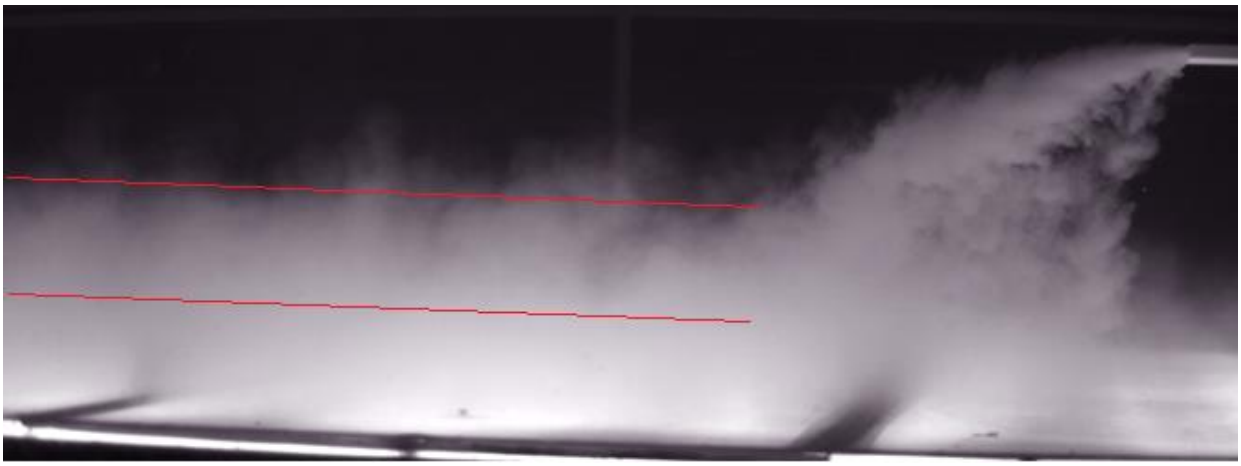

Figure 4.5: Still from the high speed camera recordings showing the steady-state of the flow from the diffuser. The region between the red lines is the height in the turbidity current associated with the low correlation, believed to be caused by Kelvin-Helmholtz instabilities.

Apart from the statistical analysis and visual observations, the data of the different experiments can be compared to directly observe the changes caused by the difference in concentration between the different experiments. When comparing the velocity profiles of the different experiments, there are mainly two locations of interest. These are the impingement points, which give insight into how the different initial concentrations influence the processes at this location, and locations 5A and 6A, which are located at the same absolute distance from the diffuser mouth for all experiments, allowing for a direct comparison of the velocity profiles further upstream.

In the impingement region, one of the key observations has been the increase in measured velocity after impingement, which can be observed when comparing profiles 3A and 4A in Figure 4.1. This increase has been observed for all experiments, but was significantly larger for the experiment with the highest initial concentration. This leads to the conclusion that the impingement is more aggressive for higher initial concentrations at constant diffuser height. This aggressive impingement and the resulting high velocities could pose a problem for deep sea mining operations as it could lead to the resuspension of bed material. The critical velocity for this to happen depends on the type of bed sediment as well as on the degree of consolidation of the bed [5]. Another notable difference between the experiments is the velocity component sideways to the discharge direction that was measured 20 cm to the left of the impingement point for all experiments. It was found that this velocity component is highest for the experiment with the largest initial concentration, being 1.4 and 2 times larger in magnitude than for diffuser 2 and 3 respectively. This is an interesting finding for deep sea mining as sediment transport in this direction is undesirable as it may lead to the burying of nodules which could decrease the production of the miner.

When comparing locations 5A and 6A of different diffusers Figure 4.1, it is observed that the larger the initial concentration, the lower the velocity at these locations. This means that a larger initial concentration results in the turbidity current dying out and the sediment transport being halted closer to the diffuser, as is shown in Figure 4.1. It should be noted that this total distance is a combination of the impingement distance and runout distance, which will be elaborated on further in section 4.4 and 4.5 respectively.

4.3 Turbidity current concentration

The concentration inside the plume and turbidity current have been determined based on the SNR measured by the ADV. It gives an indication of the decrease in concentration away from the source. A decrease in concentration is caused by both dilution due to the entrainment of ambient water and settling of particles. Combining the concentrations, turbidity current dimensions and velocities gives some valuable insight into the sediment transport away from the diffuser.
This section will only give a few examples of the created concentration profiles for the purpose of explaining the data processing as well as showing the key observations. For the complete collection of created concentration (and SNR) profiles, one should consult Appendix C.

4.3.1 *Concentration profiles*

The SNR data that has been used for creating the concentration profiles has been recorded simultaneously with the velocity. This means that the concentrations profiles have been created for the same locations as have been discussed in section 4.2.1. For processing the data a similar process has been performed as for the velocity. To summarize, the mean value over a 30-second time period is used for creating the profiles, after which the data points were also plotted in a probability density function as well as in the frequency domain to analyse bias and periodic behaviour.
Figure 4.6 below shows an example of one of the created concentration profiles. The x-axis shows the normalised concentration c/c_0, where c_0 is the initial concentration of each diffuser. In the figure below the displayed concentration is the average of a single 15 mm profile. The normalised concentration allows for a better comparison between the different diffusers because it shows the decrease in concentration away from the diffuser relative to the initial value. For equal dimensions of the plume/current this means that a larger decrease indicated more sediment deposition. Some concentration profiles show two values of the concentration at one height, the reason for which is explained in section 3.5.1.

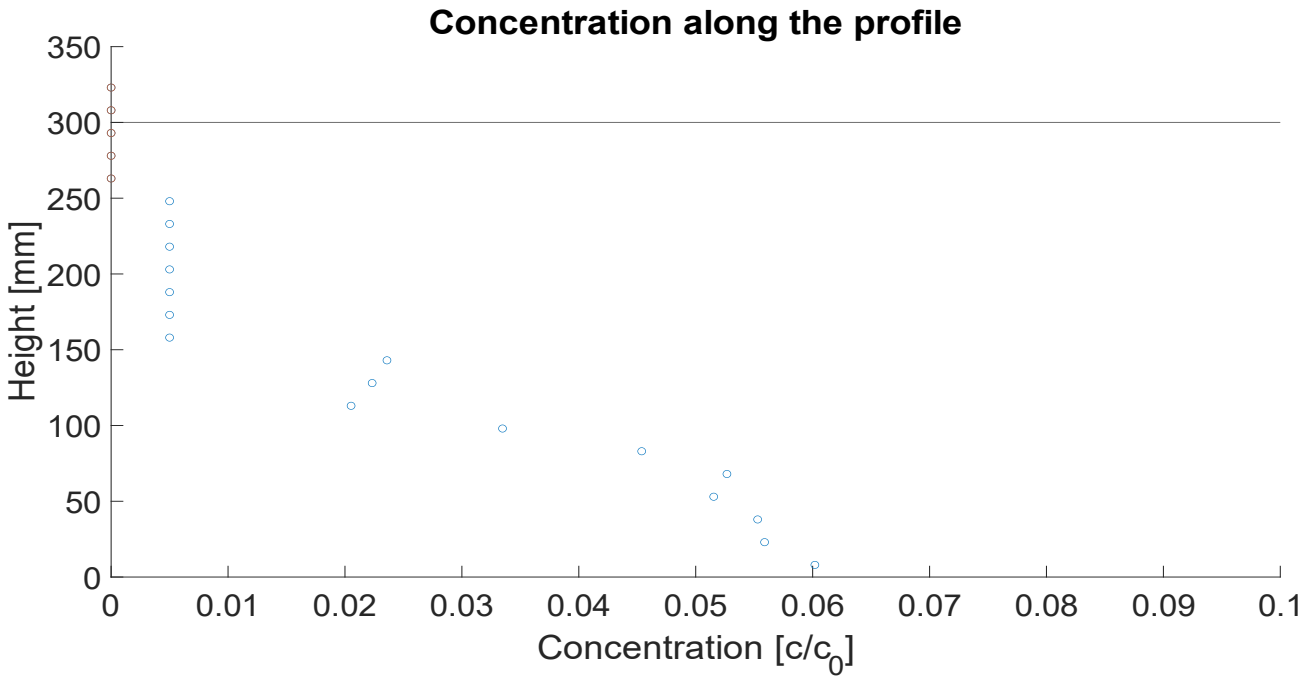

Figure 4.6: Concentration profile of diffuser 3 at location 3A (130 cm from the diffuser mouth)

4.3.2 *Analysis of concentration profiles*

For the analysis of the SNR data the same steps have been undertaken as for the velocity profiles, being the Fourier analysis and putting the data into histograms, which has led to a number of notable observations. When looking at the SNR signal over time, an example of which is displayed in panel (b) of Figure 4.7, one can observe the contours of a periodic motion around the mean. As panel (a) of Figure 4.7 shows, this can be translated into a notable peak at the low range of frequencies between 0 and 0.2 Hz. Based on this, the data

can be filtered and translated back into the time domain using an inverse Fourier transform. The result of this can be seen in panel (c) of Figure 4.7, and reveals the periodic behaviour of the SNR signal. This periodic motion can also be observed in the histograms of the data, by it having a bimodal distribution. The presence of sediment clouds with a seemingly higher density were already observed during the experiments and confirmed during inspection of the videos, captured during the experiments. The SNR data confirms this observation by showing that there is indeed a periodicity in the signal. The cause of this remains unknown. As Figure 4.8 shows, this phenomenon can also be observed at different locations. The left panel of this figure shows the SNR data measured at 4 cm from the bed, while the right panel shows the SNR data at 7 cm from the bed for the same location, profile 4A. The notable difference between them is the way in which the periodicity of the concentration manifests itself in the SNR data. For the location close to the bottom, where the concentration is higher, the SNR shows dips towards lower values. These are believed to be caused by waves of higher concentration, in the concentration range in which an increase in concentration leads to a decrease in SNR, as it was discussed in section 3.5.1. The location further above the bottom, characterised by a lower mean concentration and SNR, shows peaks in the SNR, also believed to be caused by waves of high concentrations. Both these figures show a strong fluctuation of the SNR over time which seem to confirm the visual observation of high density waves inside the turbidity current. Based on this, it was found that the concentration is not as constant over time as the velocity.

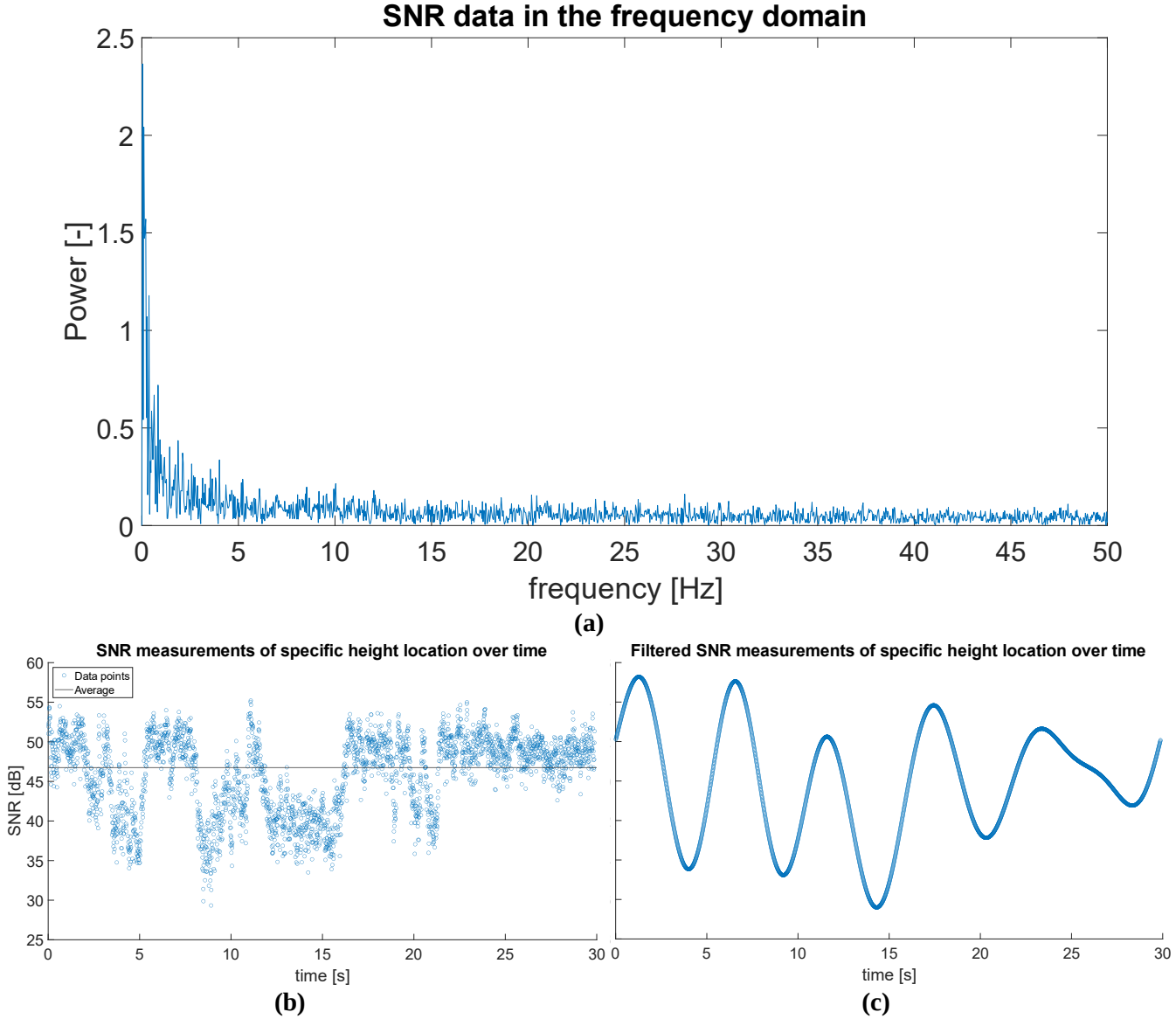

Figure 4.7: Statistical analysis of one of the concentration profiles (diffuser 1, location 5A). (a) data points of 1 specific height location of the profile in the frequency domain, showing large peaks between 0 and 0.4 Hz. (b) measured SNR over time. (c) filtered SNR over time

These figures are an example of the critical attitude required when analysing the SNR data for the purpose of calculating the concentration. As explained before, each SNR value corresponds to two concentration values. Therefore when one takes the time average of the SNR, two possible concentrations follow for that location. For the left panel of Figure 4.8, the time average of the SNR signal is about 48 dB (indicated by the horizontal black line), which would suggest the concentration to be either 0.1 or 105 g/L. Given the initial concentration of this particular experiment and the position of this measurement, the high concentration of 105 g/L as an average seems unlikely, leading to the conclusion that the average concentration over time at this location is 0.1 g/L. However, as stated before, visual observations and SNR measurements at other locations have led to the conclusion that both the SNR and concentration show periodic behaviour, and the dips in SNR values in the left panel of Figure 4.8 are believed to be caused by these observed peaks. By simply taking the average, these dips in the SNR value cause the average SNR to decease, which in term leads to a low calculated concentration, even though observations have shown the dips in the SNR value to be the result of an increase in concentration. And thus using the average of the SNR for determining the concentration may lead to a wrong conclusion. Furthermore, because the relation between the SNR and concentration is not linear, errors will occur when the average SNR is used for determining the average concentration. The average SNR can only be accurately applied for small ranges of SNR values, at which this relation can be assumed to be linear. For larger ranges of measured SNR values, the average concentration should only be calculated by taking the individual SNR values and translating these to individual concentration values, which results in the average concentration over time. As a result, using the average SNR is not the most accurate method for determining the average concentration over time in the turbidity current. To circumnavigate this problem, a solution could be to not use the average SNR, but to use the individual SNR values to calculate the correct concentrations. Afterwards, these concentrations can be averaged over time to find the concentration of the turbidity current. However, despite taking the SNR signal over time, calculating this to concentration values over time and then taking the time average giving a quantitatively more reliable result, it was deemed to labour intensive for the time available, as it would require an inspection of every SNR signal over time for every height at every profile, amounting to about 220 sets of SNR values which require a translation to concentration. This process will have to be done by comparing the SNR signal values with video imagery of every profile. Therefore it was decided, despite the above, to create the profiles of Appendix C using a time average of the SNR value, as combining the SNR and resulting concentration profiles gives a rough indication of the concentrations inside the current. This is argued to be more efficient in determining the general decrease in concentration values away from the diffuser.

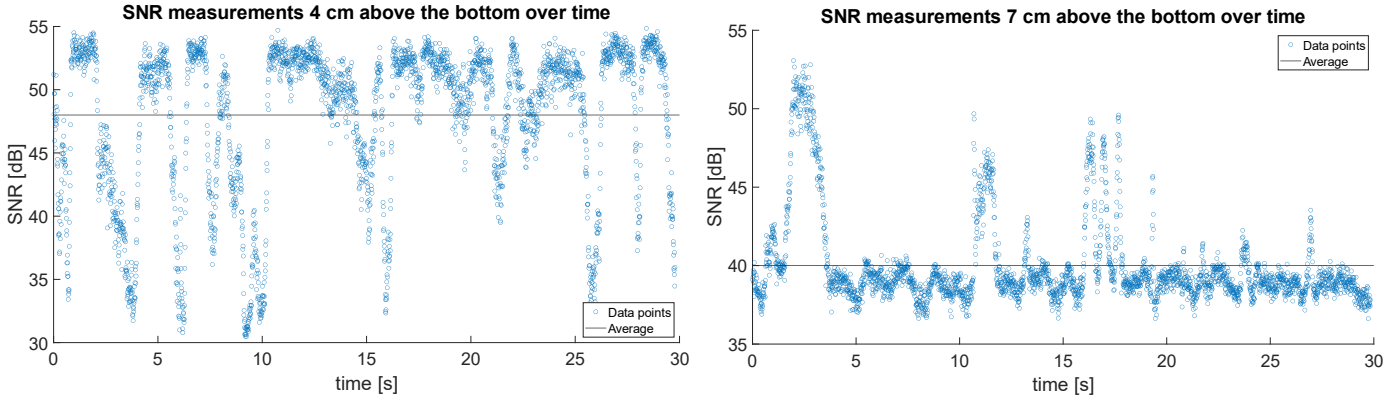

Figure 4.8: The SNR over time for diffuser 1 at location 4A. The panel on the left is from a height of 4 cm above the bed and shows a mean value of 48 dB, with dips in the SNR to around 30-35 dB. The right panel is from a height of 7 cm above the bed and shows a mean value of 40 dB, with peak to around 50 dB. The lower mean value at a larger height (right panel) can be attributed to a lower concentration away from the bed. The dips and peaks in the signal are believed to be due to temporary surges of high concentrations.

When comparing the SNR/concentration measurements of the different diffusers, the following observations have been made. For the experiment with the highest initial concentration of 120 g/L, the dilution in the first phase is the strongest as in decreases to about $1/5^{th}$ of the initial concentration in the first few centimetres of the buoyant jet/plume. Based on the imagery of the final deposition layer as shown in Figure 4.9, this is believed to be caused by the settling of most of the particles in these first centimetres directly after leaving the

diffuser. Next, an increase in the measured SNR value can be observed for all diffusers when comparing the profiles of locations 3A and 4A. Given the expected concentration in this location (low concentration calibration curve regime), the increase in SNR at this location will generally be associated with an increase in concentration. It should however be noted that the height of the profile significantly decreases after impingement. Therefore the increase in SNR is believed to be due to the decreased dimensions which causes the sediment to be pressed into a tighter space, resulting in the concentration to temporarily rise. After location 4A, the SNR starts to decrease again away from the diffuser. A comparison between the SNR measurements of the different diffusers furthermore shows that for location 6A (150 cm form the diffuser), the SNR values for diffuser 1 are the lowest, indicating that, as was the case with the velocity, the SNR decreases the fastest for a higher initial concentration. This leads to the conclusion that for this sediment type a higher initial concentration leads to less spatial spread of the turbidity current.

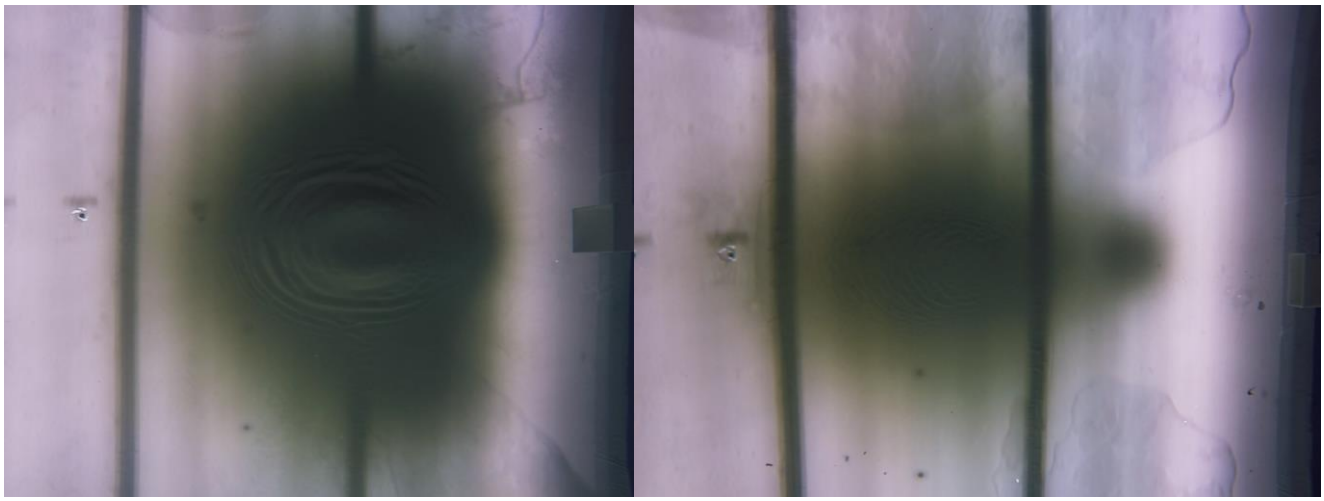

Figure 4.9: Video image of the sediment deposition around the impingement point after 10 minutes of discharging

[This page is intentionally left blank]

4.4 Impingement

The previous two section have already discussed the velocity and SNR behaviour in and directly after the impingement point by comparing locations 3A and 4A, giving insight into the behaviour of the wall jet and turbidity current at this location and the effect of different concentrations. Figure 4.10 shows the emerging turbidity current after impingement for one of the experiments. Comparing the video images of the different experiments reveals further differences between the different concentrations.

When comparing the different experiments in Figure 4.12, the impingement distance is the shortest for diffuser 1, while diffuser 3 can be seen to extend outside the field of view of the camera. The impingement distance for the three experiments have been found to be 21, 41 and 130 cm respectively. The shorter impingement distances for the experiments with higher concentrations is caused by the higher density, which is dominant for the settling of the plume in this phase of the flow. A shorter impingement distance has the direct consequence that the angle at which the plume impinges the bottom with respect to the horizontal is larger (given an equal discharge height), which can also be observed in Figure 4.12. Figure 4.11 shows the top view of the experiments as filmed with a GoPro. These stills show the circular outflow shape that is typically associated with a more vertical impingement. This outflow also explains the higher velocity measured in the direction perpendicular to the discharge direction for these two experiments when compared to the experiment of diffuser 3.

Figure 4.10: Still from the high speed camera recordings of diffuser 2, showing the initial horizontal spread just after impingement, associated with the increase in horizontal velocity as observed by the ADV as discussed in section 4.2.2.

Figure 4.11: Stills from GoPro videos showing the outflow shape of the current the moment after first impingement for diffusers 1 and 2 respectively

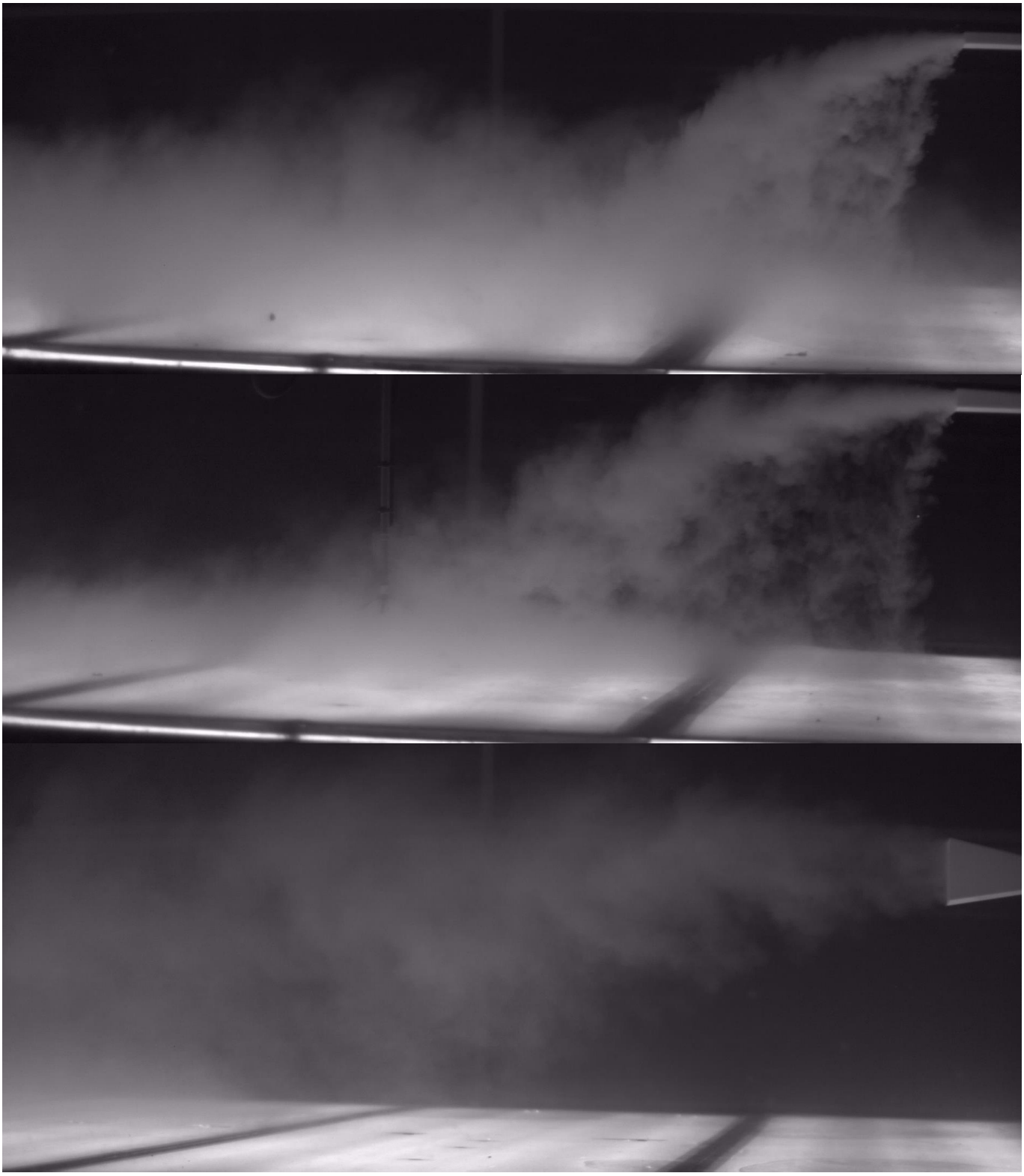

Figure 4.12: Stills from the high speed camera recordings of all three diffusers (diffusers 1, 2 and 3 from top to bottom respectively). Diffuser 1 discharging the mixture with the highest concentration shows a more vertical impingement closer to the diffuser. These stills show that the lower the concentration becomes (higher momentum/buoyancy ratio), the larger the impingement distance and the smaller the impingement angle with the bed.

4.5 Analysis of the runout distance

To explain and find a possible reason for the findings from the experiments, the process of the slurry discharge will be separated into two different phases. The first phase is the discharge form the diffuser until the impingement on the bottom. This phase includes the jet behaviour and the deflection of the plume towards the bottom. For the second phase the moment right after impingement will be considered, which consists of a short

lived wall jet and the turbidity current. As explained before, this first phase is dominated by the density difference between the slurry and the ambient water. Results from the experiments, discussed in section 4.4, have shown that **a higher initial concentration leads to a deflection of the plume towards the bottom over a shorter distance resulting in an impingement point closer to the diffuser** with a larger angle with respect to the bottom. The second phase can be regarded as a separate process in which flow originates from impingement point. The impingement point can be seen as the source of the wall jet and turbidity current, with its own source parameters, such as the sediment flux, velocity profile, momentum and volume flow. From the experiments it is known that the initial concentration of the discharged fluid influences these parameters, most notably the velocity profile and dimensions of the current leaving from the impingement point. Because the dying out of the turbidity current is known to be caused by the settling of the suspended solids, which during this phase is dominated by their individual settling velocity, it is believed that analysing and comparing the velocity profiles and heights of the current after impingement can give valuable insights into the runout distance of turbidity currents resulting from a fluid impingement with the bottom. In order to explain the runout distances of the turbidity currents emerging from the impingement points, different theoretical approaches can be used.

One of these methods, originally designed for the sedimentation process in hopper dredgers, is the Camp model. This model argues that the total distance required for settling is determined by mainly three things: settling velocity, horizontal velocity, and height above the bottom. Apart from this, also the temperature of the water (influencing viscosity and density) and turbulence play a role. Figure 4.13 shows a representation of the Camp model in which V_s is the settling velocity, S_0 the horizontal velocity and H_w the height of the upmost particle above the bottom. This first panel assumes a uniform velocity profile and therefore shows a straight line of the particles. In reality however, the velocity profile will show a shape with a velocity maximum near the bottom. As a result, the particle trajectory of the camp model will be adjusted to show a 'dip', caused by the increase in horizontal velocity as the particle travels down towards the bottom. This is shown in the second panel of Figure 4.13.

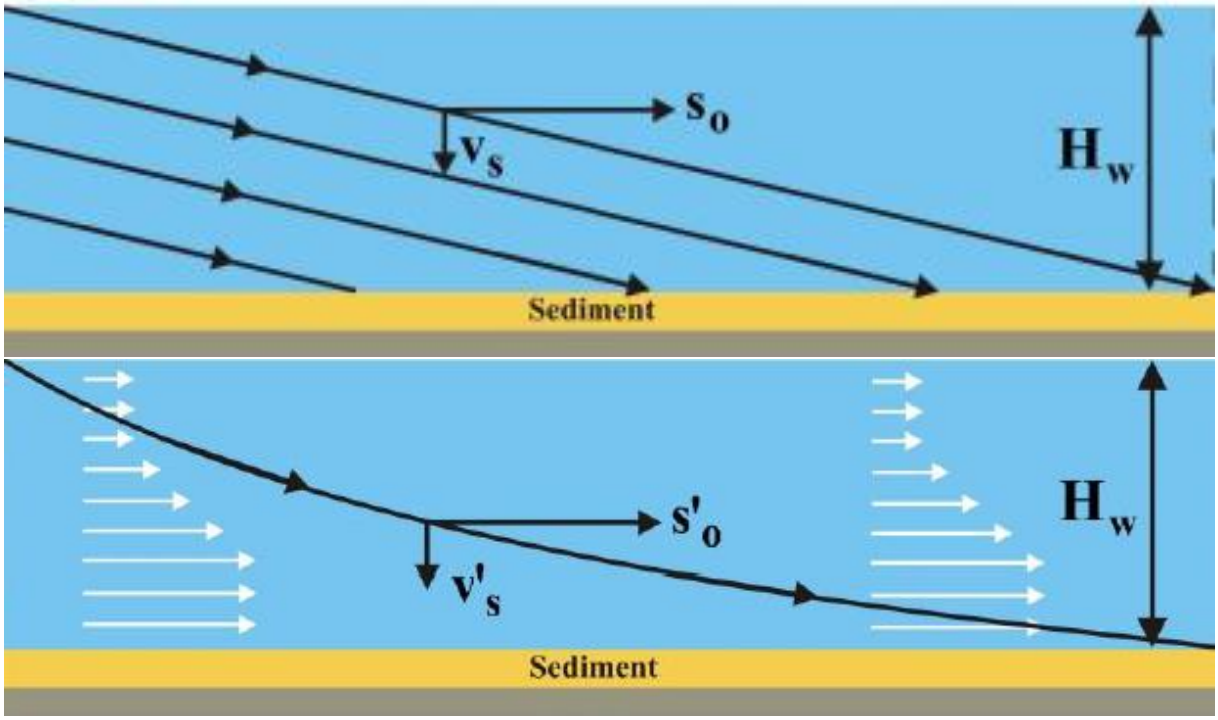

Figure 4.13: Camp model assuming a uniform and non-uniform velocity profile [102]

Because for all experiments performed for this research the settling velocity of the particles were equal, focus will be on the height above the bottom and the horizontal velocity of the particles. An increase of either of these two results in an increase in sedimentation distance, for turbidity currents usually referred to as runout distance. Theoretically, the settling velocity is not constant but increases over distance as the concentration

decreases, which leads to an increase in the hindered settling velocity as explained in section 2.3.1. However, due to the low concentrations found in the turbidity currents from the experiments this effect is small and can be neglected for simplicity. Furthermore, some differences between the Camp model and the situation from the experiments should be highlighted. One of these is the difference in outflow shape. Because the Camp model assumes a constant volume flow and a rectangular basin with constant dimensions, the horizontal velocity does not decrease as it does for the experiments. Instead, the velocity remains constant over the entire length of the basin because the flow in the Camp model essentially behaves like rectangular duct flow. For the experiments it is known that especially for the high initial concentration the outflow is radial, and the scale of the experiment is chosen such that reflection against the side walls should not occur. As a result, the trajectory of particles in a turbidity current as observed in the experiments is expected not to show a dip due to an increase in velocity further down in the water column, but rather a bulge due to the increasing ratio of settling versus horizontal velocity. It should also be kept in mind that the driving force in the Camp model is the continuous volume flow that is being fed into the basin. For a turbidity current on the other hand, the driving force is the density difference with the ambient. As particles settle over time, this driving force therefore decreases which creates a feedback loop of continuously decreasing velocity and more settling particles, something which is not taken into account when applying the Camp model. As a result, the runout distance of a turbidity current is expected to be smaller than the sedimentation distance as would be calculated using the Camp model.
However, despite the differences the Camp model does offer insight into the importance of height and velocity. Because in the Camp model the lowest product of initial height and horizontal velocity results in the smallest sedimentation distance, the same is assumed to be true for the runout distance of turbidity currents. As a results, comparing the initial height and velocity of the velocity profiles measured after impingement of the different experiments could allow for predictions to be made as to which turbidity current will have a longer runout distance. When applying this to the experiment results and comparing velocity profiles 4A of diffusers 1 and 2, it is found that the turbidity current from diffuser 1 has a slightly smaller height and higher peak velocity, the latter believed to be due to the earlier mentioned aggressive vertical impingement. When comparing the velocities at similar heights above the bottom near the top of the currents however, it is found that these are almost equal to each other. The larger total height of the turbidity current of diffuser 2 is believed to be caused by the larger volume flow of this experiments, which logically results in a larger height given that the measured velocity is slightly smaller than for diffuser 1. Based on the above, this would mean that based on the Camp model the turbidity currents from both diffusers are expected to have similar runout distances.

Another method for comparing the turbidity currents resulting from the different experiments is by looking at the potential energy involved. Multiple studies have pointed out that the potential energy is a good measure for the runout distance and driving force of turbidity currents [103] [104]. One of these studies, which looked into the factors influencing the deposit geometry of turbidity currents, found that an increase in flow density (which means an increase in concentration) resulted in a longer runout distance [103]. It should be noted however that the experiments that are being compared in that study have been performed by lock-exchange experiments using a constant volume, meaning that an increase in density/concentration is the result of an increase in the amount of sediment added to this constant volume, thus resulting in an increase of the sediment flux. For experiments of the same density but an increased volume it was also found that this resulted in an increase of the runout distance. The increase of runout distance of both occasions was ascribed to the increase of (gravitational) potential energy. Potential energy in this case is the product of mass, gravity and height, so both an increase in volume, which leads to an increase in mass, and an increase in density, which also increases mass (for an equal volume) increase the potential energy.
Potential energy can be analysed by looking as the total potential energy, or by looking at the potential energy per unit volume. When looking at the potential energy per unit volume, it is the density of the ambient fluid and turbidity current fluid, and not the total mass that is being compared. For turbidity currents the potential energy per unit volume can be expressed using the following equation [103]:

$$E = \frac{1}{2}\rho_f g\left(\frac{\rho_f - \rho}{\rho}\right)d \tag{35}$$

Where E is the potential energy per unit volume, ρ the density of the ambient, and d the thickness of the flow. When applying this to the findings from the experiments, the following is concluded. When comparing the turbidity currents from diffusers 1 and 2, the flow thickness is slightly higher for diffuser 2. Furthermore, the concentration profiles (Appendix C) show higher concentrations after impingement (location 4A) for diffuser 2. These observed higher concentrations in the profiles of diffuser 2 is caused by the large amount of particles settling directly in the impingement zone during the experiments of diffuser 1. As a result of the higher concentrations, the fluid density of the turbidity current from diffuser 2 is also higher. This results in the potential energy per unit volume as calculated using Equation (35) being larger for the turbidity current of diffuser 2. Based on this, it is believed that the smaller current height and lower concentration after impingement, resulting from a higher initial concentration being discharged from the diffuser, results in a smaller runout distance for the turbidity current.

To summarize, the total distance between the diffuser from which the slurry is being discharged and the position at which the velocity reaches values of (near) zero, is a combination of the impingement and runout distances, where the runout distance is being measured from the starting point of the turbidity current (the impingement point in this case) and the location at which the turbidity current ceases to ensue further. It should be noted that this is the case for horizontal jets with an initial horizontal velocity relative to the bottom of non-zero, as are being considered in this research. The experiment results of this research have shown a smaller impingement distance for higher initial concentrations. The exact location where the velocity profiles of the turbidity currents of different diffusers approach zero have not been found for every diffuser because of the location choices at which velocity measurements have been performed. However, the measurements at locations just after the impingement point, combined with a theoretical analysis have shown that the runout distance for the higher initial concentration experiments is likely to be similar or lower than the runout distance of turbidity currents resulting from experiments with a smaller initial concentration. This results in a smaller total spreading distance of the flow for a higher initial concentration, in accordance to what has been found during the experiments, shown in Figure 4.1.

4.6 Experiments with clay

As explained before, the experiments for this research have been performed using spherical glass particles as sediment instead of real clay. Being larger in diameter and therefore settling over a shorter distance as well as rheology are among the reasons for using these spherical glass particles, as it is more practical for experimental purposes. However, as real deep sea mining operations will take place in locations where the seabed is formed by clay, performing experiments with it could give valuable insights into the behaviour of sediment plumes and turbidity currents when formed out of clay particles instead of spherical glass. For this reason it was decided to also perform a number of experiments in the same experimental setup using a clay mixture. Because of the complexity and lack of experience with clay experiments in this setup, these tests only consisted of visual experiments using the FASTEC high speed camera. Apart from these results, a lot of valuable lessons have been learned regarding experimenting with clay on this scale and in this specific setup. Appendix D has been created specifically to discuss the recommendations for future experiments with clay in the dredging lab of the 3mE faculty of the TU Delft.
Apart from the sediment, all other characteristics of the experiments were initially kept equal to the glass particle experiments. The first experiment was performed with the 20 g/L concentration and the largest diffuser (diffuser 3). The next experiment was planned to use diffuser 2 and the same concentration as was used during the glass particle experiments, being 80 g/L. During mixing however it was found that the maximum achievable concentration was 35 g/L. Bringing the clay into suspension using the experimental setup proved difficult as large clumps of clay remained on the bottom. Because of this finding, it was decided to perform the second experiment using this maximum achievable concentration of 35 g/L and the largest diffuser. As a consequence the only difference between the two clay experiments caused by the increased concentration is the sediment flux. This higher concentration and thus density resulted in the second experiment having a larger buoyancy flux compared to the 20 g/L experiment. Because the same volume flow was used, the second experiment has a smaller momentum/buoyancy ratio, as is the case for the ‘high concentration experiments’ with the glass particles.

Figure 4.14 shows the steady state of both experiments. These stills from the high speed camera recordings show a significant difference in behaviour of the plume for the two different concentrations. The plume with the initial concentration of 20 g/L can be seen to have a large horizontal reach without deflecting much towards to bottom. This shape and reach is comparable to the lower most panel of Figure 4.12, showing a still from the glass particle experiment with the same initial concentration. The second still in Figure 4.14 shows a very different behaviour for the plume with the initial concentration of 35 g/L. This higher density plume deflects towards the bottom at a distance comparable to those found in the 80 and 140 g/L glass particle experiments, and impinges the bottom in a more vertical manner than the plume of the 20 g/L (clay) experiment. What these results clearly show is the difference caused by the concentration difference for the initial phase of the discharge, during which the settling of the plume is dominated by density differences between the discharged mixture and the ambient water. Due to the deflection towards the bottom of the higher density mixture, the height of the ensuing turbidity current is much smaller than for the 20 g/L experiment. This current height is believed to be beneficial for limiting the total reach of the turbidity current as after impingement a turbidity current dies out due to the settling of individual particles and is thus dominated by the terminal settling velocities of the individual particles involved. Therefore a lower current height would most likely result in the individual particles to settle over a shorter distance.
Because of the scale of the experiment and size of the tank, it was found that due to reflection the experiments could only last about 1 to 2 minutes and therefore mainly give insight into the initial phase of the discharging process as described above. The turbidity currents of both experiments started to reflect from the back and side walls, causing the sediment clouds to move up, something which on the ocean floor would not occur. Therefore the observations done during these experiments mainly gave insight into the initial stage of the discharge of the mixture and were not usable for getting information regarding the process inside the turbidity current itself.

Figure 4.14: Stills from the high speed recordings of both clay experiments at 40 seconds into the experiment (timed from the moment the mixture first leaves the diffuser)

[This page is intentionally left blank]

5. Discussion, conclusions & recommendations

The objective of this research was to find the influence of the initial concentration of discharged slurries on the spatial spread of the turbidity current. Through experimenting answers on the research questions have been found which have helped reaching the main research objective. Apart from the results that were looked for, also some limitations of the setup have been found which have led to some suggestions and recommendations for future research.

5.1 Discussion

The results of the experiments as discussed in the previous chapter have been used to answer the research questions and to formulate a conclusion regarding the general influence of the initial concentration of the discharged slurry on the spatial spread of the turbidity current, which was the research objective. Despite the overall good results, the experiments highlighted some limitations of the setup and measurement devices.

One of the most notable limitations found was the inability of the ADV to measure velocities in turbulent currents. This resulted in both uncertainties in front of the diffuser and at the interface between the turbidity current and clear water above it, in which Kelvin-Helmholtz instabilities were observed. Because of this, for a range of height of some of the velocity profiles, no clear value of the average velocity could be found. One possible solution would be to use an ADV with a higher sampling frequency, as this is known to improve the correlation of the data. Despite this limitation, the ADV has shown to be a reliable device in other situations and allows for velocity profiles to be measured relatively easy, although a device which is able to measure longer profiles would make the experiments significantly less labour intensive and more efficient.
Also some uncertainties remain regarding the concentration calculations based on the SNR signal measurements. Different calibrations for relating the SNR to concentration values show very similar results, but are not 100% reproducible. The overall shape of the calibration curve and the concentration at which the maximum SNR is measured were the same after each calibration, but the exact SNR values corresponding to each calibration showed a small shift, indicating some bias in the measurements. Despite this uncertainty, the SNR measurements were consistent over the course of the research and as such, the SNR is believed to be a good indication of the concentration of the current. Therefore expanding knowledge of this method could prove to be beneficial for future research.
Furthermore, given the periodicity and dips and peaks, especially if not spread symmetrically around the mean, leads to the question whether calculating the average concentration is useful, as for acquiring a better understanding of the processes inside the individual turbidity currents it can be argued that it is more useful to analyse the SNR signal over time, as shown in Figure 4.7 and Figure 4.8. The aim of this research however is to find the influence of the initial concentration on the sediment transport away from the diffuser, and for this purpose finding the average concentration over time at different locations is useful for comparing the average sediment transport over a longer period of time.

Based on the literature review, the expectations of the experiments were to find a relation between concentration and spatial spread of the turbidity current. The lower momentum/buoyancy ratio for buoyant jets with higher concentrations combined with the assumption that during the initial phase (plume impingement) the mixture density is the dominant factor for the settling, the expectations were to find that an increase in initial concentration would lead to a decrease in the total range of the turbidity current. The experiments confirmed these expectations, but also showed some adverse effects of increasing the concentration on the spread of the turbidity current, most notably the sediment transport perpendicular to the discharge direction.

Perhaps one of the most influential decisions that was made, was to keep the sediment flux (and therefore buoyancy flux) constant for each experiment. The concentration was increased by decreasing the total volume flow which was achieved by adding less total water. As explained earlier in the report, this decision was made based upon the assumption that the sediment flux is determined mainly by the miner width, velocity and cutting

depth and is therefore a result of design choices which cannot be altered during operations. Taking a constant sediment flux also shows the effect of reduced water intake, important for the BAT concept as introduced in chapter 1. It should however be noted that a change in concentration during the experiments could also have been achieved by adding more sediment to the same volume of water, hereby increasing the sediment flux. In this case not the buoyancy flux but the momentum flux would have been the constant throughout the experiments, with the buoyancy flux increasing for a higher concentration. Although this choice would have changed the quantitative results of the experiments, qualitatively the differences between each concentration would be comparable, as for this method the momentum/buoyancy ratio would decrease for an increase in concentration, just as it did for the actual experiments. Therefore it is believed that despite the method that would have been chosen, the conclusions regarding the influence of the initial concentration would remain the same.

5.2 Conclusions

The goal of this research was to find the influence of the initial concentration of a discharges slurry on the spatial spread of the turbidity current, with the research objective being defined as follows:

'Determine how changing the initial volumetric concentration of the discharge mixture influences the flow parameters after impingement and sediment flux inside the turbidity current for a constant sediment flux and discharge velocity through measurement of velocity and concentration profiles. Subsequently use the findings to identify how the spread of sediment can be limited for the benefit of the ecosystems around the mining area.'

In order to reach this objective a set of 7 research questions have been formulated, which will now be answered below.

- Increasing the concentration for a constant sediment flux has shown to decrease the impingement distance away from the diffuser. For a constant discharge height, this results in the impingement angle with respect to the horizontal to increase (a more vertical impingement) for a higher concentration.

- It has been shown that increasing the initial concentration leads to a more vertical impingement and as such, a circular outflow shape. This same outflow shape has not been observed for the low concentration experiment. A consequence of this circular outflow shape is a higher velocity component perpendicular to the discharge direction as compared to the low concentration experiment.

- The video images of the experiments have shown a clear wall jet after impingement for the mixtures with a high concentration and corresponding vertical impingement. Inspection of the velocity profiles has shown an increase in peak velocity after impingement for these experiments with a high concentration. Comparing the 140 and 80 g/L experiments has led to the conclusion that a higher concentration leads to a larger velocity increase (both absolute and relative) after impingement.

- The head velocity of the turbidity current which forms after impingement also increases for higher concentrations

- SNR measurements have shown that a high initial concentration of 140 and 80 g/L quickly decreases after leaving the diffuser. Based on the decrease of the SNR signal to clear water values over a shorter distance for higher initial concentrations, it was concluded that the concentration in the turbidity current decreases over a shorter distance and as such leads to the turbidity current to die out over a shorter distance.

- Increasing the initial concentration for a constant discharge velocity results in the velocity to be higher after impingement, caused by a more aggressive impingement. After this the velocity profiles for the experiments with a higher initial concentration show a fast decrease in velocity and reach velocities of near zero at a shorter distance from the diffuser than lower initial concentrations do. Higher concentration do however result in a larger velocity component in the direction perpendicular to the discharge direction, resulting in more spread of sediment towards the sides.

- The faster decrease in concentration and velocity for experiments with a higher initial concentration combined with smaller turbidity current dimensions (shown by the profile heights in Figure 4.1), led to the conclusion that the sediment transport away from the diffuser is stopped in a shorter distance for higher initial concentrations. This has been confirmed by observations of the deposition layer after experiments of equal length, which showed more sediment deposition closer to the diffuser for experiments with a higher initial concentration. Given the equal sediment flux this means that the sediment is transported over a smaller distance for a higher initial concentration

Based on the answers on the research questions above, the following conclusion has been drawn regarding the research objective:

- It is believed that a higher concentration than the 1% volumetric concentration that is currently being assumed by deep sea mining companies could prove to be beneficial in preventing the spatial spread of the sediment plume and subsequent turbidity current resulting from the sediment discharge of the deep sea mining vehicle. It is believed that in general, increasing the initial concentration of the discharged slurry, and thereby decreasing the momentum/buoyancy ratio of the buoyant jet, directly leads to both the velocity and concentration of the turbidity current to decrease over a shorter total distance. As such, the total reach of the turbidity current resulting from the slurry discharge from a deep sea mining vehicle can be decreased by using a higher initial concentration of said slurry. It should however be noted that a large increase in concentration has the adverse effect of an aggressive impingement, leading to larger velocities in the ensuing wall jet than would otherwise be the case, and further research is required to determine the exact effect that the concentration has on this, as a too large velocity could cause the resuspension of bed material. It is believed that mainly the higher density difference with the ambient water plays a vital role in decreasing the spatial spread of the sediment plumes produced by deep sea mining operations. The higher density achieved by a high concentration results in the plume to deflect towards to bottom over a shorter distance, a decrease in turbidity current height and an increase in turbidity current velocity. This decrease in height is beneficial for the later stage of the turbidity current in which the dying out is dominated by the settling velocity of individual particles. The increase in velocity however causes the particles in suspension to be carried away from the impingement point further. As concluded in section 4.5, the runout distance of the turbidity current can be minimized by using a concentration which results in the lowest combination of horizontal velocity and turbidity current height after impingement. For this research the experiments with the highest initial concentration proved to result in the lowest total distance (measured from the diffuser) needed to reach a velocity of zero. This distance is the combination of the impingement and runout distance.

It should be noted that the conclusions from this research are applicable to horizontal sediment-laden jets which result in a sediment jet and plume with an initial relative horizontal velocity with the bottom of non-zero, which means that the total distance between the diffuser and stopping point of the turbidity current is a combination of the impingement distance and runout distance.

5.3 Recommendations

Based on the results of this research and the experience gained during experimenting, the following recommendations are given for future research:

- As explained in the analysis and conclusion, the results of this research show the decay of velocity and concentration of a sediment-laden jet and subsequent turbidity current for a slurry that is being discharged with an initial horizontal velocity of non-zero relative to the bottom. As for real deep sea mining operations it is expected that the forward velocity of the miner and discharge velocity of the slurry will be equal, it is important to gain insight into the effect that initial concentration has on the sediment transport away from the impingement point for this zero initial relative velocity case, for which the impingement is expected to be vertical for all initial concentrations. Such experiments would allow for the runout distance of the turbidity currents to be tested for a vertical impingement and with a zero initial vertical velocity (something not achieved by using vertical jets). It would be valuable to measure velocities and concentrations in such experiments at multiple distances from the impingement point, resulting in velocity measurements away from the impingement point at equal distances for all experiments, something which was not the case for the experiments performed for the research in this thesis. For experiments with a zero initial horizontal velocity relative to the bottom, the following possibilities have been thought of:
    - Using a moving instead of a stationary jet would include the effects of both the wake of a miner as well as that of a relative velocity of zero between the discharged fluid and the bottom. For this the aim should be to have a jet which moves forward at the same velocity at which the slurry is being discharged from the diffuser.
    - Instead of using a moving jet and all the practical challenges that this will give rise to, another possibility could be to perform experiments in which mixtures are being released vertically instead of horizontally. Because a vertical jet would give the mixture an initial vertical velocity which should be zero, as with a deep sea mining operation, a solution could be to perform what essentially is a vertical lock-exchange experiment. By releasing mixtures with different concentrations into the water column the effect of the density differences on the vertical descend and vertical impingement could be measured. This way experiments could be performed in which the mixtures have a relative horizontal velocity with the bottom of zero while also not discharging them with an initial vertical velocity, allowing them to descend as a plume under the influence of gravity. A disadvantage of this would be that, while taking away the difficulties of using a moving jet, only experiments with a constant volume (as with lock-exchange experiments) can be performed, instead of continuous flow experiments.

- A valuable piece of information would be the height of the sediment deposition resulting from the experiments, as it would give more insight into the sediment transport and deposition around the impingement point. For this purpose the bottom height measurement function of the ADV can be used. This would allow to measure the deposition layer height over a grid of coordinates and as a result find the volume of sediment deposited at different locations. In order to do this however enough space above the modular tank is required and as such it should be performed before the blackout curtains are placed over the modular tank, as it prevents these measurements to be performed efficiently.

- During this research only the concentration was changed between experiments, resulting in the conclusion that a higher concentration leads to a more limited spatial spread of the sediment. It was however also found that the experiments with a higher concentration have a more vertical impingement, causing an aggressive impact of the sediment on the bed, resulting in an increase in velocity and a velocity component perpendicular to the discharge direction. Performing experiments with this high concentration at different height could give insight into the effect that this has on the impingement, as it could help prevent the aggressive impingement, as well as result in a more horizontal impingement. This horizontal impingement is expected to decrease the velocity component perpendicular to the discharge velocity which is believed to be desirable for deep sea mining operations

as a sidewards velocity could bury nodules. At the same time a more horizontal impact due to a lower discharge height is also expected to give more momentum into the discharge direction, which possibly leads to an extent of the spatial spread of the turbidity current.

- A better understanding of the concentration measurement using the ADV is advisable. For this study it was found that a correlation can be found between the SNR and concentration, but still some uncertainties remain regarding the determination of the correct concentration and the applicability of the method overall. As discussed in section 4.3.2, a further analysis is required into the processing of the SNR data, to get a better insight into the way the data should be handled and looked at, as it was found that is behaves quite differently than the velocity data, showing fluctuations with a much higher magnitude. Also some bias in the calibration data was observed. As a result of both, a better understanding of the influence of the presence of scatters (the concentration) on the backscatter intensity, which ultimately determines the SNR, is advised.

- As a result of the findings of this research that a higher concentration proved to result in less spatial spread of the sediment but a more aggressive impingement, it is recommended to start testing with a sediment bed already present. This might give a better understanding of the effect that different impingements and the velocity increased associated with this impingement have on the possible resuspension of material, which is assumed to be unwanted in deep sea mining operations.

- As real deep sea mining operations will take place in areas where clay is the present sediment type, it is recommended to expand knowledge regarding clay experiments and to perform more experiments with clay, of which the first step was undertaken in this research. Using clay instead of glass particles adds the effects of the changing rheology for high concentration and flocculation, the latter of which could play an important role in limiting the spread of the sediment plume.

Recommendations specifically related to experimenting with clay in the modular tank in the dredging lab at the 3mE faculty of the TU Delft can be found in Appendix D.

Bibliography

[1] D. O. B. Jones, S. Kaiser, A. K. Sweetman, C. R. Smith, L. Menot, A. Vink, D. Trueblood, J. Greinert en D. S. M. Billett, „Biological responses to disturbance frmo simulated deep-sea polymetallic nodule mining," *PLoS ONE,* 2017.

[2] M. Bashir, S. H. Kim, E. Kiosidou, H. Wolgamot and W. Zhang, "A Concept for Seabed Rare Earth Mining in the Eastern South Pacific," University of Southhamption, Southhampton, 2012.

[3] J. C. Drazen, C. R. Smith, K. M. Gjerde, S. H. D. Haddock, G. S. Carter, C. A. Choy, M. R. Clark, P. Dutrieux, E. Goetze, C. Hauton and M. Hatta, "Midwater ecosystems must be considered when evaluating environmental risks of deep-sea mining," *PNAS,* 2020.

[4] K. A. Miller, K. F. Thompson, P. Johnston and D. Santillo, "An Overview of Seabed Mining Including the Current State of Development, Environmental Impacts, and Knowledge Gaps," *Frontiers of Marine Science,* 2018.

[5] B. Gillard, K. Purkiani, D. Chatzievangelou, A. Vink, M. H. Iversen and L. Thomsen, "Physical and hydrodynamic properties of deep sea mining-generated, abyssal sediment plumes in the Clarion Clipperton Fracture Zone (eastern-central Pacific)," *ELEMENTA: Science of the Anthropocene,* 2019.

[6] D. O. B. Jones, J. A. Ardron, A. Colaço and J. M. Durden, "Environmental considerations for impact and preservation refernce zones for deep-sea polymetallic nodule mining," *Marine Policy,* 2018.

[7] Blue Nodules, "Blue Nodules Deliverable report D3.4 Report describing the process flow overview," Blue Nodules, 2019b.

[8] H. U. Oebius, H. J. Becker, S. Rolinski and J. A. Jankowski, "Parametrization and evaluation of marine environmental impacts produced by deep-sea manganese nodule mining," *Deep-sea research part II: Topical studies in oceanography,* pp. 3453-3467, 2001.

[9] J. Spearman, J. Taylor, N. Crossouard, A. Cooper, M. Turnbull, A. Manning, M. Lee and B. Murton, "Measurement and modelling of deep sea sediment plumes and implications for deep sea mining," *Scientific Reports,* 2020.

[10] M. A. Atmanand and G. A. Ramadass, "Concepts of Deep-Sea Mining Technologies," in *Deep-Sea Mining: Resource Potential, Technical and Environmental Considerations*, Cham, Springer International Publishing AG, 2017, pp. 305-343.

[11] S. E. Volkmann and F. Lehnen, "Production key figures for planning the mining of manganese nodules," *Marine Geosources & Geotechnology,* pp. 360-375, 2017.

[12] R. Sharma and S. Smith, "Deep-Sea Mining and the Environment: An Introduction," in *Environmental Issues of Deep-Sea Mining: Impacts, Concsequences and Policy Perspectives*, Cham, Springer Nature Switzerland AG, 2019, pp. 4-22.

[13] Blue Nodules, "Blue Nodules Deliverable report D3.6 Process model for a pre-prototype sediment seperator," Blue Nodules, 2020d.

[14] Blue Nodules, "Blue Nodules Deliverable report D5.4 Report on properties of plume source material, tailings and processing water," Blue Nodules, 2020f.

[15] S. Rajput and N. K. Thakur, "Sedimentation Pattern," in *Geological Controls for Gas Hydrate Formations and Unconventionals,* Amsterdam, Elsevier, 2016, pp. 69-106.

[16] J. A. Ardron, E. Simon-Lledó, O. B. Jones and H. A. Ruhl, "Detecting the Effects of Deep-Seabed Nodule Mining: Simulations Using Megafaunal Data From the Clarion-Clipperton Zone," *Frontiers in Marine Science* , p. 604, 2019.

[17] P. P. E. Weaver and D. Billett, "Environmental Impacts of Nodule, Crust and Sulphide Mining: An Overview," in *Environmental issues of Deep-Sea Mining: Impacts, Consequences and Policy Perspectives*, Cham, Springer Nature Switzerland AG, 2019, pp. 27-62.

[18] M. R. Chowdhury and F. Y. Testik, "A review of gravity currents formed by submerged single-port discharges in inland and coastal waters," *Environmental Fluid Mechanics,* pp. 265-293, 2014.

[19] Blue Nodules, “Blue Nodules Deliverable report D2.3 Detailed Design of the Nodules Collectors,” Blue Nodules, 2020c.

[20] Blue Nodules, “Blue Nodules Deliverable report D2.12 Design report for full-scale mining,” Blue Nodules, 2020b.

[21] Blue Nodules, “Blue Nodules Deliverable report D1.7 Environmental Impact Assessment (EIA) components for test mining up to prototype level (TRL 6),” Blue Nodules, 2020a.

[22] G. H. Jirka and R. L. Domeker, “Hydrodynamic Classification of Submerged Single-Port Discharges,” *Journal of Hydraulic Engineering,* 1991.

[23] I. G. Papakonstantis and G. C. Christodoulou, “Spreading of round dense jets impinging on a horizontal bottom,” *Hydro-environment Research,* pp. 289-300, 2010.

[24] T. Bleninger and G. H. Jirka, “Modelling and environmentally sound management of brine discharges from desalination plants,” *Desalination,* pp. 585-597, 2007.

[25] O. E. Sequeiros, R. Mosquera and F. Pedocchi, “Internal Structure of a Self-Accelerating Turbidity Current,” *Journal of Geophysical Research: Oceans,* pp. 6260-6276, 2018.

[26] D. Shao and A. W. Law, “Turbulent mass and momentum transport of a circular offset dense jet,” *Journal of Turbulence,* vol. 2009, pp. 1-24, 2009.

[27] J. C. Drazen, C. R. Smith, K. M. Gjerde, W. Au, J. Black, G. Carter, M. Clark and J. M. Durden, “Report of the workshop Evaluating the nature of midwater mining plumes and their potential effects on midwater ecosystems,” *Research Ideas and Outcomes,* p. 5: e33527, 2019.

[28] Blue Nodules, “Blue Nodules Deliverable report D2.8 Detailed design of SWOE return systems and water management,” Blue Nodules, 2019a.

[29] F. Pedocchi and M. H. García, “Acoustic measurement of suspended sediment concentration profiles in an oscillatory boundary layer,” *Continental Shelf Research,* 2011.

[30] O. Chmiel, I. Bastelt and A. Malcherek, “Applicability of Acoustic Concentration Measurements in Suspensions of Artificial and Natural Sediments Using and Acoustic Doppler Velocimeter,” *Acoustics,* pp. 59-77, 2018.

[31] S. A. Hosseini, A. Shamsai and B. Ataie-Ashtiani, “Synchronous measurements of the velocity and concentration in low density turbidity currents using an Acoustic Doppler Velocimeter,” *FLow Measurement and Instrumentation,* pp. 59-68, 2006.

[32] P. D. Thorne and D. M. Hanes, “A review of acoustic measurement of small-scale sediment processes,” *Continental shelf research,* pp. 603-632, 2001.

[33] Blue Nodules, “Blue Nodules Deliverable report D4.5 Mining Platform,” Blue Nodules, 2020e.

[34] Blue Nodules, “Blue Nodules Deliverable report D2.4 Initial Design of Vehicle Propulsion and Propulsion Test Performance,” Blue Nodules, 2017b.

[35] Blue Nodules, “YouTube,” 3 August 2020. [Online]. Available: https://www.youtube.com/watch?v=pCus0hTsibc&t=230s. [Accessed 10 March 2021].

[36] Blue Nodules, “Blue Nodules Deliverable report D1.1 Terms of Reference,” Blue Nodules, 2017a.

[37] M. Nabavi, “Three-dimensional asymmetric flow through a planar diffuser: Effects of divergence angle, Reynolds number and aspect ratio,” *International Communications in Heat and Mass Transfer,* pp. 17-20, 2009.

[38] F. M. White, Fluid Mechanics: 4th (fourth) edition, Boston: WCB/McGraw-Hill, 1998.

[39] T. P. Chong, P. F. Joseph and P. A. O. L. Davies, “A Parametric Study of Passive Flow Control for a Short, High Area Ratio 90 deg Curved Diffuser,” *Journal of Fluids Engineering,* p. Vol. 130, 2008.

[40] J. Oosterhuis, “Oscillatory flows in jet pumps,” University of Twente, Enschede, 2016.

[41] H. Schlichting and K. Gersten, Boundary-Layer Theory, Berlin Heidelberg: Springer-Verlag, 2017.

[42] L. R. Reneau, J. P. Johnston and S. J. Kline, “Performance and Design of Straight, Two-Dimensional Diffusers,” *Journal of Basic Engineering,* pp. 141-150, 1967.

[43] V. Chandavari and S. Palekar, “Diffuser angle control to avoid flow separation,” *International Journal of Technical Research Applications,* pp. 16-21, 2014.

[44] X. Meng, Z. Zuo, M. Nishi and S. Liu, “A Numerical Study on the Flow Mechanism of Performance Improvement of aWide-Angle Diffuser by Inserting a Short Splitter Vane,” *Processes,* 2020.

[45] C. A. Moore and S. J. Kline, “Some Effects of Vanes and of Turbulence in Two-Dimensional Wide-Angle Subsonic Diffusers,” NACA, 1958.

[46] D. L. Cochran and S. J. Kline, “Use of Short Flat Vanes for Producing Efficient Wide-Angle Two-Dimensional Subsonic Diffusers,” NACA, 1958.

[47] M. Taherian and A. Mohammadian, “Buoyant Jets in Cross-Flows: Review, Developments and Applications,” *Journal of Marine Science and Engineering,* 2021.

[48] S. N. Chan and H. W. Lee, “A Particle Tracking Model for Sedimentation from Buoyant Jets,” *Journal of Hydraulic Engineering,* 2016.

[49] M. Kapil, B. R. Sutherland and Balasubramanian, “Spreading and sedimentation from bottom-propagating particle-bearing jets,” *Journal of Fluid Mechanics,* p. 907, 2020.

[50] S. N. Chan, “Mixing and Deposition of Sediment-Laden Buoyant Jets,” University of Hong Kong, Hong Kong, 2013.

[51] W. Y. Lee, A. C. Y. Li and H. W. Lee, “Structure of a Horionztal Sediment-Laden Momentum Jet,” *Journal of Hydraulic Engineering,* pp. 124-140, 2013.

[52] P. Papanicolaou and E. List, “Investigations of Round Vertical Turbulent Buoyant Jets,” *Journal of Fluid Mechanics,* pp. 341-391, 1988.

[53] S. N. Michas and P. N. Papanicolaou, “Horizontal round heated jets into calm uniform ambient,” *Desalination,* pp. 803-815, 2009.

[54] S. A. Miedema, Dredging Engineering Special Topics, Delft: TU Delft Open, 2019.

[55] A. J. Manning, J. R. Spearman, R. J. S. Whitehouse, E. L. Pidduck, J. V. Baugh and K. L. Spencer, “Flocculation Dynamics of Mud: Sand Mixed Suspensions,” in *Sediment Transport: Processes and Their Modelling Applications,* IntechOpen, 2013, pp. 119-164.

[56] J. R. Spearman, A. J. Manning and R. J. S. Whitehouse, “The settling dynamics of flocculating mud and sand mixtures: part 2 - numerical modelling,” *Ocean Dynamics,* pp. 351-370, 2011.

[57] M. Tilston, R. W. C. Arnott, C. D. Rennie and B. Long, “The influence of grain size on the velocity and sediment concentration profiles and depositional record of turbidity currents,” *Geology,* pp. 839-842, 2015.

[58] M. G. Wells and R. M. Dorrell, “Turbulence Processes Within Turbidity Currents,” *Annual Reviews,* pp. 59-83, 2021.

[59] G. F. Lane-Serff and T. J. Moran, “Sedimentation form Buoyant Jets,” *Journal of Hydraulic Engineering,* pp. 166-174, 2005.

[60] M. C. Lippert and A. W. Woods, “Experiments on the sedimentation front in steady particle-driven gravity currents,” *Journal of Fluid Mechanics,* p. A20, 2020.

[61] J. H. Baas and W. D. McCaffrey, “Coupling between suspended sediment distribution and turbulence structure in a laboratory turbidity current,” *Journal of Geophysical Research,* 2005.

[62] S. Nomura, G. D. Cesare, M. Furuichi, Y. Takeda and H. Sakaguchi, “Quasi-stationary flow structure in turbidity currents,” *International Journal of Sediment Research,* pp. 659-665, 2020.

[63] B. Kneller and C. Buckee, “The structure and fluid mechanics of turbidity currents: a review of some recent studies and their geological implications,” *Sedimentology,* pp. 62-94, 2000.

[64] T. Preseren, F. Steinman, B. Sirok and T. Bajcar, “The theoretical densimetric Froude number values with favourable effect on the clarifier,” *Chemical Engineering and Processing: Process Intensification,* pp. 97-105, 2013.

[65] P. T. Slatter, “Transitional and Turbulent Flow of Non-Newtonian Slurries in Pipes,” University of Cape Town, Cape Town, 1995.

[66] K. Ono, P. Plink-Björnklunk, J. G. Eggenhuisen and M. J. B. Cartigny, “Froude supercritical flow processes and sedimentary structures: New insights from experiments with a wide range of grain sizes,” *Sedimentology*, 2019.

[67] I. Tosun, D. Uner and C. Ozgen, “Critical Reynolds number for Newtonian flow in rectangular ducts,” *Ind. Eng. Chem. Res.*, pp. 1955-1957, 1988.

[68] E. Shashi Menon, Transmission pipeline calculations and simulations manual, Oxford: Gulf Professional Publishing, 2015.

[69] R. P. Chhabra and J. F. Richardson, Non-Newtonian Flow in the Process Industries, Oxford: Butterworth-Heinemann, 1999.

[70] N. Mangesana, R. S. Chikuku, A. N. Mainza, I. Govender, A. P. v. d. Westhuizen and M. Narashima, “The effect of particle size and solids concentration on the rheology of silica sand based suspensions,” *Journal of The Southern African Institue of Mining and Metallurgy,* pp. 237-243, 2008.

[71] K. E. Ugwu, A. C. Ofomatah and S. I. Eze, “Influence of solids concentration on the flow characteristics and settling rate of coal-water slurries,” *Journal of Energy and Natural Resources,* pp. 21-24, 2013.

[72] P. Vlasak and Z. Chara, “Conveying of Solid Particles in Newtonian and Non-Newtonian Carriers,” *Particulate Science and Technology,* pp. 428-443, 2009.

[73] V. B. Nguyen, H. Kang and Y. Kim, “Effect of clay fraction and water content on rheological propertiesof sand-clay mixtures,” *Environmental Earth Sciences,* p. 576, 2018.

[74] R. Sosio and G. B. Crosta, “Rheology of concentrated granular suspensions and possible implications for debris flow modeling,” *Water Resources Research,* 2009.

[75] A. M. Sahar, J. Wissink, M. M. Mahmoud, T. G. Karayiannis and M. S. Ashrul Ishak, “Effect of hydraulic diameter and aspect ratio on single phase flow and heat transfer in a rectangular microchannel,” *Applied Thermnal Engineering,* pp. 793-814, 2017.

[76] M. Spiga and G. L. Morini, “A symmetric solution for velocity profile in laminar flow through rectangular ducts,” *International Communications in Heat and Mass Transfer,* pp. 469-475, 1994.

[77] G. Nasif, R. Balachandar and R. M. Barron, “Supercritical flow characteristics in smooth open channels with different aspect ratios,” *Physics of Fluids,* 2020.

[78] I. Albayrak and U. Lemmin, “Secondary Currents and Corresponding Surface Velocity Patterns in a Turbulent Open-Channel Flow over a Rough Bed,” *Journal of Hydraulic Engineering,* pp. 1318-1334, 2011.

[79] G. A. Priego-Hernández and F. Rivera-Trejo, “Secondary currents: Measurement and analysis,” *Atmósfera,* pp. 23-34, 2016.

[80] D. Demiral, R. M. Boes and I. Albayrak, “Effects of Secondary Currents on Turbulence Characteristics of Supercritical Open Channel Flows at Low Aspect Ratios,” *Water,* 2020.

[81] A. Noorani, R. Vinuesa, L. Brandt and P. Schlatter, “Aspect ratio effect on particle transport in turbulent duct flows,” *Physics of Fluids,* 2016.

[82] S. Jing, W. Yang and Y. Chen, “Smooth Open Channel with Increasing Aspect Ratio: Influence on Secondary Flow,” *Water,* 2019.

[83] R. Vinuesa, P. Schlatter and H. M. Nagib, “On minimum aspect ratio for duct flow facilities and the role of side walls in generating secondary flows,” *Journal of Turbulence,* pp. 588-606, 2015.

[84] W. R. Quinn, “Turbulent Free Jet Flows Issuing from Sharp-Edged Rectangular Slots: The Influence of Slot Aspect Ratio,” *Experimental Thermal and Fluid Science,* pp. 203-215, 1992.

[85] E. Faghani, B. Farhanieh, R. Maddahian and P. Faghani, “Numerical investigation of effect of aspect ratio of rectangular nozzles,” in *Second International Conference on Thermal Issues in Emerging Technologies*, Cairo, 2008.

[86] P. Koch, “Equivalent diameter of rectangular and oval ducts,” *Building Serv. Eng. Res. Technol.*, pp. 341-347, 2008.

[87] Nortek, “nortek-bv.nl,” [Online]. Available: http://www.nortek-bv.nl/nl/produkten/snelheidsmeters/vectrino-ii. [Accessed 19 April 2021].

[88] C. Sahin, M. Ozturk and B. Aydogan, “Acoustic doppler velocimeter backscatter for suspended sediment measurements: Effects of sediment size and attenuation,” *Applied Ocean Research,* 2020.

[89] P. D. Thorne, I. T. MacDonald and C. E. Vincent, “Modelling acoustic scattering by suspended flocculating sediments,” *Continental Shelf Research,* pp. 81-91, 2014.

[90] J. H. Lee and V. Chu, Turbulent Jets and Plumes, New York: Springer, 2003.

[91] V. Matousek, Dredge Pumps and Slurry Transport, Delft: TU Delft, 2004.

[92] A. Sellgren, “The choice of operating velocity in vertical solid-water pipeline systems,” *Hydrotransport 8,* pp. 211-226, 1982.

[93] J. M. v. Wijk, “Vertical Hydraulic Transport for deep sea mining,” TU Delft, Delft, 2016.

[94] X. Meng, Z. Zuo, M. Nishi and S. Liu, “A Numerical Study on the Flow Mechanism of Performance Improvement of a Wide-Angle Diffuser by Inserting a Short Splitter Vane,” *Processes*, 2020.

[95] Nortek, “The Comprehensive Manual for Velocimeters,” Nortek AS, 2018.

[96] B. MacVicar and S. Dilling, “A quality analysis of the vectrino II instrument using a new open-source MATLAB toolbox and 2D ARMA models to detect and replace spikes,” in *RiverFlow 2014*, Lausanne, 2014.

[97] D. W. Velasco and C. A. Huhta, “Experimental verification of acoustic Doppler velocimeter (ADV®) performance in fine-grained, high sediment concen-tration fluids,” SonTek, 2009.

[98] I. T. MacDonald, C. E. Vincent, P. D. Thorne and B. D. Moate, “Acoustic scattering from a suspension of flocculated sediments,” *Journal of Geophysical Research,* vol. 118, no. American Geophysical Union, pp. 2581-2594, 2013.

[99] J. Lin, Q. He, L. Guo, B. C. v. Prooijen and Z. B. Wang, “An integrated optic and acoustic (IOA) approach for measuring suspended sediment concentration in highly turbid environments,” *Marine Geology,* vol. 421, no. Elsevier, 2020.

[100] V. Martin, T. S. R. Fisher, R. G. Millar and M. C. Quick, “ADV Data Analysis for Turbulent Flows: Low Correlation Problem,” in *Hydraulic Measurements and Experimental Methods Specialty Conference (HMEM) 2002*, Estes Park, Colorado, United States, 2002.

[101] H. Chanson, “ACOUSTIC DOPPLER VELOCIMETRY (ADV) IN THE FIELD AND IN LABORATORY: PRACTICAL EXPERIENCES,” in *International Meeting on Measurements and Hydraulics of Sewers (IMMHS'08)*, Bougeunais, France, 2008.

[102] S. Miedema, Dredging Engineering Special Topics, Delft: TU Delft Open, 2019.

[103] O. Al Ja'aidi, W. McCaffrey and B. Kneller, “Factors influencing the deposit geometry of experimental turbidity currents: Implications for sand-body architecture in confined basins,” *Geological Society London Special Publications,* vol. 222, no. The Geological Society of London, pp. 45-58, 2004.

Appendices

A. Velocity profiles (x-direction)

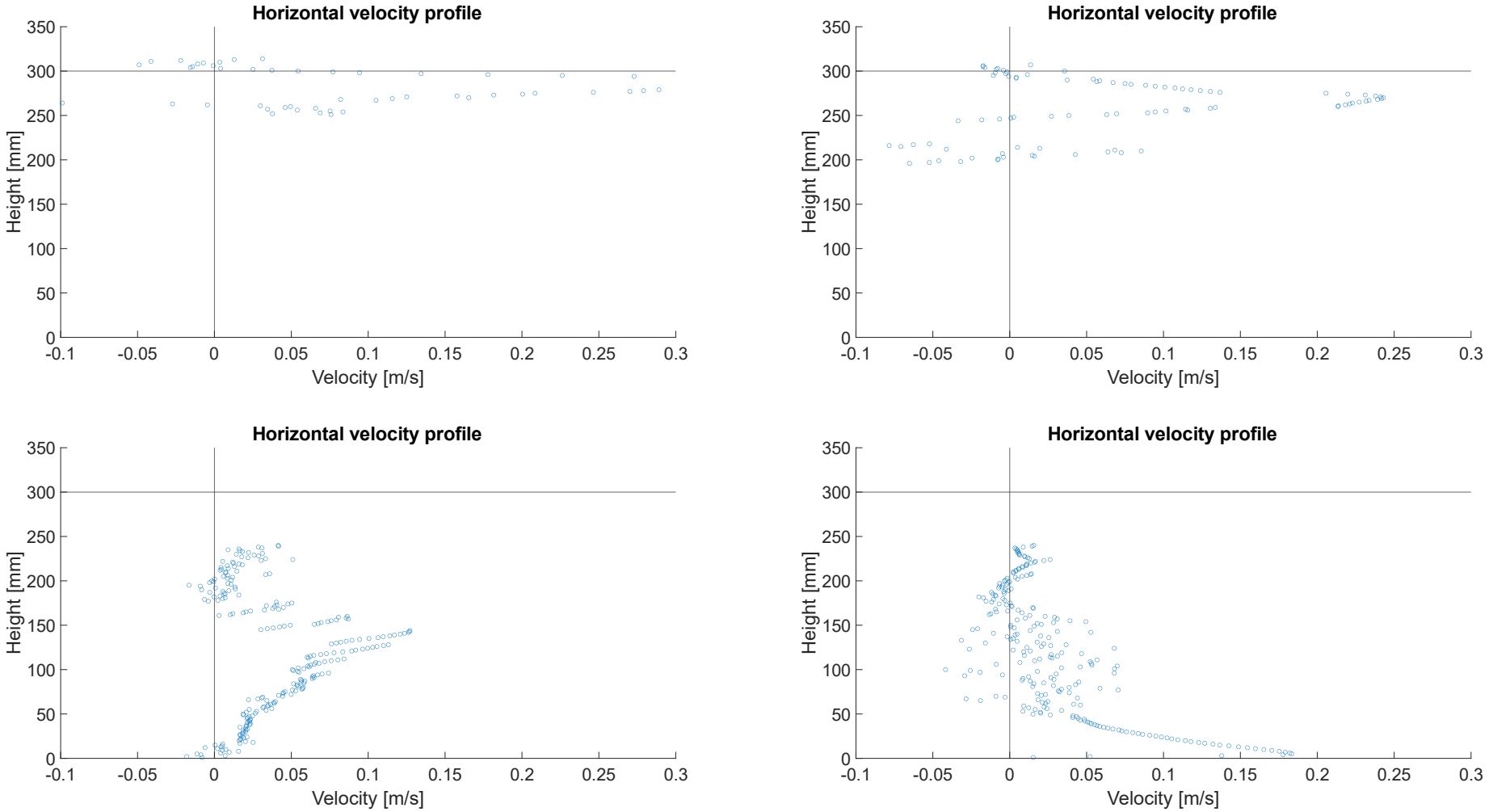

Figure A.1: Velocity profiles for diffuser 1 at x = 3.3, 11, 21 and 41 cm respectively

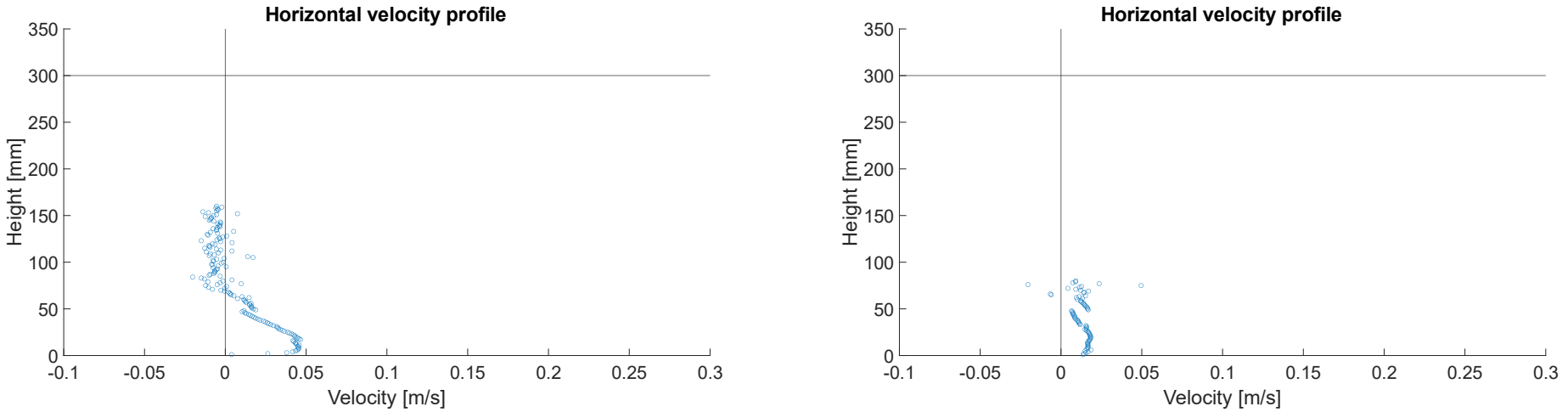

Figure A.2: Velocity profiles for diffuser 1 at x = 100 and 150 cm respectively

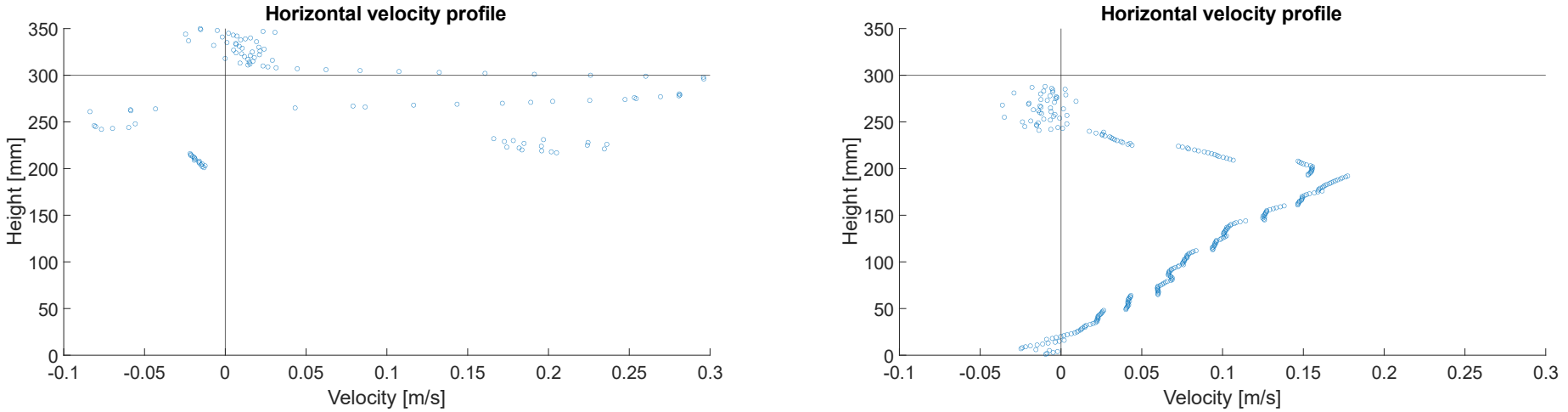

Figure A.3: Velocity profiles for diffuser 2 at x = 3.3 and 31 cm respectively

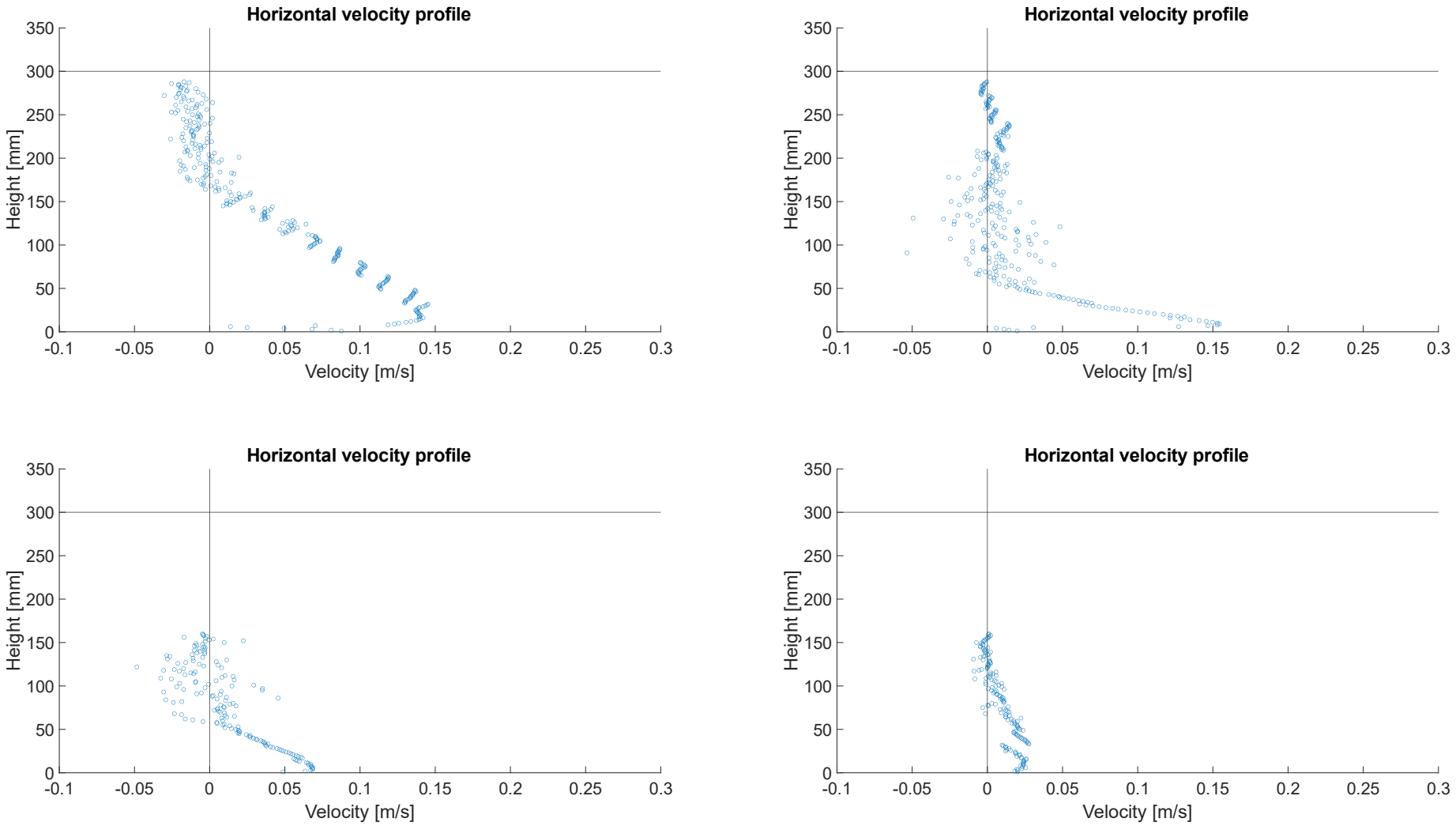

Figure A.4: Velocity profiles for diffuser 2 at x = 41, 61, 100 and 150 cm respectively

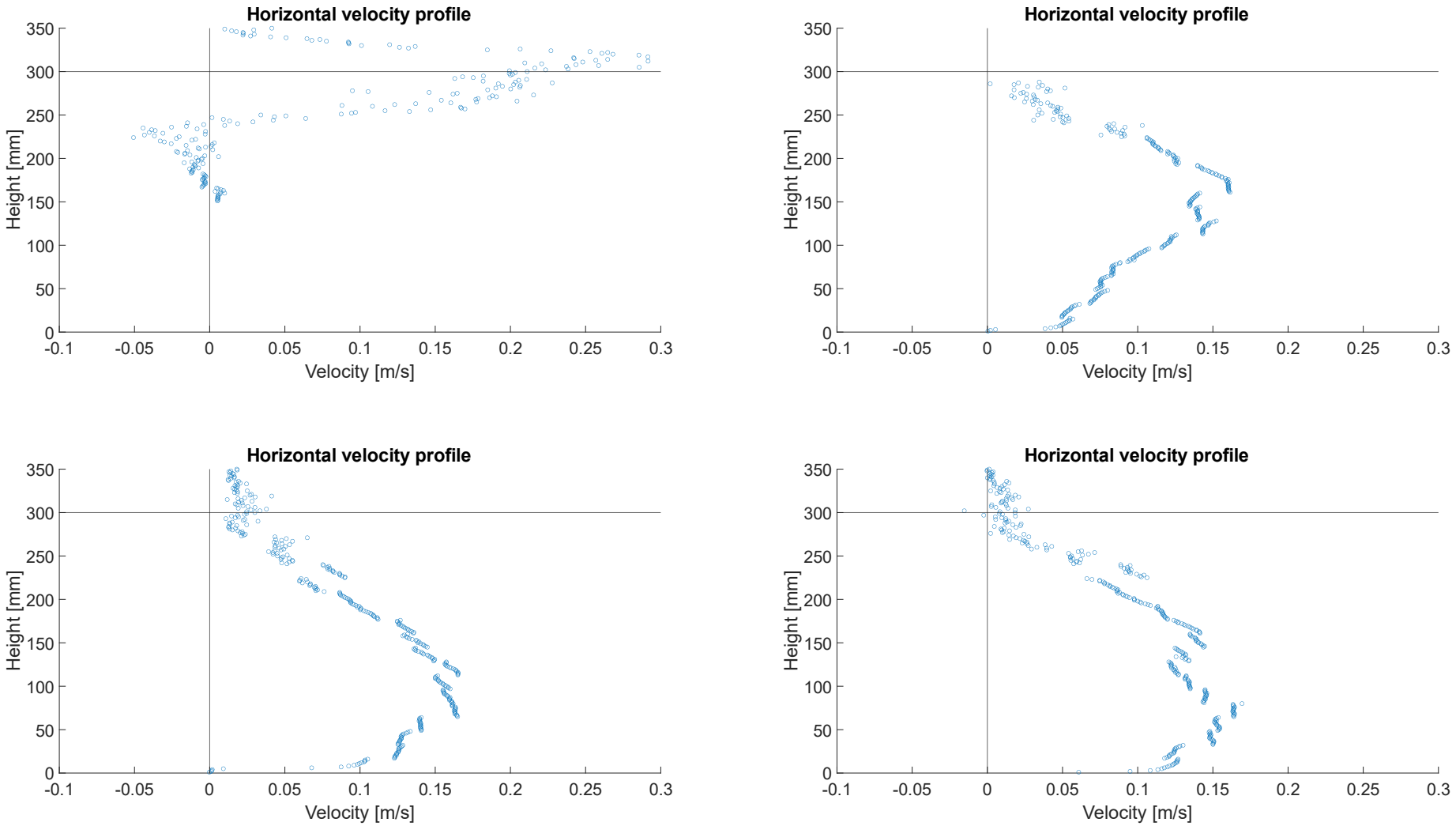

Figure A.5: Velocity profiles for diffuser 3 at x = 3.3, 100, 120 and 130 cm respectively

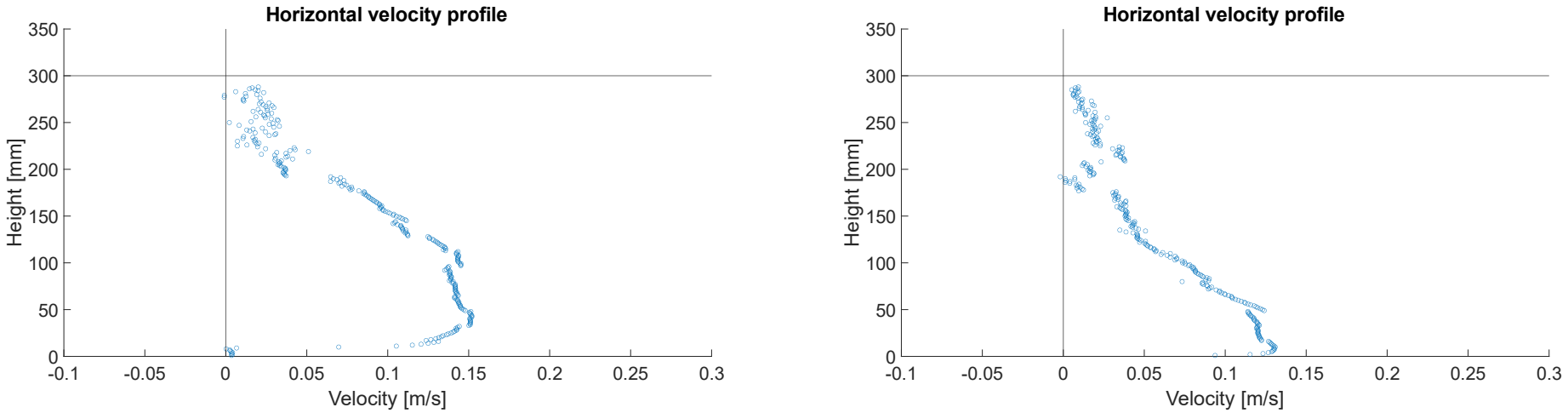

Figure A.6: Velocity profiles for diffuser 3 at x = 150 and 200 cm respectively

B. Correlation profiles

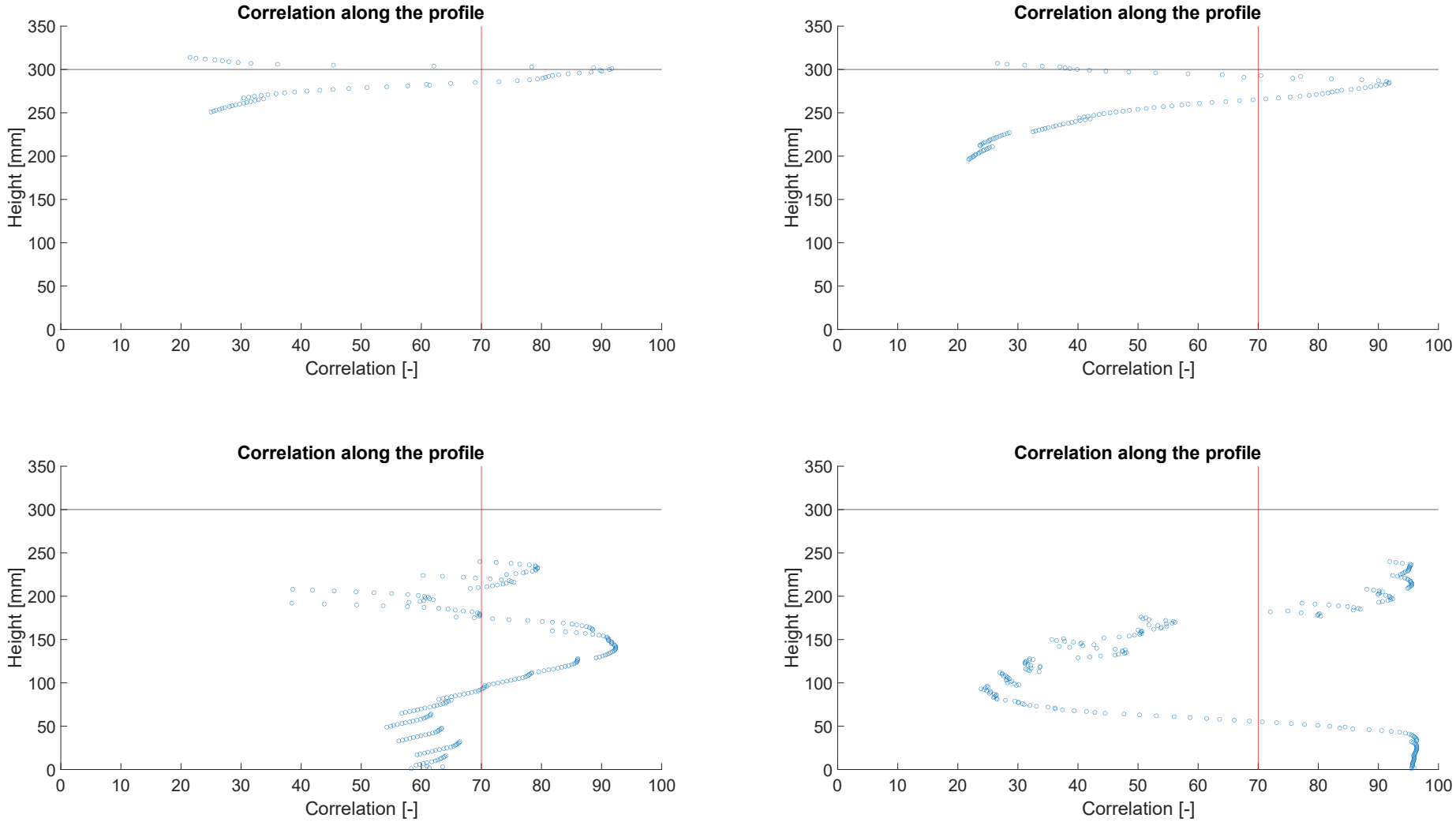

Figure B.1: Correlation profiles for diffuser 1 at x = 3.3, 11, 21 and 41 cm respectively

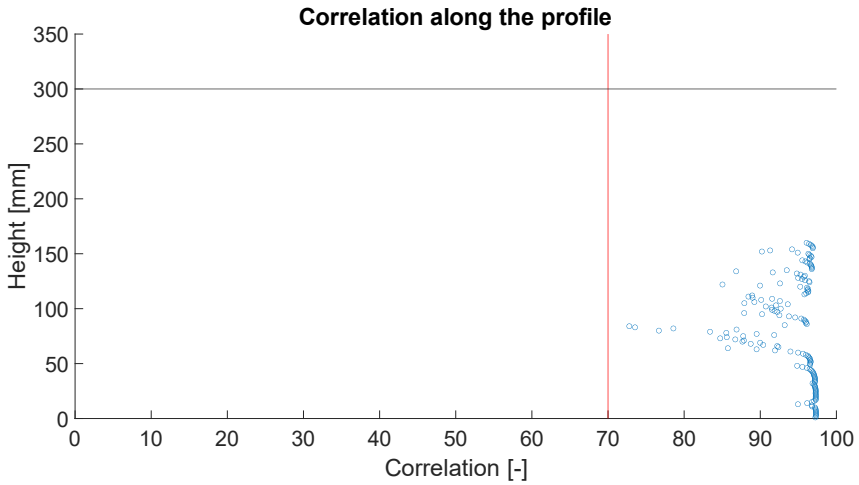

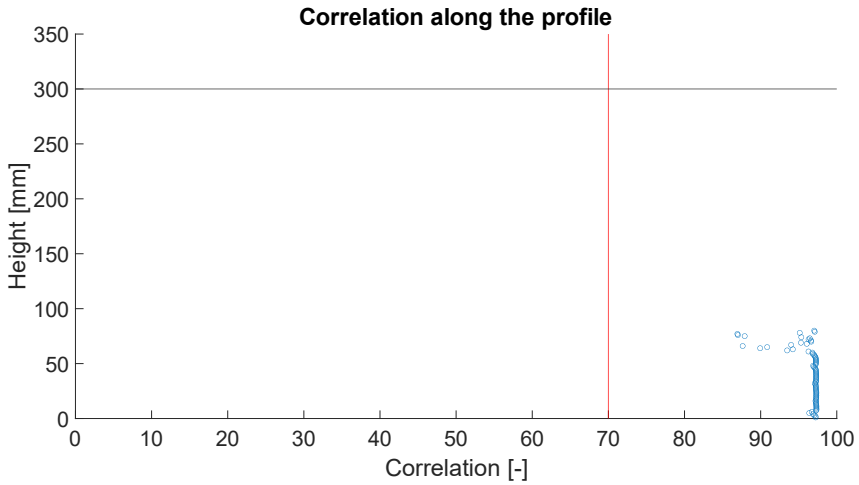

Figure B.2: Correlation profiles for diffuser 1 at x = 100 and 150 cm respectively

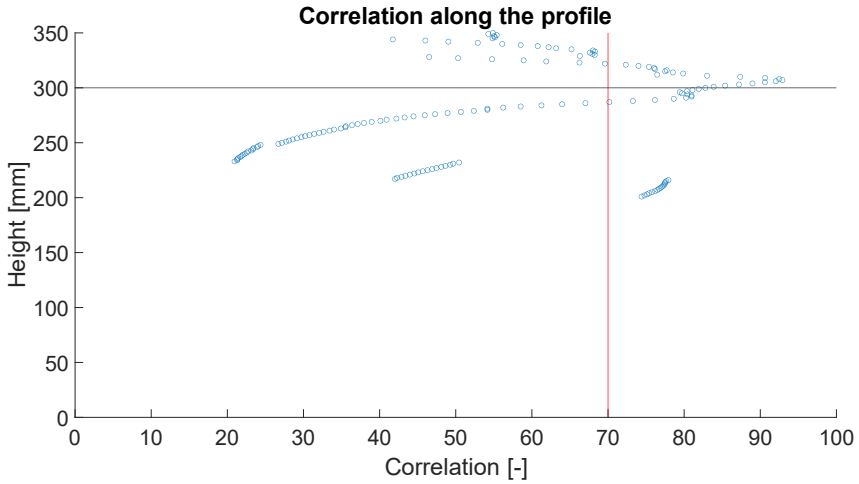

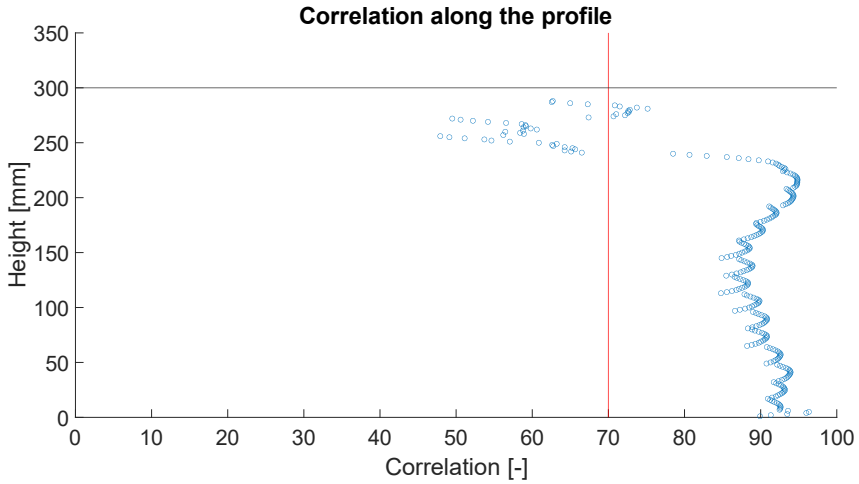

Figure B.3: Correlation profiles for diffuser 2 at x = 3.3 and 31 cm respectively

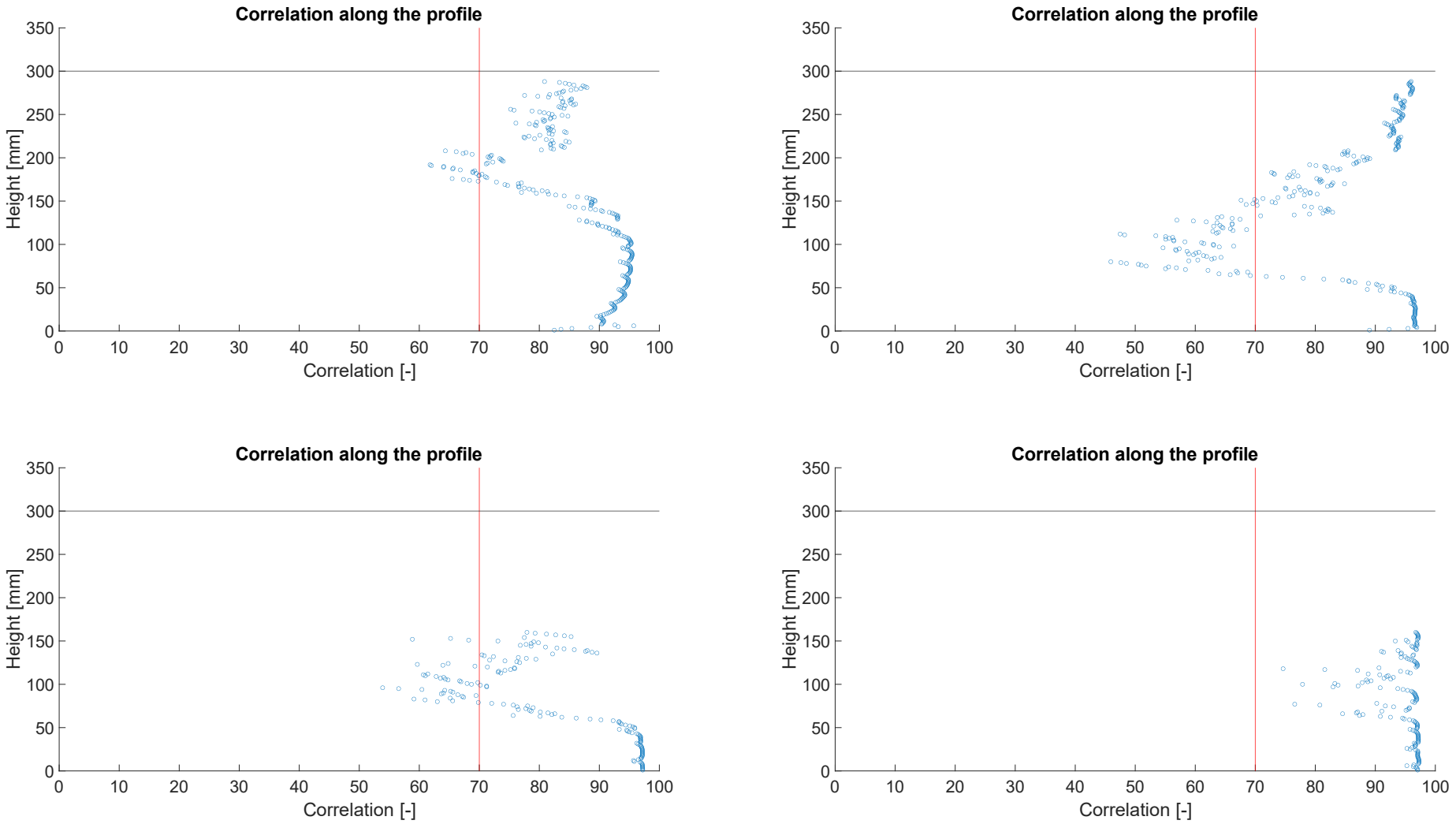

Figure B.4: Correlation profiles for diffuser 2 at x = 41, 61, 100 and 150 cm respectively

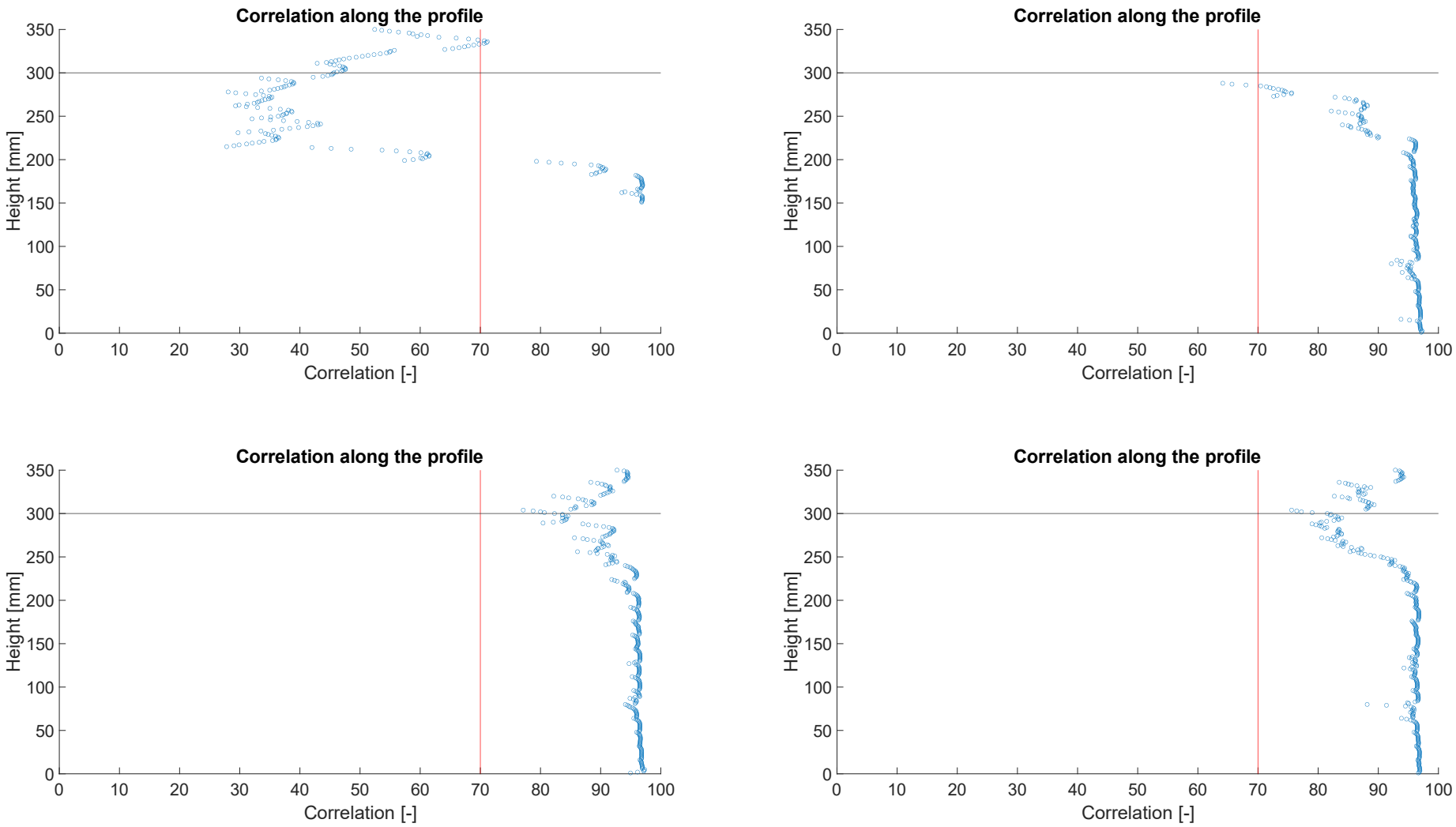

Figure B.5: Correlation profiles for diffuser 3 at x = 3.3, 100, 120 and 130 cm respectively

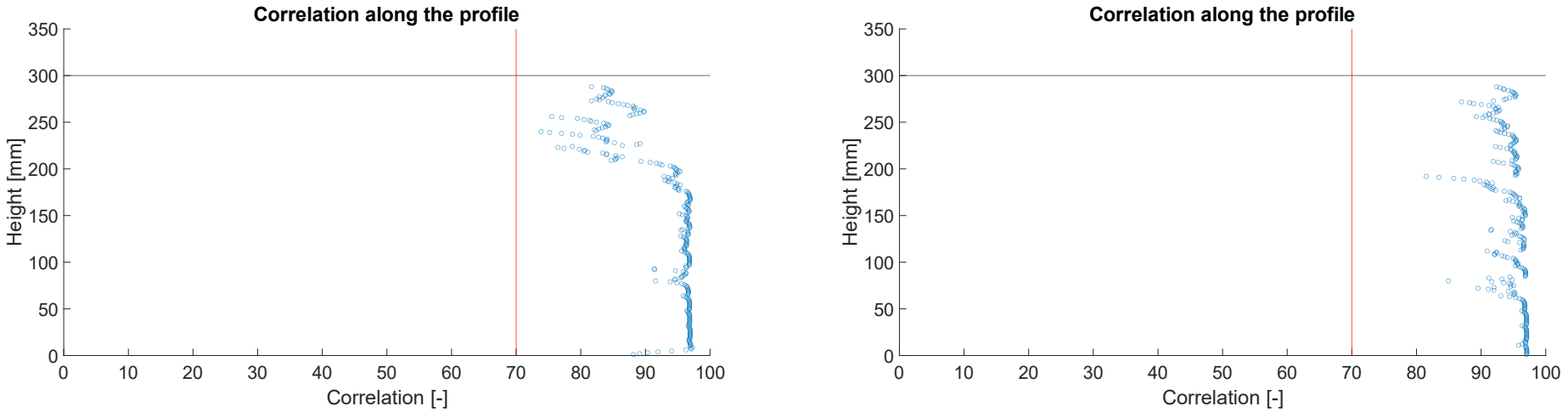

Figure B.6: Correlation profiles for diffuser 3 at x = 150 and 200 cm respectively

C. SNR and concentration profiles

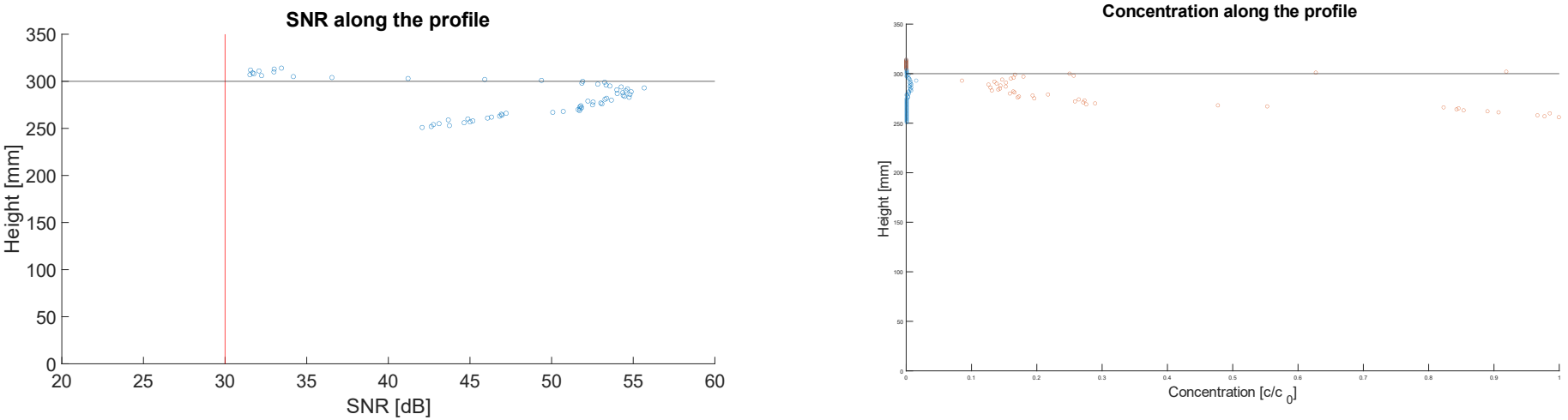

Figure C.1: SNR and resulting concentration profile for diffuser 1 at x = 3.3 cm (1A)

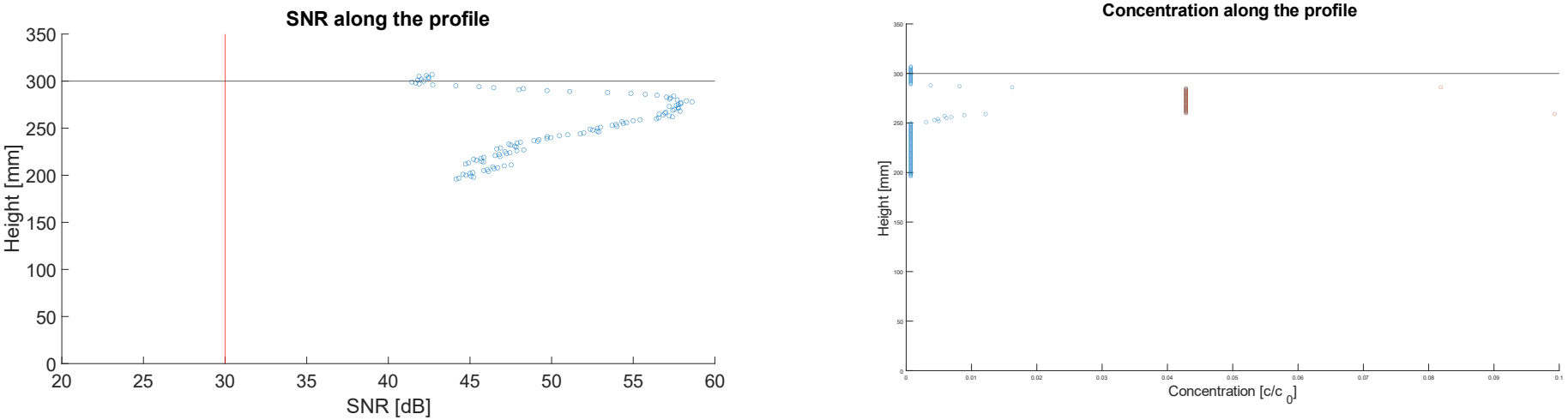

Figure C.2: SNR and resulting concentration profile for diffuser 1 at x = 11 cm (2A)

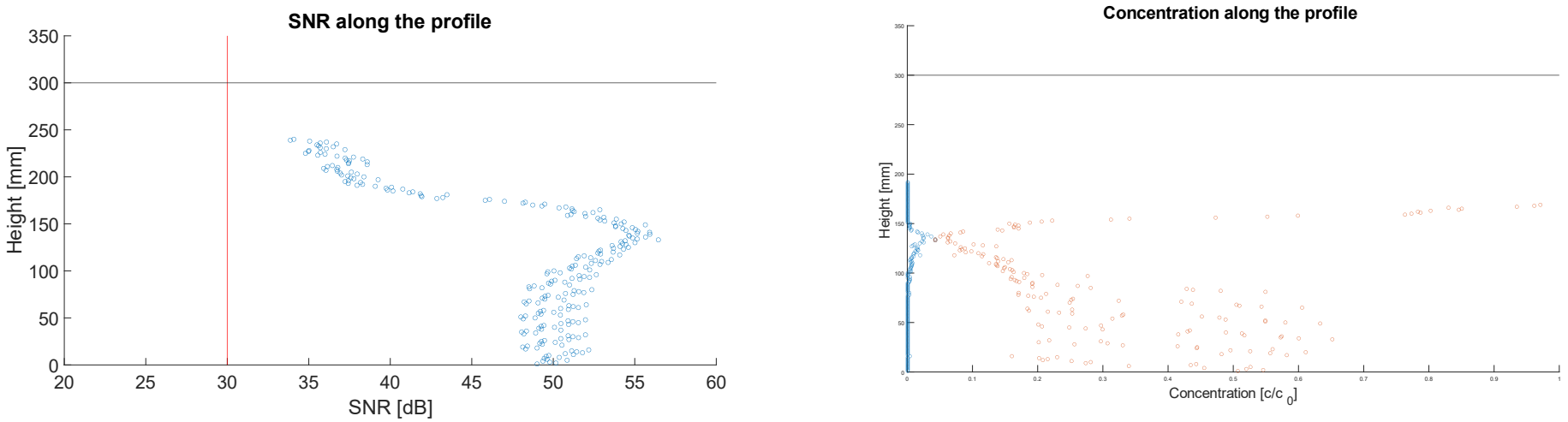

Figure C.3: SNR and resulting concentration profile for diffuser 1 at x = 21 cm (3A)

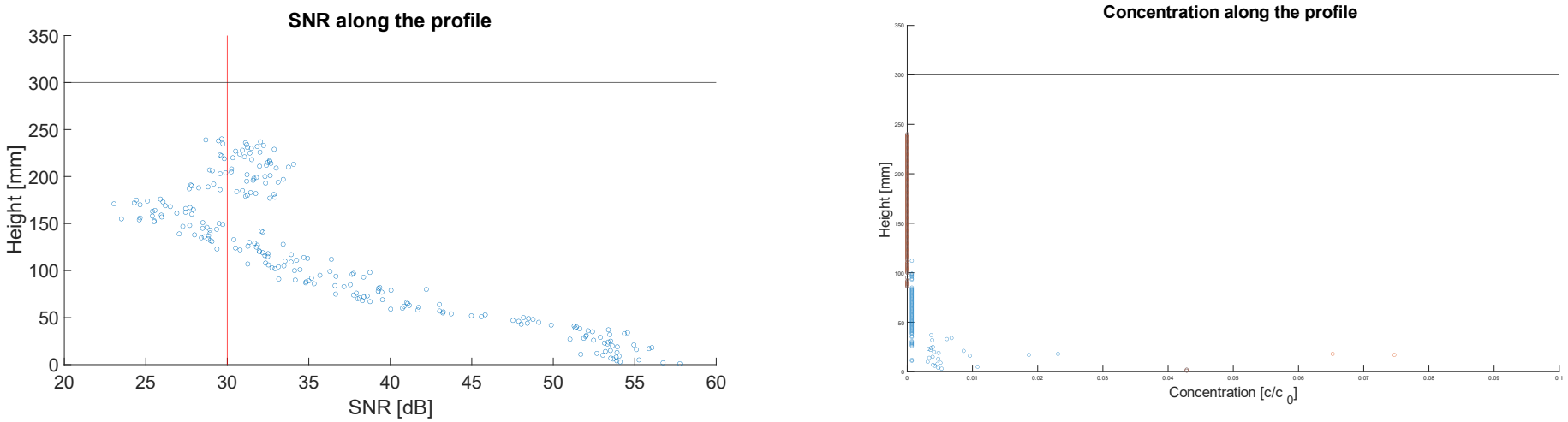

Figure C.4: SNR and resulting concentration profile for diffuser 1 at x = 41 cm (4A)

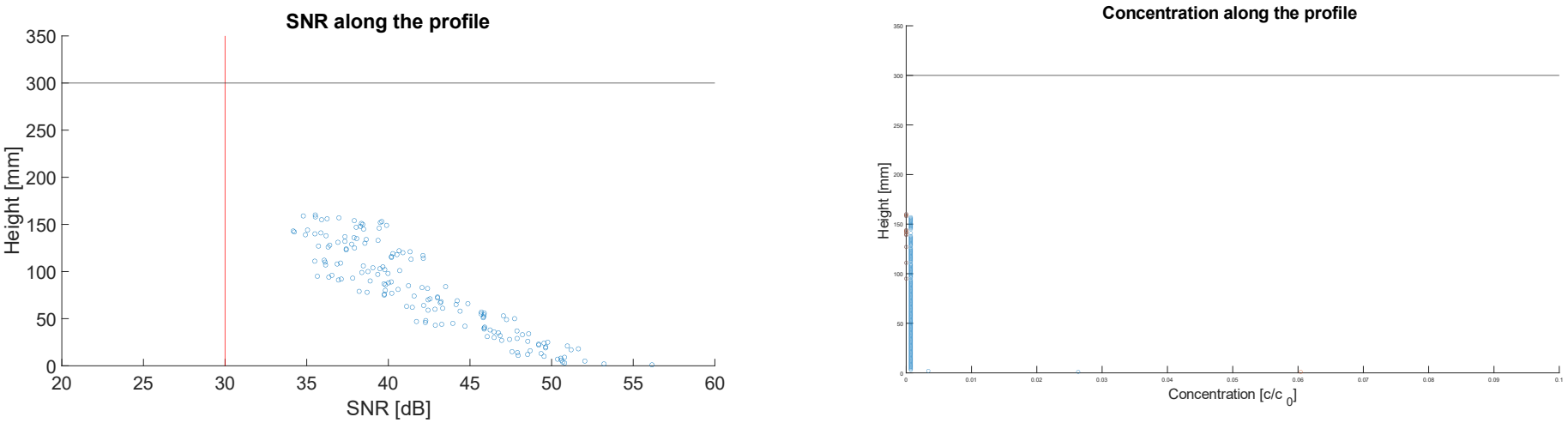

Figure C.5: SNR and resulting concentration profile for diffuser 1 at x = 100 cm (5A)

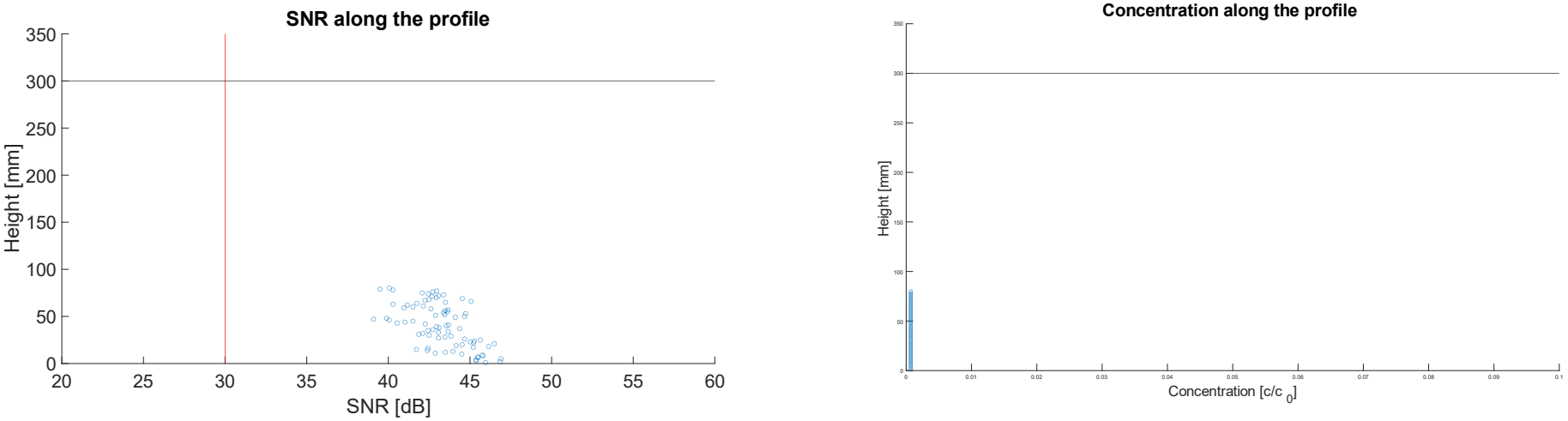

Figure C.6: SNR and resulting concentration profile for diffuser 1 at x = 150 cm (6A)

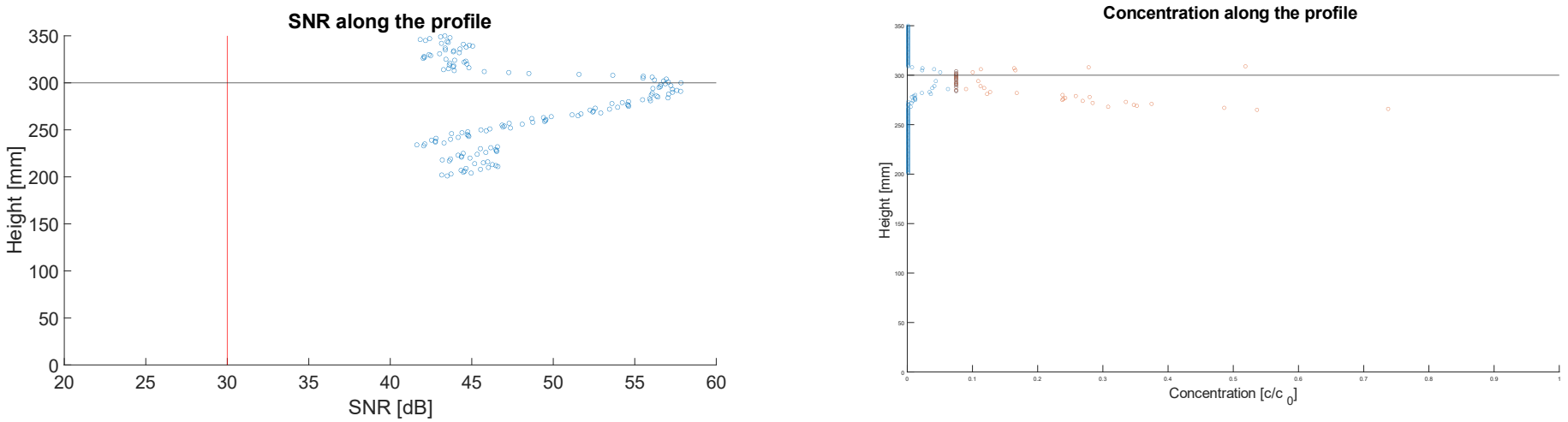

Figure C.7: SNR and resulting concentration profile for diffuser 2 at x = 3.3 cm (1A)

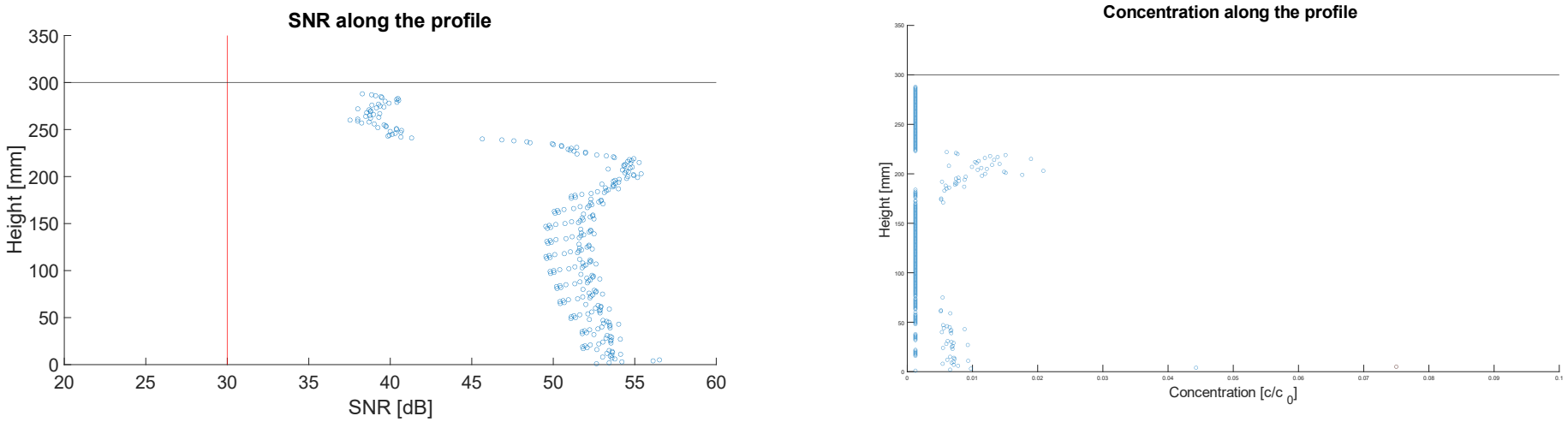

Figure C.8: SNR and resulting concentration profile for diffuser 2 at x = 31 cm (2A)

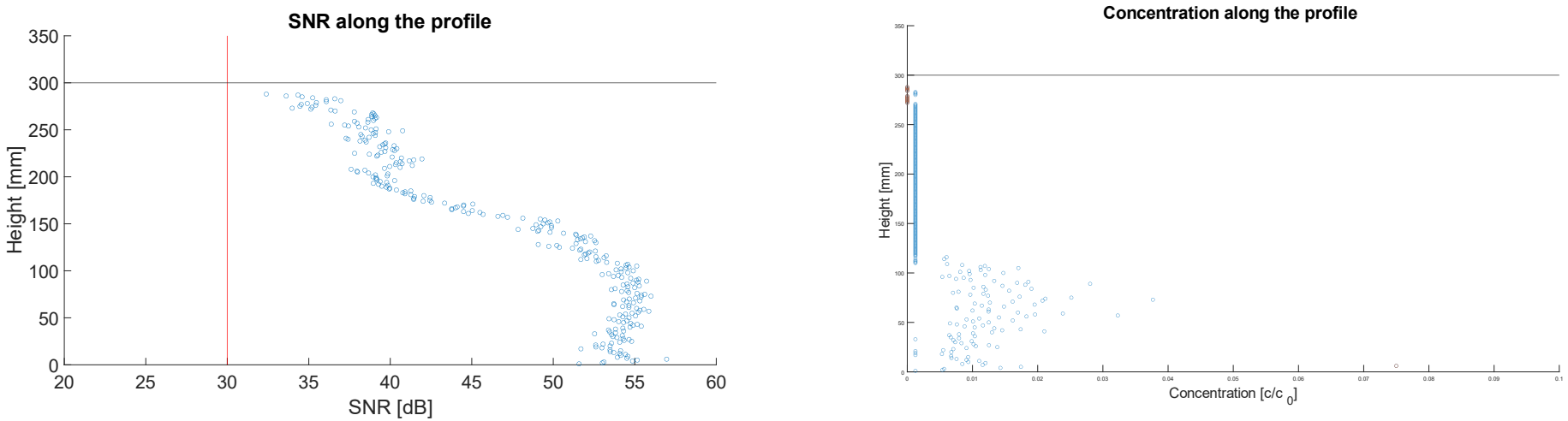

Figure C.9: SNR and resulting concentration profile for diffuser 2 at x = 41 cm (3A)

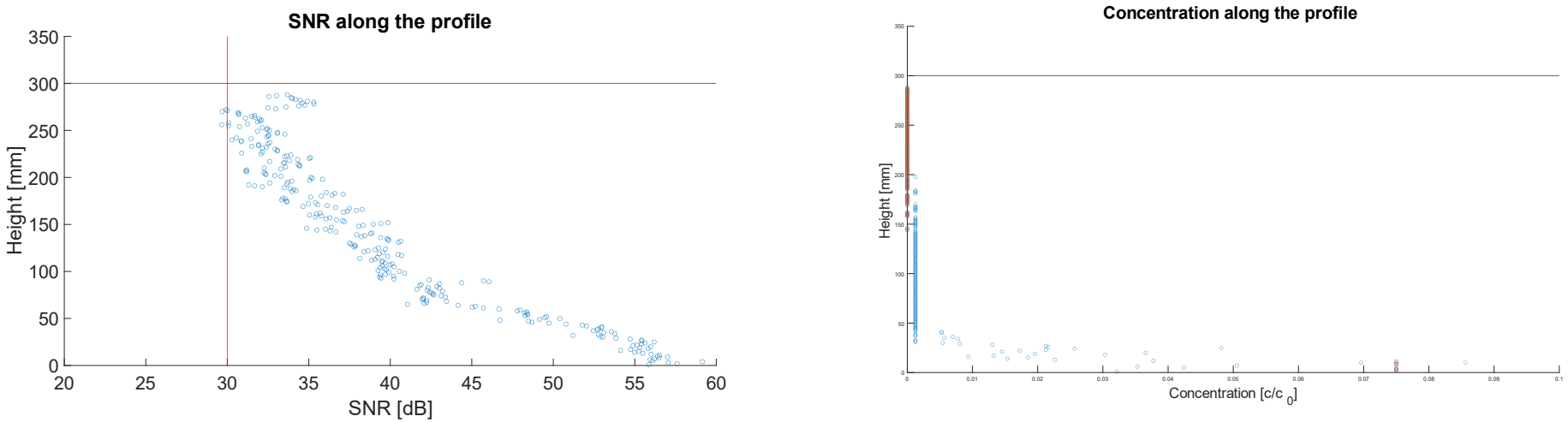

Figure C.10: SNR and resulting concentration profile for diffuser 2 at x = 61 cm (4A)

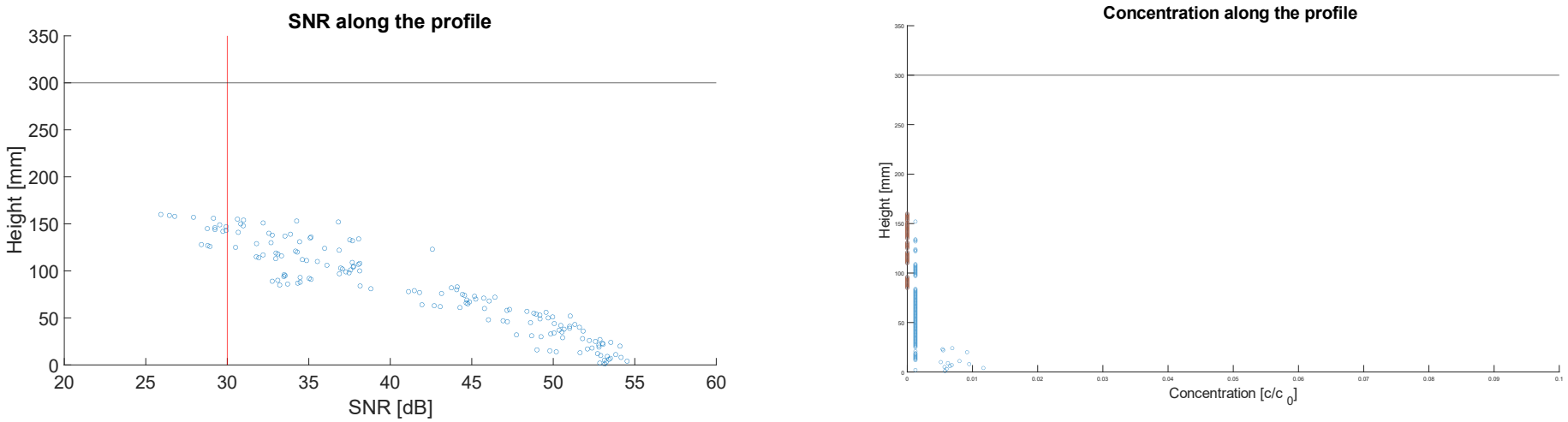

Figure C.11: SNR and resulting concentration profile for diffuser 2 at x = 100 cm (5A)

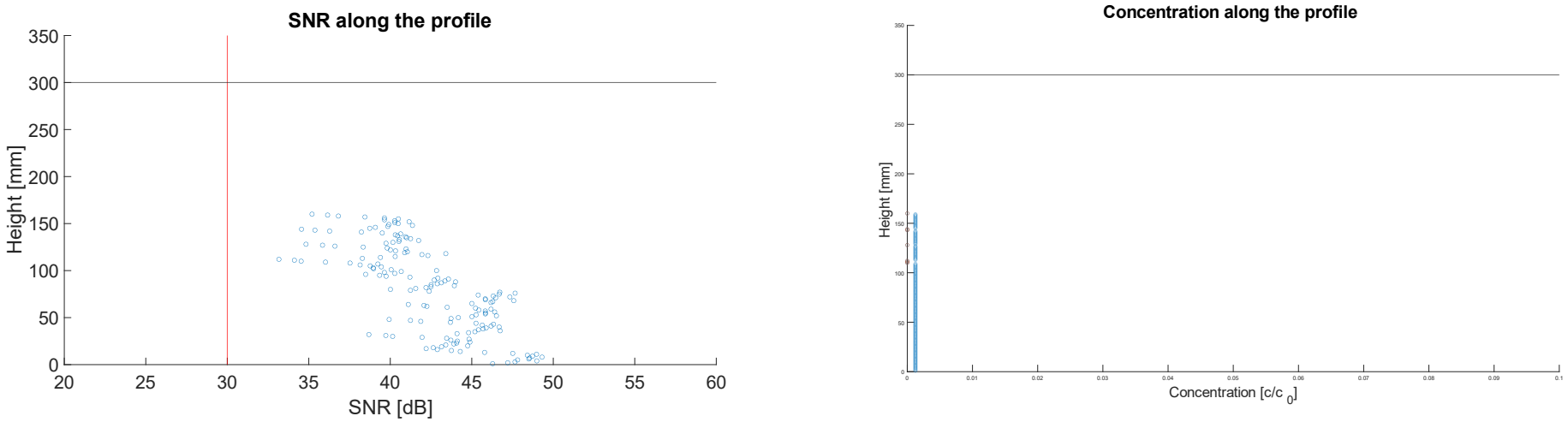

Figure C.12: SNR and resulting concentration profile for diffuser 2 at x = 150 cm (6A)

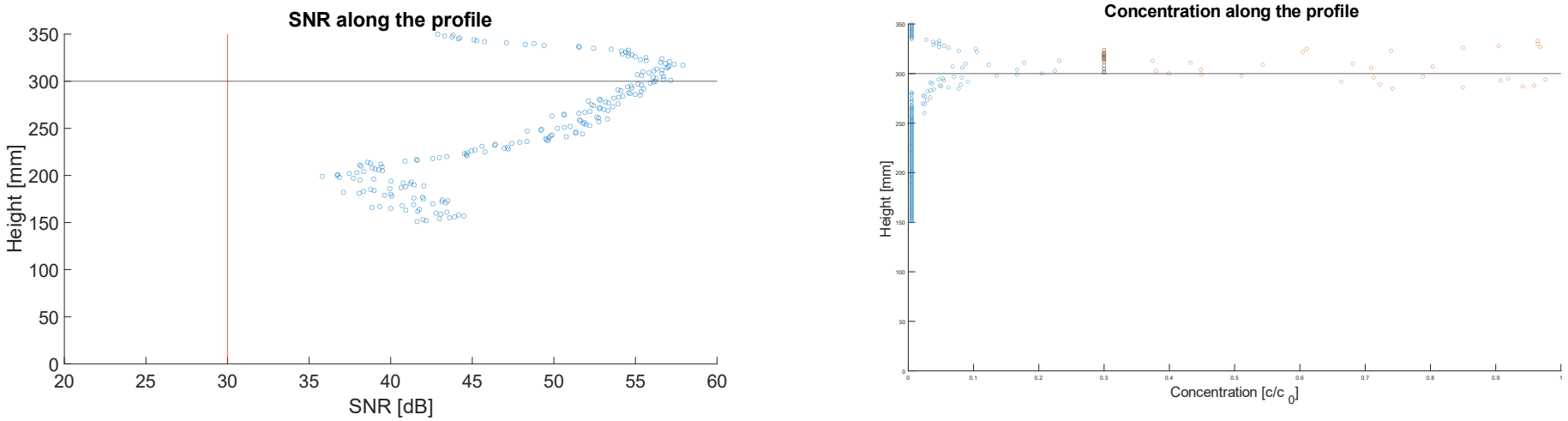

Figure C.13: SNR and resulting concentration profile for diffuser 3 at x = 3.3 cm (1A)

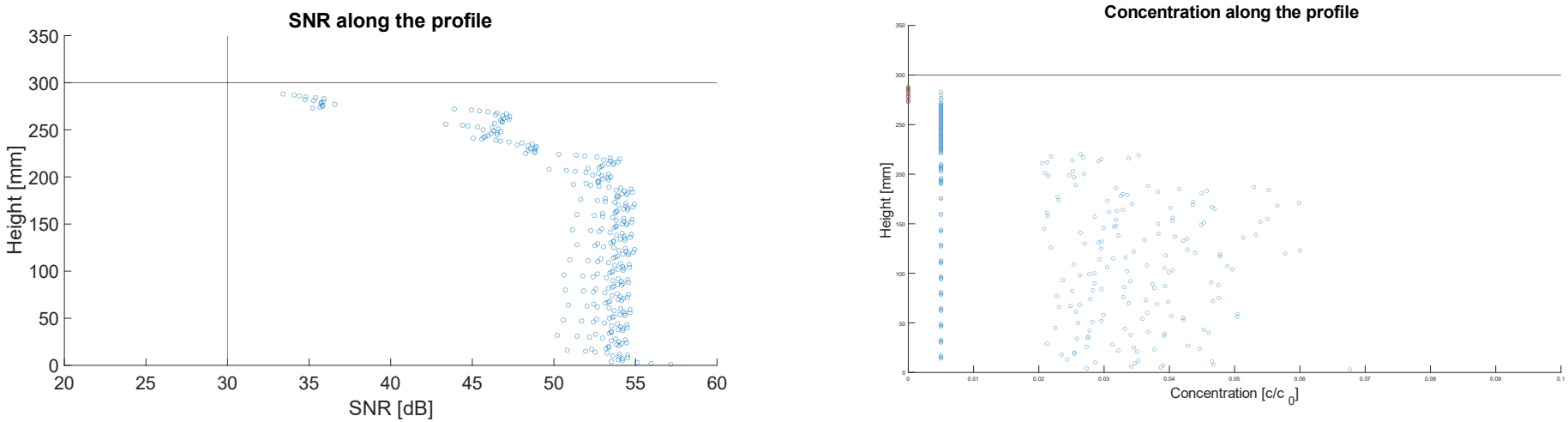

Figure C.14: SNR and resulting concentration profile for diffuser 3 at x = 100 cm (5A)

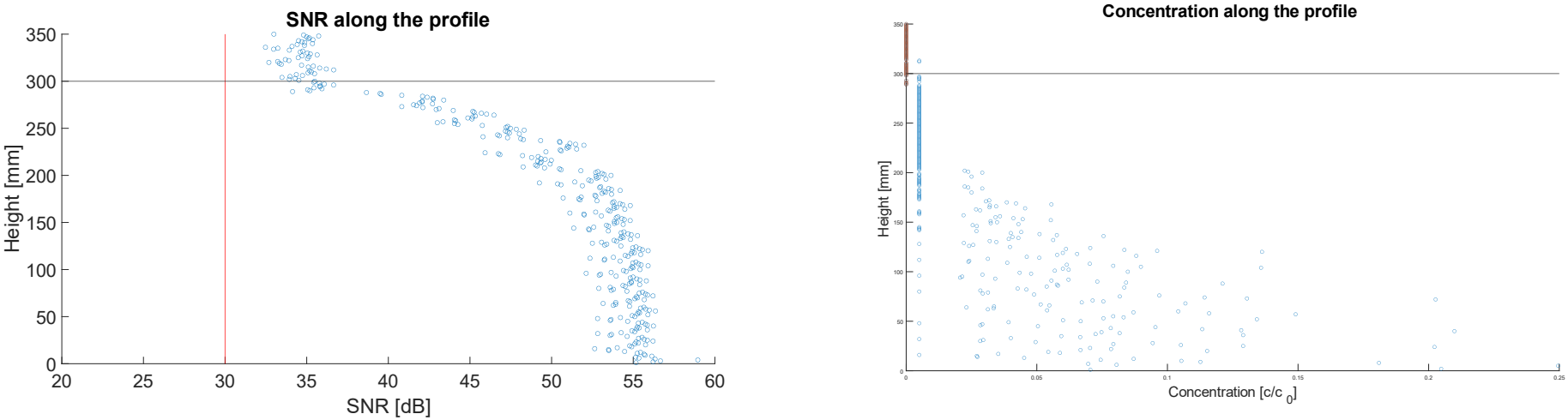

Figure C.15: SNR and resulting concentration profile for diffuser 3 at x = 120 cm (2A)

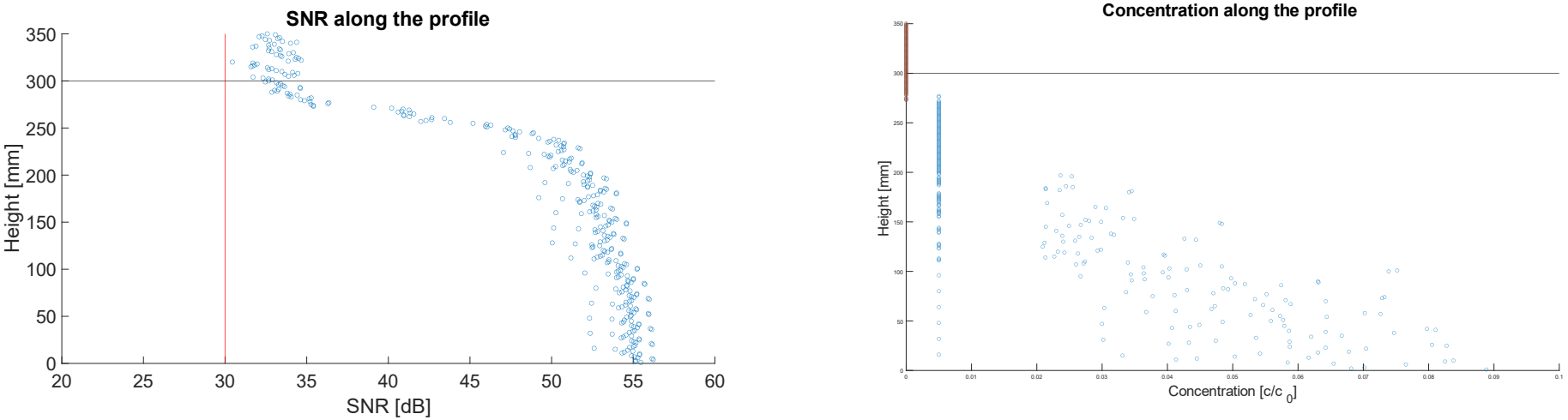

Figure C.16: SNR and resulting concentration profile for diffuser 3 at x = 130 cm (3A)

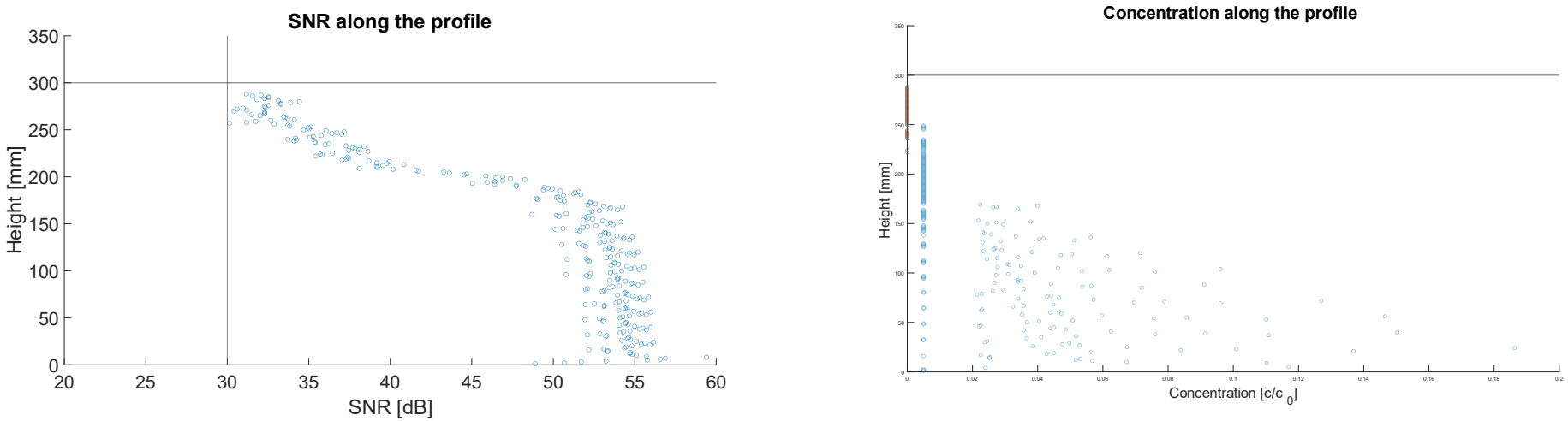

Figure C.17: SNR and resulting concentration profile for diffuser 3 at x = 150 cm (4A/6A)

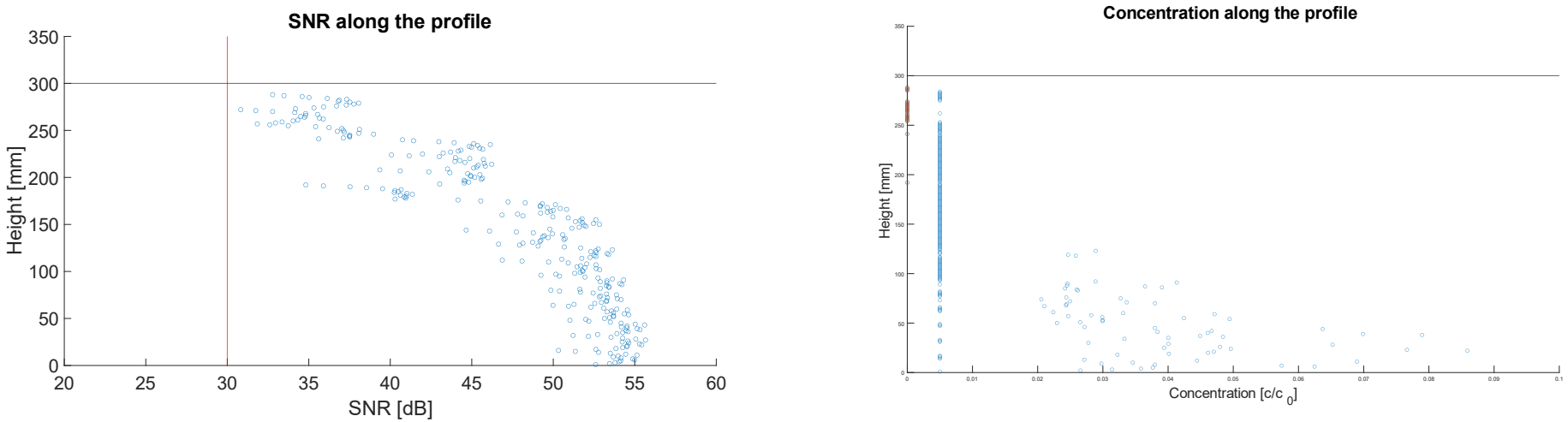

Figure C.18: SNR and resulting concentration profile for diffuser 3 at x = 200 cm (7A)

D. Recommendations for experiments with clay

As mentioned in Section 4.6, the clay experiments performed for this research could not be executed in the way envisioned based on the glass particle experiments. Mentioned in that section are the inability to reach a concentration higher than 35 g/L and the maximum experiment duration of between 1 and 2 minutes before reflection of the walls caused the tank to become completely turbid, preventing any further visual observations. Even though the ADV was not used during the experiments, it is also expected that the reflection would prevent the measuring of any profile as the time available is not enough to measure a profile consisting of more than 2 30 mm ADV profiles. Based on the lessons learned from the clay experiments performed for this research, a list of recommendations has been drawn up for the purpose of benefiting future clay experiments in the modular tank of the 3mE dredging lab. The recommendations are the following:

- The experiment scale of 1:15 as used during the experiments for this research proved to be too large. It is believed that decreasing the scale could help in elongating the total experiment duration, therefore allowing for more visual observations and possible profile measurements using the ADV. Decreasing the scale would both decrease the discharge velocity and height, which are both believed to help decrease the time scale at which the turbidity current will reach the end of the modular tank. It should be noted however that care has to be taken when choosing the scale, as keeping the buoyant jet discharge turbulent is a requirement that becomes hard to accomplish at smaller scales.
- To reach a higher concentration than 35 g/L, more preparation is required. Keeping 20 and 35 g/L in suspension for a long period of time proved not to be a problem as concentration measurements have shown. Reaching a higher concentration however, turned out to be difficult using the current setup. The pumps work well for keeping the clay in suspension, but not for bringing it in suspension. It was found that mixing the clay requires a long period of time to prevent clumps of clay from staying on the bottom. It is believed that this can be improved by pre-mixing the clay using a physical mixer instead of pumps. This could help in bringing all the added clay into suspension, after which the mixture can be pumped into the mixing tank with submersible pumps to keep it in suspension and perform the experiments. This would also allow for making a new batch of mixture while also working on the actual experiments, as both processes were found to take a lot more time than glass particle experiments.
- A smaller mixing tank should be used than the 2000 L one used for the experiments of this research. As already mentioned, the maximum running time for the experiments is 2 minutes. Depending on the volume flow of the experiment, this amounts to no more than 200 L of mixture being required. As a result, a much smaller mixing tank can be employed, which could benefit the suspension of the clay as the jet from the submersible pumps mixes more aggressively in a smaller tank.
- The water level in the modular tank should be kept low. It was found that due to the reflection of both the back and side walls the sediment cloud eventually moves towards to free surface. As a result, the water inside the modular tank stays turbid for 3-4 days, meaning that only 2 experiments can be performed per week. Decreasing the water level inside the modular tank to a height just abode the reach of the buoyant jet could improve the time needed for the settling of the particles inside the tank. Having a lower water level means the particles.